1-24-2017 12:00 AM

Synthesis of Azide-Modified NHC Coinage Metal Thiolates

Vaishnavi Somasundaram
The University of Western Ontario

Supervisor
Dr. John Corrigan
The University of Western Ontario Joint Supervisor
Dr. Mark Workentin
The University of Western Ontario

Graduate Program in Chemistry
A thesis submitted in partial fulfillment of the requirements for the degree in Master of Science

Abstract

Research on phosphine and N-heterocyclic carbene (NHC) terminated coinage metal complexes of the type L-M-X (L = NHC, Phosphine and X = S, Se) has been well-documented, however, the synthesis of coinage metal complexes of the type containing functional chalcogenolate ligands remains largely unexplored. Previous studies on sulfur containing precursors have provided an effective pathway for their incorporation onto coinage metal complexes through the generation of trimethylsilylsulfides and thiolates.

The reaction of NHC-coinage metal salts, [(NHC)MX] (X = halide, carboxylate, *etc*.), with an azide-modified ligand affords clickable NHC-coinage metal thiolates: [(^{i}Pr$_2$-bimy)Au-1-SCH$_2$-2,5-(CH$_3$)$_2$Ph-4-CH$_2$N$_3$] (**1**), [(IPr)Au-1-SCH$_2$-2,5-(CH$_3$)$_2$Ph-4-CH$_2$N$_3$] (**2**), [(IPr)Ag-1-SCH$_2$-2,5-(CH$_3$)$_2$Ph-4-CH$_2$N$_3$] (**3**) and [(IPr)Cu-1-SCH$_2$-2,5-(CH$_3$)$_2$Ph-4-CH$_2$N$_3$] (**4**) (R = {CH$_2$Ph(CH$_3$)$_2$CH$_2$N$_3$}, ^{i}Pr$_2$-bimy =1,3-di-isopropylbenzimidazol-2-ylidene, IPr = 1,3-bis(2,6-di-iso-propylphenyl)imidazol-2-ylidene). Single crystal X-ray analysis of **1-4** show that they are two-coordinate, nearly linear, with a terminally bound thiolate ligand. The successful conversion of [(NHC)MX] from X = halide, carboxylate, *etc*. to X = SR is further confirmed by heteronuclear spectroscopy, and elemental analysis. The complexes are also found to be luminescent at 298 K. The results of the UV-Vis and photoluminescence spectroscopy are also presented.

The Strain Promoted Alkyne-Azide Cycloaddition (SPAAC) reaction of one of the complexes with bicyclononynylmethanol (BCN-OH), a cyclooctyne, has also been demonstrated in order to illustrate the reactivity of the azide moiety toward strained-alkynes (**5**). Additionally, the reaction kinetics have also been determined, further confirming that the azide moiety is available for SPAAC reaction. Altogether, a novel approach towards functional coinage-metal thiolate complexes is presented for post-assembly modifications through SPAAC chemistry.

Co-Authorship Statement

The work described here in Chapter 2 and 3 of this dissertation are the results of contributions from the author, Vaishnavi Somasundaram, under the supervision of Profs. John F. Corrigan and Mark. S. Workentin from Western University.

Dr. John F. Corrigan performed the crystal structure analyses for the complexes **1 – 4** described in Chapter 2.

Praveen Gunawardene provided the author with BCN-OH, which was used in the cycloaddition reaction and rate kinetics described in Chapter 3. All other synthesis, characterisation, and data analysis described in the thesis were done by the author under the supervision of Profs. John F. Corrigan and Mark. S. Workentin.

Acknowledgements

First and foremost, I would like to thank my supervisors John Corrigan and Mark Workentin. Thank you for being there to provide the guidance and support I needed to complete my master's thesis work.

A very special thanks goes out to my friends and lab mates Willis, Alex P, Kyle, Alex V, Mahmood, Tanya, Tommy, Raj and Alec for all the good times and late nights in lab we've shared these past two years. They made my time here all the more enjoyable. I am also lucky to have met Praveen here at Western and his willingness to help in whatever way possible, insightful discussions, and supportive ear went a long way in helping me complete this work.

Finally, I would also like to express my profound gratitude to my family and friends (Soma, Senthi, Birn, Birathan, Birhavi, Dhurks and Nuj) for their constant love and support throughout my studies.

Table of Contents

List of Figures

List of Schemes

List of Appendices

List of Abbreviations

Å angstrom

bimy benzimidazole-2-ylidene

br broad

°C degree Celsius

CI chemical ionization

DMF dimethylformamide

ESI electrospay ionization

g gram

HRMS high resolution mass spectrometry

m (NMR) multiplet

mL milliliter

m.p. melting point

Me methyl

MHz megahertz

NHC N-heterocyclic carbene

NMR nuclear magnetic resonance

OAc acetate anion

Ph phenyl

PFA paraformaldehyde

ppm part per million

^{i}Pr isopropyl

quart quartet

quin quintet

s (NMR) singlet

sep (NMR) septet

THF tetrahydrofuran

1. Introduction

1.1 Coinage Metal Complexes

Complexes of group 11 elements (Cu, Ag, Au), also conventionally known as coinage metals, have become very well-established in the last few decades owing to their unique structural properties, which has led to their widespread application in a wide variety of fields such as catalysis, materials chemistry and medicine. The application of coinage metal complexes in catalysis can be seen in the large number of reports dealing with this topic.[1] Gold derivatives are primarily used in cycloisomerization and C-H activation;[2] silver derivatives have been used in alkene diboration and ring opening polymerization;[3] copper derivatives have been used in reduction and cycloaddition reactions.[4] Due to their luminescent properties, there have also been several studies that report functional materials containing various coinage metal complexes that enhance the optical properties in desirable and predictable ways.[5] Finally, due to the cytotoxicity of coinage metal complexes that can be regulated through structural and electronic modifications, they have found extensive use in medicinal applications.[6] Ag(I) complexes have demonstrated profound antimicrobial activities[7] and have been extensively by the review by Young's group.[8] Au(I) complexes have demonstrated antitumor properties in many cancer cell lines such as breast cancer cells, where mitochondria-targeted chemotherapeutic cationic Au(I) complexes possesses selective toxicity toward breast cancer cells.[9] In recent years, it has been found that coinage metals can form stable coordination complexes with N-heterocyclic carbene ligands, which have shown to possess desired properties such as antimicrobial and antitumor activity.[7,10] Regardless of the application, synthetically accessible coinage-metal complexes of the type L–M–X, where L = NHC and X = monoanionic donors such as halides, thiolates *etc*. are gaining increasing relevance.

1.2 Electronic and Steric Properties of N-Heterocyclic Carbenes (NHCs)

During the past decades, N-heterocyclic carbenes (NHCs) have emerged as a versatile class of dative ligands in metal coordination chemistry, because they can form a robust metal-ligand bond with an electron-rich metal center.[11] Wanzlick and co-workers first investigated the reactivity and stability of NHCs in the early 1960's,[12] and shortly thereafter reported the first application of NHCs as ligands for metal complexes. It was shown that the reaction of 1,3- diphenylimidazolium salts with mercuric(II) acetate leads to deprotonation of the imidazolium salt to generate an NHC-ligated mercury complex, as shown below in **Scheme 1.1**.

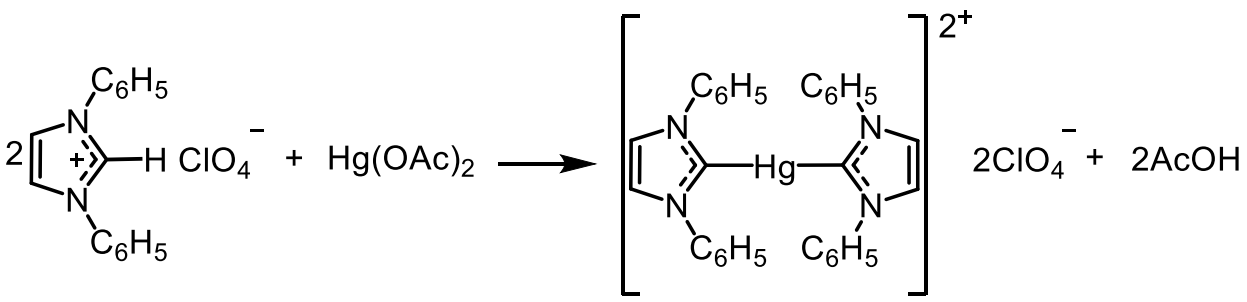

Scheme 1.1: NHC ligated mercury complex synthesized by Wanzlick group.

Ofele and co-workers later showed that applying heat to the imidazolium salts of chromium generates an NHC-chromium complex, NHC–$Cr(CO)_5$.[13] The insightful studies by Wanzlick and Ofele lead to the isolation of the first stable, easy-to-synthesize NHC, 1,3-di(adamantyl)imidazol-2-ylidene (IAd) by Arduengo *et al.* in 1991.[14] Together, these groundbreaking discoveries influenced the wave of experimental and theoretical studies of novel NHCs that followed. These studies have established that NHCs are strong sigma donor ligands that can bind firmly to many different transition metal ions with various oxidation states, where the vast majority of NHC-transition metal complexes having been synthesized through deprotonation of N,N′-disubstituted benzimidazolium salts.[15] Furthermore, changes to the reactivity profile of NHCs can be easily

modified by adjusting the electronic and steric features of the NHC. Typically, the electronic properties of NHCs can be easily tuned by introducing electron donating or electron withdrawing functional groups, while the sterics can be controlled by manipulating the steric bulkiness of the N-substituents in the NHC. For example, appending large auxiliary molecules such as substituted phenyl groups to the N-substituents in NHCs can increase the steric bulkiness of the NHC, which produces predictable changes in the overall reactivity of the NHC.[16] In order to quantify the steric factors characterizing these ligands, Nolan developed a method where one can measure the volume of a sphere that is centered around a metal, buried by overlap with the various NHC ligands, denoted as $\%V_{Bur}$.[17] The bulkier the ligand, the larger the volume that will be occupied by the ligand within the sphere ie. $\%V_{Bur}$ is larger. Nolan's model allows for the quantification of the subtle steric differences within the NHC class of ligands, allowing for fine tuning of the NHC's reactivity profile. In this model (**Fig 1.1**), the metal atom is centered in the core of a defined radius (3Å) and the average bond length between the coordinating C of the NHC and the metal atom is set to 2Å.

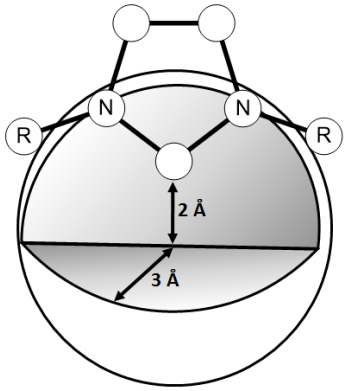

Fig 1.1: Nolan's method of measuring percent buried volume ($\%V_{Bur}$).

The $\%V_{Bur}$ has been calculated for several saturated and unsaturated NHCs using crystallography data, such as those shown in **Fig 1.2**. As can be seen, N-alkyl substituents such as

the *iso*-propyl groups in 1,3-di-isopropylbenzimidazole-2-ylidene possess the lowest percent buried volume,[18] which increases upon substitution of the N-substituents with aryl groups in 1,3-bis(2,6-di-iso-propylphenyl)imidazol-2-ylidene (IPr).[19] Cyclic (alkyl)(amino)carbenes (CAAC) are a class of NHCs bearing only one nitrogen substituent, introduced by Bertrand *et al*. and feature one amino group of a typical NHC replaced with an alkyl group thereby introducing a tunable steric environment.[20]

As shown above, $\%V_{Bur}$ measurements have been proven useful in providing a steric evaluation of an NHC. The electronic properties of NHCs are commonly assessed using the Tolman Electronic Parameter (TEP).[21] The TEP measures the electron-donating ability of a ligand, L by determining the infrared-stretching frequencies of the carbonyl ligands in model transition metal carbonyl complexes such as *cis*-[LIrCl(CO)$_2$] or *cis*-[LRhCl(CO)$_2$]. Mathematical formulae have been derived to correlate the TEP values obtained from different complexes. The more electron-donating the ligand of interest the more electron-rich the metal center becomes which then increases the degree of π-backbonding into the carbonyl ligands and thus reducing the bond order and thereby lowering the infrared stretching frequency.

Together, the synthetically attractive features and the ability to tune the properties of NHCs has led to them to be used extensively in transition metal and main group chemistry. Specifically, the development of coinage metal(I)-centered complexes has been explored with a variety of coordinating ligands possessing either hard (N, and O) and soft (S, P, and carbene C) donor atom sets. However, due to the advantages of the NHCs-based coordinating ligands described above and the lability of metal-halide bonds, metal-NHC-halides [(NHC)MX] are generally used as the precursor to access these types of complexes.

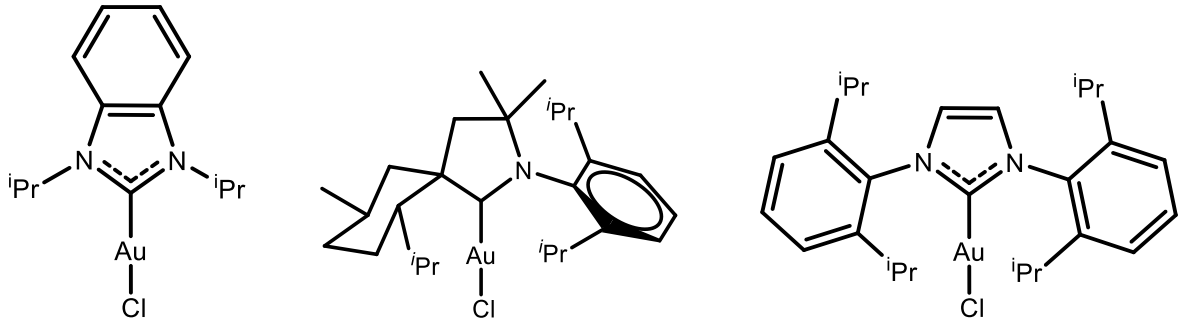

(a) (b) (c)

Fig 1.2: Percent buried volumes of various NHCs using AuCl model with length at 2Å: (a) $^{i}Pr_2$-bimy – 27.9 (b) IPr – 44.5 (c) CAAC – 51.2.

1.3 NHC-Metal-Halido Complexes

NHC bound group 11 metal halides serve as precursors to making various isolable monomeric metal carbene complexes possessing anionic heteroatomic ligands (such as amido, alkoxy, and thiol groups) that have a wide scope of applications. Of these complexes, NHC–Ag complexes are the most widely studied due to their relative ease of synthesis, affordability, and effective use as transmetallating agents. The chemistry of NHC–Cu complexes has received relatively less attention compared to the other coinage metals. To date, the applications of NHC-Cu complexes are focused on use in catalysis such as in various transformations of CO_2, like the carboxylation of various substrates, and the reduction of CO_2 to CO or formic acid derivatives.[22]

For the preparation of Cu and Ag metal complexes, the most common route is through the reaction of an appropriate imidazolium salt with a metal base to afford [(NHC)MX] (X = halide, carboxylate, *etc.*) precursors, which can be subsequently transformed to the desired metal complex. However, it should be noted that [(NHC)AgX] can serve as an effective transmetallating agent to

make [(NHC)CuX] in the presence of a copper base, where the driving force for the formation of NHC-Cu is the stronger NHC–Cu bond relative to the NHC–Ag bond.[23]

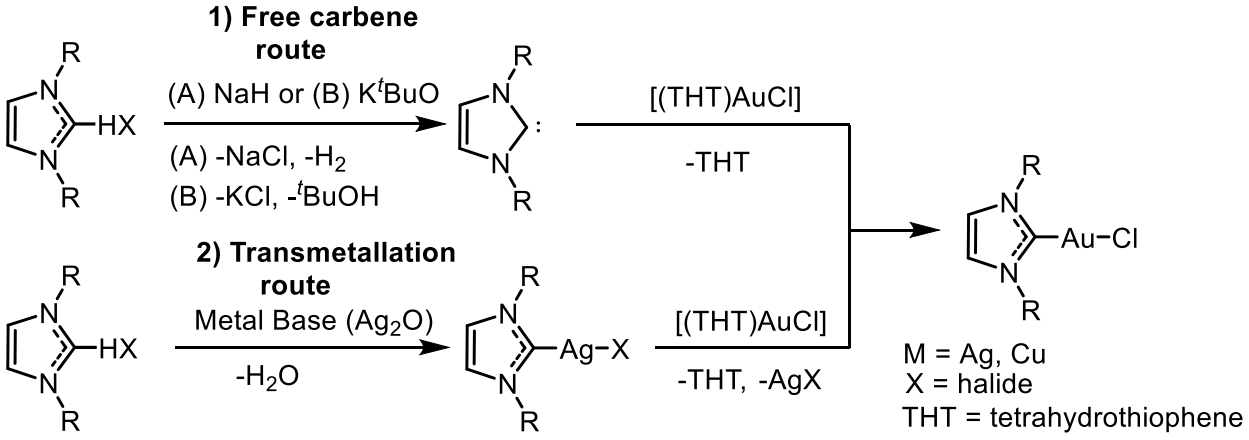

Scheme 1.2: Synthetic route to the preparation of [(NHC)AuCl] complexes.

In the case of NHC-Au complexes, the most commonly used methodologies involve: 1) reaction of free carbene with gold (I) precursors[24] or 2) carbene transfer from Ag or Cu–NHC precursors (**Scheme 1.2**).[25,26] Both approaches, although efficient, require multiple steps, and inert conditions. For the carbene route, an excess of relatively expensive bases (NaH or KO^{t}Bu) are needed in order to deprotonate the imidazolium salt, and one equivalent of metal is wasted during the transmetallation procedures. In 2013, the Nolan group devised an improved, scalable one-step economical procedure for the synthesis of [(NHC)AuCl] that proceeds under mild conditions in air using technical grade solvents.[27] In this methodology, the imidazolium salt is reacted with [(THT)AuCl] in the presence of K_2CO_3 to afford the product in high yields (**Scheme 1.3**).

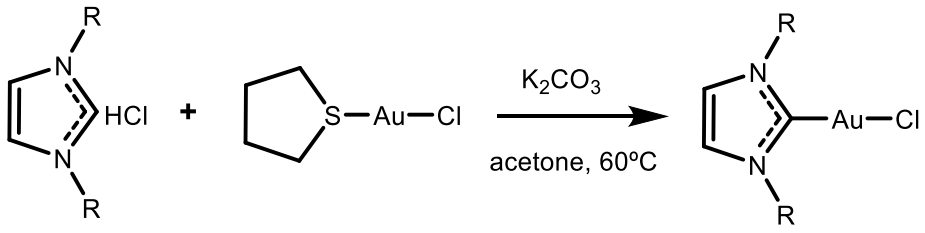

Scheme 1.3: Alternate route to the preparation of [(NHC)AuCl] proposed by Nolan group.[27]

1.4 NHC-Metal-Chalcogenolate Complexes

Studies on both monomeric and cyclic Ag(I) and Cu(I) chalcogenolates have revealed rich photophysical properties.[5] The synthesis of these species proceeds by the reaction of an [(NHC)MX] (X = halide, carboxylate, *etc*.) precursor with aryl and alkyl silyl-chalcogenolate reagents under inert conditions to give NHC-metal-thiolate complexes in good yields. In general, using chalcogenate reagents with trimethylsilyl moieties (instead of other counter-substituents) allows for the facile preparation of metal-chalcogenolate complexes as they are relatively easy to handle, have good solubility in common organic solvents, and the silane by-product is easily removed by evaporation. Furthermore, tuning the electronic structure of chalcogenate ligand (and/or carbene) can afford these metal-chalcogenolates as linear complexes, or as cyclic clusters. In 2012, the Corrigan group showed 1,3-di-isopropylbenzimidazol-2-ylidene ($^{i}Pr_2$-bimy) and its relatively smaller size, based on $\%V_{Bur}$, can be used to stabilize polynuclear Cu(I) and Ag(I) phenylchalcogenolate clusters prepared from phenylchalcogentrimethylsilanes.[28] The reaction shown in **Scheme 1.4**, proceeds with the formation of the by-product trimethylsilylchloride, $ClSiMe_3$ or trimethylsilylacetate, $AcOSiMe_3$ which can be easily removed by evaporation.

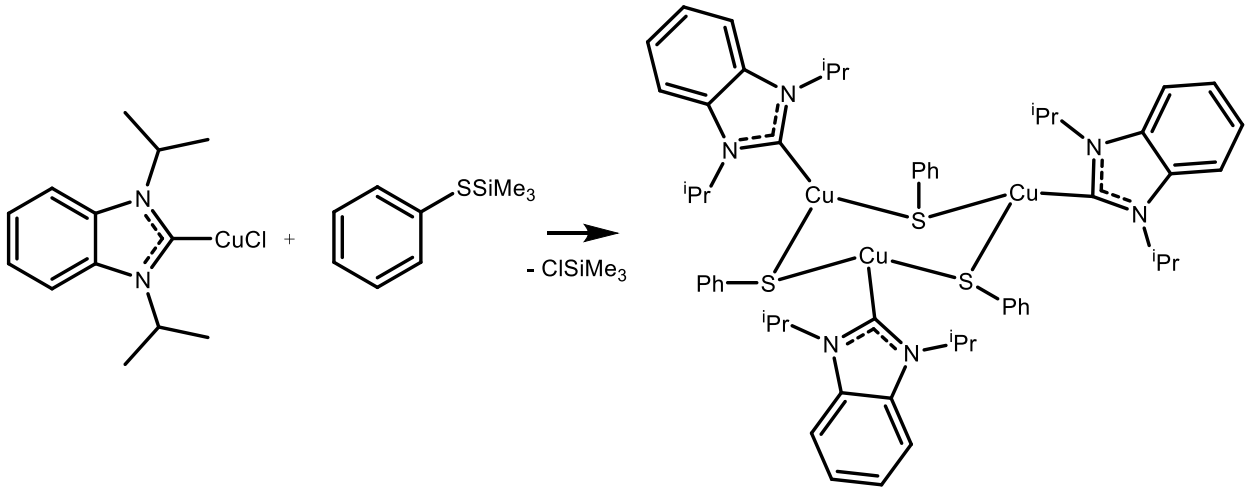

Scheme 1.4: Synthesis of NHC copper phenylthiolate cluster, $[Cu_3(\mu\text{-}SPh)_3(^iPr_2\text{-}bimy)_3]$ by Corrigan group.[28]

The molecular structure of the NHC coinage metal thiolate clusters was determined by X-ray crystallography (**Fig 1.3**). The silver analogue consists of an eight membered Ag_4S_4 ring framework with two Ag environments that are four coordinate and two three-coordinate Ag sites. In the case of the copper analogue, the Cu_3E_3 (E = S, Se) ring adopts a chair confirmation and the three Cu(I) are three-coordinate.

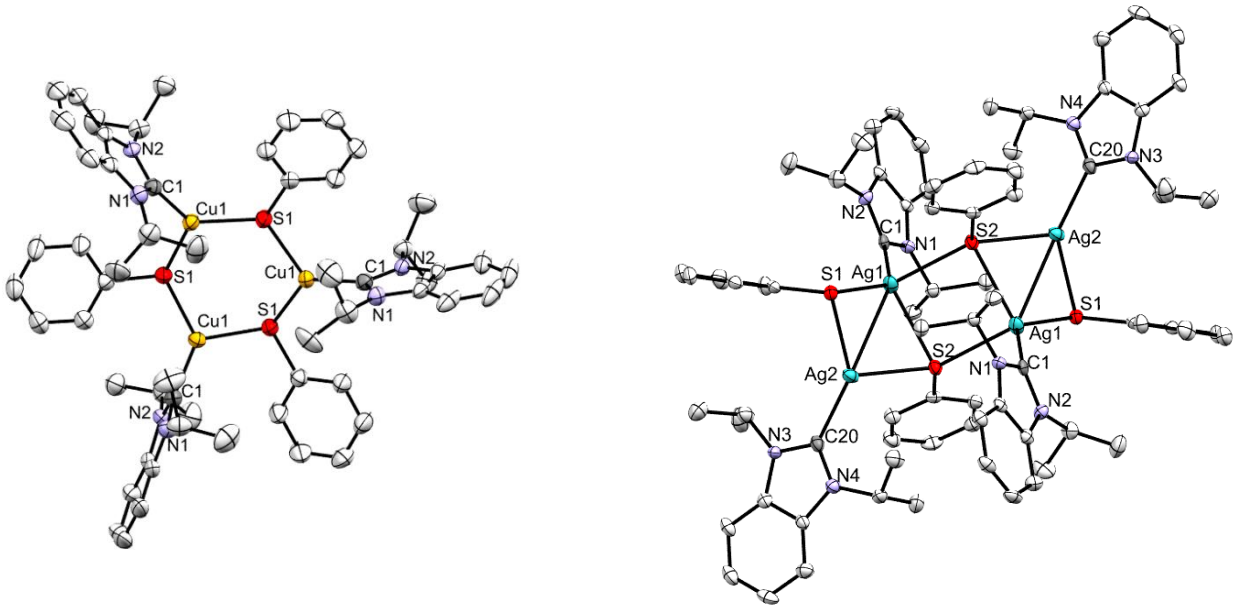

Fig 1.3: Crystal structures of $[Cu_3(\mu\text{-SePh})_3(^{i}Pr_2\text{-bimy})_3]$ and $[Ag_4(\mu\text{-SPh})_4(^{i}Pr_2\text{-bimy})_4]$.[28]

Another approach to the synthesis of silver thiolates employs free carbenes to solubilize $[AgSR]_n$ coordination polymers to make [(NHC)AgSR], as shown in **Scheme 1.5 (A)**. Following established methods, when reacting AgX with a thiol in the presence of a base such as triethylamine, a network of repeating [AgSR] units, generally understood as coordination polymers, is produced (**Scheme 1.5 (B)**).[29] An equilibrium is established between soluble complex species and the polymer, the high thiophilicity of Ag(I) and labile coordination modes ultimately drive the reaction forward as the insoluble silver thiolate self-assembly is formed.

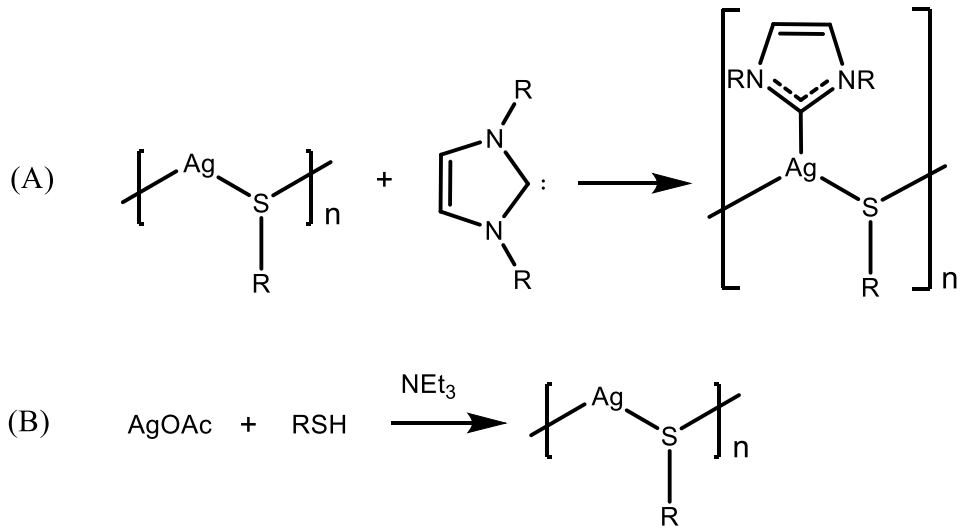

Scheme 1.5: (A) Synthesis of [(NHC)AgSR] clusters using coordination polymer precursor. (B) Synthesis of [AgSR] coordination polymer.

It has been reported that the steric bulkiness and solubilizing substituents on the ligands can influence the aggregation processes.[30] In 1989, Dance predicted a chain structure consisting of $M_4(SR)_4$ cycles for [CuSR] and [AgSR] compounds.[31] Powder X-ray diffraction data have illustrated chain structures, although lamellar structures consisting of alternating layers of silver thiolates have also been proposed depending on the organic substituent on sulfur.[32] Subsequently, an ancillary ligand such as phosphines and carbenes is added in order to dissolve polymeric [AgSR]. The strong affinity of phosphines, and carbenes for Ag(I) facilitates the break down of the polymeric chain to form the desired mononuclear complexes or cyclic clusters.

1.5 Click Chemistry

"Click chemistry" was a term first coined by K.B. Sharpless to describe reactions between pairs of functional groups that occur rapidly and chemoselectively with each other under mild

conditions and can be performed in a wide range of both organic and aqueous solvents.[33] The Workentin group has demonstrated the utility of click chemistry as an efficient method for the post-assembly surface modification of gold nanoparticles, [34] due to its high yields, simple reaction conditions and ease of post-treatment. There have been many types of click reactions described in literature, which include 1,4 Michael addition reactions between maleimides and thiols, 1,3-dipolar cycloadditon reactions between cyclooctyne and nitrones, the inverse electron demand Diels-Alder tetrazine ligation and the Staudinger ligation between a phosphine and azide.[35] Of these, 1,3 dipolar cycloaddition reactions are an extremely versatile class of chemical reaction that has found widespread utility in in heterocyclic chemistry, natural product synthesis, and medicinal chemistry. In the chemical transformation, a 1,3- dipole reacts with an alkene or alkyne termed the dipolarphile, giving rise to a five-membered ring through a 1,3 cycloaddition.[36] Studies on the mechanism of these types of reaction have shown that it proceeds in a concerted fashion. The reaction of alkynes with azide dipoles to form 1,2,3-triazoles is by far the most widely used 1,3 dipolar cycloaddition reaction **(Scheme 1.6**). This reaction was first reported by Arthur Michael in 1893 and developed further by Rolf Huisgen, and is arguably the gold standard in the conjugation of two substrates that is otherwise difficult to achieve. The main advantage to using alkyne-azide cycloaddition chemistry in conjugation studies is that azides are generally chemically inert, robust and easy to synthesize, allowing for facile incorporation of the dipolar moiety.[37] The original Huisgen 1,3-dipolar cycloaddition reaction required high temperature or pressure in order to overcome the reaction barrier. In 2002, it was found that addition of catalytic amounts of a Cu(I) salt could be added in what is now known as the Cu-catalyzed azide-alkyne cycloaddition (CuAAC), in order to make the reaction proceed faster.[38]

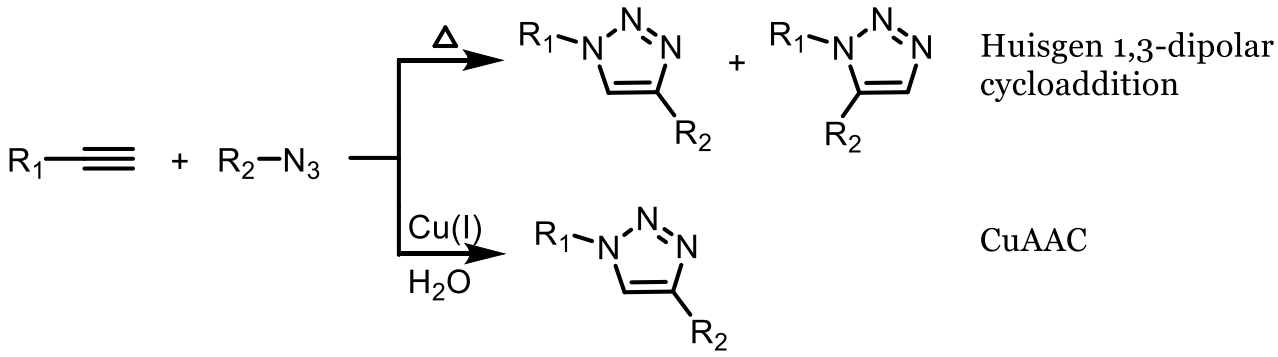

Scheme 1.6: Synthetic pathways for alkyne-azide cycloaddition.

Another strategy was later developed by the Bertozzi group that utilizes the ring strain in cyclooctyne rings to promote the cycloaddition reaction between the alkyne and azide moieties in the absence of synthetically-disadvantageous copper catalysts.[39] This class of click reaction has been termed the "strain-promoted alkyne-azide cycloaddition" (SPAAC) (**Scheme 1.7**), and has shown to be highly chemoselective and biocompatible, proceeds efficiently at ambient temperature and exhibits rapid reaction kinetics compared to other classes of click reactions. For these reasons, this metal-free cycloaddition reaction has found widespread utility in biological applications such as *in vivo* chromophoric labelling of protein glycans and lipids, protein and oligonucleotide modification and tissue reengineering.[40]

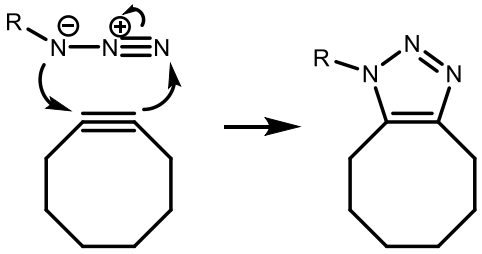

Scheme 1.7: Strain-promoted alkyne-azide cycloaddition reaction occurring through concerted mechanism.

1.6 Photoluminescence

Photoluminescence involves the absorption of energy by a material followed by the emission of light. Excitation of a molecule can subsequently lead to 2 major relaxation pathways termed fluorescence and phosphorescence. Fluorescence is generally fast (nanosecond time scale) while phosphorescence is slow (longer time scale, up to days). Fluorescence occurs when a chemical species absorbs a photon and is excited to a singlet electronic excited state, relaxes to the lowest excited state, and then the excited electron transitions back to the ground state emitting a lower-energy photon than the photon initially absorbed. Refer to the coloured arrows in **Fig 1.4** through this section. Just like fluorescence, in phosphorescence a molecule is excited into a singlet electronic state. Subsequently, the singlet state couples to a triplet electronic excited state via a process called intersystem crossing followed by transition from the excited triplet state to a singlet ground state emitting a photon of lower-energy. Alternatively, the molecule can also relax back to the ground state by non-radiative mechanisms. [41]

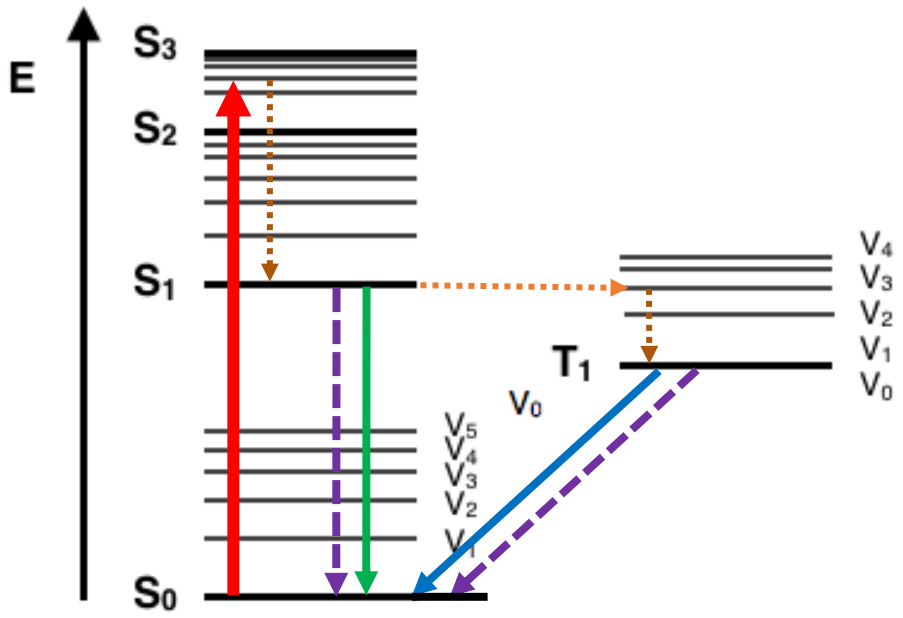

Fig 1.4: Jablonski diagram depicting absorbance (red), vibrational relaxation and internal conversion (brown), intersystem crossing (orange), and non-radiative relaxation (purple), fluorescence (green) and phosphorescence (blue) relaxation pathways**.**

Photoluminescence of NHC-coinage metal complexes are less investigated than other coinage metal complexes.[42,43] While there are several studies on the photoluminescence of NHC–Ag and NHC–Au complexes, reports on NHC–Cu are virtually non-existent. In many cases the attached ligand or metal–metal interaction can result in very interesting electronic properties allowing for the possibility of applications as luminescent chemosensors or optoelectronic on/off switches.[43] Typically, the emissive properties of these complexes are strongly dictated by the nature of the ligand (X = thiolates, carboxylates, *etc*.) and the NHC. In the cases where molecular aggregation due to metal interactions occur, such as aurophilic interactions, a featureless band

appears corresponding to a metal centered (MC) transition. Thus, [(NHC)MX] (X = monoanionic ligand) complexes typically display dual emissions arising from the NHC and X.[44]

1.7 Silver Chalcogenide Nanoclusters

Nanostructured metal clusters (NCs) consist of a metal core surrounded by a protecting shell of organic ligands. They can form isolable particles ranging typically between 1 – 10 nm in size. The particles are well-defined structures with discrete size distributions.[45] NCs have been characterized by NMR, UV-Vis spectroscopy, mass spectrometry, electrochemistry, and X-ray crystallography. Noble metals have a high affinity for chalcogen atoms and thus noble metals bonded to thiolate ligands (M–SR where M = Ag or Au) are very stable against degradation in both the solution and solid state.[46] Thus noble metal thiolate-protected nanoclusters are an attractive target in the creation of stable highly functional nanomaterials in a range of fields including catalysis, biosensing, photochemistry, drug delivery and medical therapy.[47]

With the advancements in reaction methods and development of better and more efficient reagents, metal chalcogenide clusters have become a well-documented area of NC research. Fenske *et al*. have studied and crystallographically characterized an extensive library metal chalcogenide clusters containing a silver sulfide core, surrounded by a protecting shell of thiolate ligands and $[Ag_{490}S_{188}(S^tC_5H_{11})_{114}$ is the largest silver sulfide cluster reported to date.[48] The nanocluster (**Fig 1.5**) features an Ag_2S core size of 2.5 nm and is protected by a shell of silver *tert*-butylthiolate moiety. The $AgS^tC_5H_{11}$ was solubilized using a bidendate phosphine ancillary ligand, namely 1,10-bis(diphenylphosphinomethyl) benzophenanthrene (dppdb).

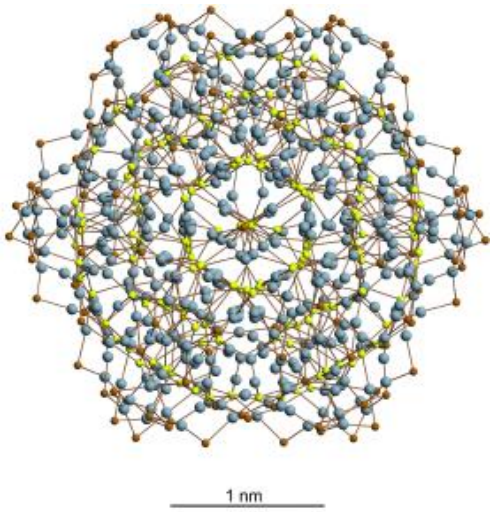

Fig 1.5: Crystal structure of largest reported Ag_2S cluster, $[Ag_{490}S_{188}(SC_5H_{11})_{114}$.[48]

The surfaces of these are protected by ligands thus preventing the formation of the thermodynamically stable binary silver chalcogenide salts. These clusters can be formed reproducibly at room temperature, whereas higher temperatures favour the formation of amorphous Ag_2S. The preparation of these nanometer sized metal-chalcogenide clusters involves the reaction of carbene or phosphine stabilized silver thiolates L-Ag-SR with silylated reagents, [49] of the type $E(SiMe_3)_2$ where E = S, Se as shown in **equation 1.1**.

$$xLAgSR + yE(SiMe_3)_2 \rightarrow L_xAg_xE_y(SR)_{x-z} + zRSSiMe_3 \quad (1.1)$$

Silylated chalcogen reagents offer a facile approach to the introduction of these chalcogenide functionalities onto the surface of nanoclusters. These reagents provide a soluble source of chalcogen under mild reaction conditions, which makes them an attractive chalcogen delivery agent. The silane byproduct, $RSSiMe_3$, in **equation 1.1** is soluble in common organic solvents and does not interfere with the crystallization process. It is speculated that the steric effects

of the ligands along with the unique synergism of the metal, nature of the ligand and solvent environment are responsible for the selection of the thermodynamically stable cluster size.[50] In the case of Au, various sizes have been reported with the same ligand, whereas Ag clusters have a much more constrained relationship between size and ligand type. DFT calculations indicated that the charge density of the sulfur atom, governed by the nature of the ligand strongly influence the electronic properties of the nanoparticles.

1.8 Project Objectives

The area of coinage metal chalcogenolate chemistry is well-understood owing to the current research progress in the area. The incorporation of functionalities that allows for post-assembly modifications to metal chalcogenolates are highly underdeveloped, however since the primary focus has been towards the development of synthetic methodologies, and investigation of photophysical properties of these metal chalcogenolates. Herein, the synthesis of azide-functionalized benzyl- and propyl-based thiolate ligands and their subsequent reaction with coinage metal salts bearing NHC ancillary ligands of the type [(NHC)MX] is presented. The development of these 'clickable NHC-metal complexes' allows for facile and rapid post-assembly modifications to the structural features on the surface of the metal complex through SPAAC chemistry. These clickable coinage metal complexes have been fully characterized and the photoluminescent properties have been explored and compared to model complexes. Of the thiolate ligands explored, the azide-modified benzyl thiol was chosen as ligand of choice for incorporation into metal thiolate clusters due to several desirable features such as its relative yields, ease-of-handling, and its predisposition to crystallization.

Chapter 2 will discuss the preparation of the novel clickable NHC-metal thiolate complexes of Au, Ag, and Cu. The chapter also details the characterization of these novel azide-modified

complexes by heteronuclear spectroscopy (^{1}H and ^{13}C), elemental analysis, and X-ray crystallography. Following characterization, the azide-modified NHC-metal thiolate complexes are reacted with a strained alkyne, bicylcononynylmethanol (BCN-OH), in order to demonstrate that these complexes are both facile to synthesize and easy to modify via strain-promoted alkyne-azide cycloadditions (SPAAC) reaction.

Chapter 3 highlights the optimized synthetic protocol of the azide-terminated thiol precursors. The precursors are fully characterized by NMR spectroscopy, UV-vis absorption spectroscopy, FT-IR and mass spectrometry.

1.9 References

[1] Rivilla, I.; Gómez-Emeterio, B. P.; Fructos, M. R.; Díaz-Requejo, M. M.; Perez, P. J. *Organometallics.* **2011**, 30, 2855.

[2] Morn-Poladura, R.; Rubio, E.; Gonzalez, J. M. *Angew. Chem. Int. Ed.* **2015**, 54, 3052.

[3] Samantaray, M. K.; Katiyar, V.; Pang, K.; Nanavati, H.; Ghosh, P. *J. Organ. Chem*. **2007**, 692, 1672.

[4] Konetski, D.; Gong, T.; Bowman, C. N. *Langmuir*, **2016**, 32, 8195.

[5] Yam, V. W.; Lee, K. W.; Ko, C. C.; Zhu, N. *J. Am. Chem. Soc.* **2009**, 131, 912.

[6] Lin, J. C. Y.; Huang, R. T. W.; Lee, C. S.; Bhattacharyya, A.; Hwang, W. S.; Lin, I. J. B. *Chem. Rev*. **2009**, 109, 3561.

[7] Hindi, K. M.; Siciliano, T. J.; Durmus, S.; Panzner, M. J.; Medvetz, D. A.; Reddy, D. V.; Hogue, L. A.; Hovis, C. E.; Hilliard, J. K.; Mallet, R.; Tessier, C. A.; Cannon, C. L.; Youngs, W. J. *J. Med. Chem*. **2008**, 51, 1577.

[8] Kascatan-Nebioglu, A.; Panzner, M. J.; Tessier, C. A.; Cannon, C. L.; Youngs, W. J. *Coord. Chem. Rev*. **2007**, 251, 884.

[9] Hickey, J. L.; Ruhayel, R. A.; Barnard, P. J.; Baker, M. V.; Berners-Price, S. J.; Filipovska, A. *J. Am. Chem. Soc.* **2008**, 130**,** 12570.

[10] Ray, S.; Mohan, R.; Singh, J. K.; Samantaray, M. K.; Shaikh, M. M.; Panda, D.; Ghosh, P. *J. Am. Chem. Soc*. **2007**, 129, 15042.

[11] Muskawar, P. N.; Karthikeyan, P.; Aswar, S. A.; Bhagat, P. R.; Senthil Kumar, S. *Arab. J. Chem*. **2016**, 9, 1765.

[12] Wanzlick, H. W.; Schönherr, H. J. *Angew. Chem. Int. Ed.* **1968**, 7**,** 141.

[13] Öfele, K. *Angew. Chem. Int. Ed.* **1968**, 7**,** 950-950.

[14] Arduengo, A. J.; Harlow, R. L.; Kline, M. *J. Am. Chem. Soc.* **1991**, 113**,** 361.

[15] Hopkinson, M. N.; Richter, C.; Schedler, M.; Glorius, F. *Nature*. **2014**, 510, 485.

[16] Poater, A.; Falivene, L.; Urbina-Blanco, C. A.; Manzini, S.; Nolan, S. P.; Cavallo, L. *Dalton Trans.* **2013**, 42, 7433.

[17] Clavier, H.; Nolan, S. P. *Chem. Comm.* **2010**, 46**,** 841.

[18] Jothibasu, R.; Huynh, H. V.; Koh, L. L. *J. Organomet. Chem.* **2008**, 693**,** 374.

[19] Fructos, M. R.; Belderrain, T. R.; Frémont, P.; Scott, N. M.; Nolan, S. P.; Díaz-Requejo, M.; Pérez, P. J. *Angew. Chem. Int. Ed.* **2005**, 117**,** 5418.

[20] Soleilhavoup, M.; Bertrand, G. *Acc. Chem. Res.* **2015**, 48, 256.

[21] Tolman, C. A. et al. *Chem. Rev.* **1977**, 77, 313.

[22] Zhang, L.; Hou, Z. *Chem. Sci.* **2013**, 4**,** 3395.

[23] Boehme, C.; Frenking, G. *Organometallics.* **1998**, 17, 5801.

[24] Nolan, S. P. *Acc. Chem. Res.* **2011**, 44**,** 91.

[25] Fremont, P.; Scott, N. M.; Stevens, E. D.; Nolan, S. P. *Organometallics.* **2005**, 24**,** 2411.

[26] Furst, M. L.; Cazin, C. J. *Chem. Comm.* **2010**, 46**,** 6924.

[27] Collado, A.; Gómez-Suárez, A.; Martin, A. R.; Slawin, A. Z.; Nolan, S. P. *Chem. Comm.* **2013**, 49**,** 5541.

[28] Humenny, W. J.; Mitzinger, S.; Khadka, C. B.; Khalili Najafabadi, B.; Vieira, I.; Corrigan, J. F. *Dalton Trans.* **2012**, 41**,** 4413.

[29] Teo, B. K.; Xu, Y. H.; Deng, Y. J.; Zou, Y. H. *Inorg. Chem.* **2001**, 40**,** 6794.

[30] Su, W.; Cao, R.; Hong, M.; Lu, J. *Inorg. Chem. Comm.* **1999**, 2**,** 241.

[31] Dance, I. G.; Fitzpatrick, L. J.; Craig, D. C.; Scudder, M. L. *Inorg. Chem.* **1989**, 28**,** 1853.

[32] Dance, I. G.; Fisher, K. J.; Banda, R. H.; Scudder, M. L. *Inorg. Chem*. **1991**, 30**,** 183.

[33] Kolb, H. C.; Finn, M. G.; Sharpless, K. B. *Angew. Chem. Int. Ed.* **2001**, 40**,** 2004.

[34] Gobbo, P.; Luo, W.; Cho, S. J.; Wang, X.; Biesinger, M.; Hudson, R. H.; Workentin, M. S. *Org. Biomol. Chem.* **2015**, 13, 4605.

[35] McKay, S.; Finn, M. G. *Chem. Biol.* **2014**, 21**,** 1075.

[36] Huisgen, R. *Angew. Chem. Int. Ed.* **1963**, 2**,** 565.

[37] Zhang, X.; Zhang, Y. *Molecules.* **2013**, 18**,** 7145.

[38] Rostovtsev, V. V.; Green, L. G.; Fokin, V. V.; Sharpless, K. B. *Angew. Chem. Int. Ed.* **2002**, 114**,** 2708.

[39] Agard, N. J.; Prescher, J. A.; Bertozzi, C. R. *J. Am. Chem. Soc.* **2004**, 126**,** 15046.

[40] Mbua, N. E., Guo, J.; Wolfert, M. A.; Boons, G. J. *ChemBioChem.* **2011**, 12**,** 1912.

[41] Parker, C. A. *Elsevier Pub. Co*. **1968**, 243.

[42] Yam, V. W.; Cheng, C. C. *Chem. Soc. Rev.* **2008**, 37**,** 1806.

[43] Omary, M. A.; Mohamed, A. A.; Rawashdeh-Omary, M. A.; Fackler, J. P. *Coord. Chem. Rev.* **2005**, 249**,** 1372.

[44] Yam, V. W.; Ko, C. C.; Zhu, N. *J. Am. Chem. Soc.* **2009**, 131**,** 912.

[45] Gimeno, M. C.; Laguna, A.; Visbal, R. *Organometallics.* **2012**, 31**,** 7146.

[46] Schmid, G.; Baumle, M.; Geerkens, M.; Heim, I.; Sawitowski, T. *Chem. Soc. Rev.* **1999**, 28**,** 179.

[47] Majdalawieh, A.; Kanan, M. C.; El-Kadri, O.; Kanan, S. M. *J. Nanosci. Nanotechnol.* **2014**, 14**,** 47570.

[48] Anson, C. E.; Eichhöfer, A.; Issac, I.; Fenske, D.; Fuhr, O.; Sevillano, P.; Persau, C.; Zhang, J. *Angew. Chem. Int. Ed.* **2008**, 47**,** 1326.

[49] So, J. H.; Boudjouk, P. *Synthesis.* **1989,** 306.

[50] Joshi, C. P.; Bootharaju, M. S.; Bakr, O. M. *J. Phys. Chem. Lett.*, **2015**, 6, 3023.

2. Synthesis of Azide Functionalized Coinage Metal (Cu, Ag, and Au) Complexes

Group 11 metals (Cu, Ag, and Au) traditionally known as coinage metals, can combine with various anionic or neutral ligands to form coordination compounds that have intriguing spectroscopic and optoelectronic properties.[1] There have been a handful of studies on small coinage metal complexes bearing thiolates and N-heterocyclic carbenes (NHC's) or phosphines as ancillary ligands which reveal rich photophysical properties.[2] These thiolates can adopt various nuclearities and coordination geometries as a result of the steric and electronic properties of the ligands.[3] The modification of the thiolate ligand, through the introduction of an azide functional group, makes the complex amenable to strain-promoted alkyne-azide cycloaddition (SPAAC) reactions.

In this chapter, the synthesis and characterization of azide-modified NHC metal thiolate complexes [(^{i}Pr$_2$-bimy)Au-1-SCH$_2$-2,5-(CH$_3$)$_2$Ph-4-CH$_2$N$_3$] (**1**), [(IPr)Au-1-SCH$_2$-2,5-(CH$_3$)$_2$Ph-4-CH$_2$N$_3$] (**2**), [(IPr)Ag-1-SCH$_2$-2,5-(CH$_3$)$_2$Ph-4-CH$_2$N$_3$] (**3**) and [(IPr)Cu-1-SCH$_2$-2,5-(CH$_3$)$_2$Ph-4-CH$_2$N$_3$] (**4**) are presented (R = {CH$_2$Ph(CH$_3$)$_2$CH$_2$N$_3$}, ^{i}Pr$_2$-bimy =1,3-di-isopropylbenzimidazol-2-ylidene, IPr = 1,3-bis(2,6-di-iso-propylphenyl)imidazol-2-ylidene). The azide-modified NHC metal thiolates were synthesized according to previously established methodologies for coinage metal thiolates.[2,4] Having successfully prepared these novel coinage metal complexes, they were characterized by heteronuclear spectroscopy, elemental analysis and X-ray crystallography. Subsequent to their synthesis and characterization, the SPAAC reactivity of the NHC gold complex, **2** was demonstrated through reaction between equimolar quantities of the complex and bicyclononynylmethanol (BCN-OH), which is a stable cyclooctyne that is easy

to synthesize and handle. This cycloadduct, **5** was characterized by heteronuclear spectroscopy, and the rate of its formation was determined through a ^{1}H NMR kinetic study which followed the SPAAC reaction under second-order conditions. See Chapter 3 for the optimized synthetic protocols and characterization of the novel azide terminated thiolate ligand precursors, 1-$SHCH_2$-2,5-$(CH_3)_2$-4-N_3CH_2-C_6H_2 (**6**) and 1-$SSi(CH_3)_3CH_2$-2,5-$(CH_3)_2$-4-N_3CH_2-C_6H_2 (**7**) used herein to generate complexes **1-4**. Finally, the photoluminescent properties of the complexes were probed.

2.1 Experimental

2.1.1. General Synthetic Techniques and Starting Materials

The reactions were performed using standard Schlenk techniques under a dry nitrogen atmosphere unless specified otherwise. Non-chlorinated solvents (tetrahydrofuran (THF), toluene, pentane, hexane, heptane, and diethyl ether) were dried by passage through packed columns of activated alumina using an MBraun MBSP Series solvent purification system. Chlorinated solvents ($CHCl_3$, and CH_2Cl_2) were distilled and dried over P_2O_5. Trimethylsilyl chloride (TMSCl) was distilled and dried over P_2O_5. Triethylamine was purchased from Aldrich and dried over CaH_2. Chemicals were used as received from Aldrich and/or VWR. Chloroform-*d* and dichloromethane-d_2 were purchased from Aldrich and distilled over P_2O_5. [($^{i}Pr_2$-bimy)AuCl] ($^{i}Pr_2$-bimy = 1,3-diisopropylbenzimidazolin-2-ylidene), [(IPr)AuCl], [(IPr)AgOAc], and [(IPr)CuCl] (IPr = 1,3-bis(2,6-diisopropylphenyl)imidazol-2-ylidene were prepared according to literature procedures.[5] ^{1}H, $^{13}C\{^{1}H\}$, and $^{31}P\{^{1}H\}$ NMR spectra were recorded on Varian Mercury 400 MHz, and Inova 400 MHz spectrometers and the chemical shifts (δ) were internally referenced by the residual solvent signals (chloroform-*d* and dichloromethane-d_2) to tetramethylsilane ($SiMe_4$) (^{1}H and $^{13}C\{^{1}H\}$) or 85% H_3PO_4 ($^{31}P\{^{1}H\}$). For single crystal X-ray analysis, the crystals were mounted

on a Mitegen polyimide micromount with a small amount of Paratone N Oil. All X-ray measurements were made on a Bruker Kappa Axis Apex2 diffractometer at a temperature of 110 K. The data collection strategies were a number of ω and φ scans. The frame integration was performed using SAINT.[6] The resulting raw data was scaled and absorption corrected using a multi-scan averaging of symmetry equivalent data using SADABS.[7] The structure was solved by using a dual space methodology using the SHELXT program.[8] All non-hydrogen atoms were obtained from the initial solution. The hydrogen atoms were introduced at idealized positions and were allowed to ride on the parent atom. The calculated structure factors included corrections for anomalous dispersion from the usual tabulation. The structure was refined using the SHELXL-2014 program from the SHELXTL suite of crystallographic software.[9] Graphic plots were produced using the NRCVAX program suite.[10] The structures were solved and refined by Dr. John Corrigan. Mass spectra and exact mass determinations were performed on a Bruker micrOTOF II instrument or Finningan MAT 8400. Elemental analysis was performed by Laboratoire d'Analyse Élémentaire de l'Université de Montréal, Montréal, Canada.

2.1.2 [(^{i}Pr$_2$-bimy)Au-1-SCH$_2$-2,5-(CH$_3$)$_2$Ph-4-CH$_2$N$_3$] (1)

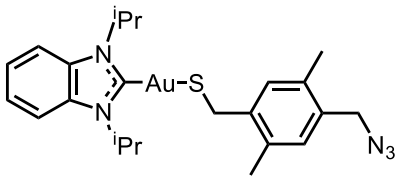

To [(^{i}Pr$_2$bimy)AuCl] (0.10 g, 0.16 mmol) in 10 mL of THF was added a solution of the azide terminated thiol, **6** (0.040 g, 0.19 mmol) in 5 mL of THF. (Synthesis of **6** discussed in chapter 3). To the solution was added NEt$_3$ (40 µL, 0.32 mmol) dropwise. The reaction was stirred at room temperature over 18 h. The solvent was evaporated under vacuum and re-dissolved in 8 mL of toluene. The white solid was filtered off by pipetting solution through glass wool and the supernatant was concentrated to ~2 mL *in vacuo* and layered with 8 mL of pentane to obtain as

colourless needles in 74 % yield (0.072 g). ^{1}H NMR (400 MHz, $CDCl_3$): δ = 7.53 (m, 2H, $Ar_{carbene}$-*H*), 7.26 (m, 2H, $Ar_{carbene}$-*H*), 7.19 (s, 1H, Ar-*H*), 6.91 (s, 1H, Ar-*H*), 5.30 (m, 2H, $(CH_3)_2CH$), 5.22 (br s, 2H, $(CH_3)_2CH$), 4.19 (s, 2H, CH_2N_3), 4.02 (s, 2H, CH_2SAu), 2.43 (s, 3H, Ar-CH_3), 2.21 (s, 3H, Ar-CH_3), 1.59 (d, 12H, $^{3}J_{HH}$ = 8Hz, $(CH_3)_2CH$). $^{13}C\{^{1}H\}$ NMR (150 MHz, $CDCl_3$): δ = 190.3, 145.2, 134.2, 133.3, 132.7, 131.8, 131.5, 130.8, 123.7, 113.16, 53.8, 53.6, 53.2, 29.5, 21.8, 19.4, 18.7. m.p. 142-146 ºC. Anal. Calcd. for $C_{23}H_{30}AuN_5S$: N, 11.56; C, 45.63; H, 4.99; S, 5.28. Found N, 11.27; C, 45.78; H, 5.00; S, 4.80. UV-Vis (CH_2Cl_2): λ_{max} = 284 nm (ε = 21,100 $M^{-1}cm^{-1}$), 292 nm (20,700 $M^{-1}cm^{-1}$), 318 nm (17,500 $M^{-1}cm^{-1}$).

2.1.3 [(IPr)Au-1-SCH_2-2,5-$(CH_3)_2$Ph-4-CH_2N_3] (2)

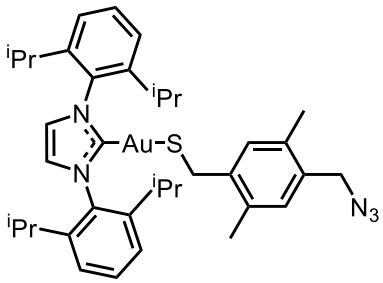

Method 1a: To a 10 mL suspension of NaH (0.0050 g, 0.21 mmol) in THF was added 0.075 g of **6** (40 mg, 0.19 mmol) in 5 mL of THF. The reaction was left to stir over 5 h. A 5 mL solution of [(IPr)AuCl] (0.12 g, 0.19 mmol) in THF was added to the reaction mixture and stirred for 18 h at room temperature. The THF solvent was evaporated under vacuum, and 10 mL of toluene was added. The white solid (NaCl) was filtered off by pipetting solution through glass wool and the supernatant was concentrated to ~2 mL *in vacuo* and layered with 8 mL of pentane to obtain as colourless plates in 72 % yield (0.10 g).

Method 1b: To [(IPr)AuCl] (0.10 g, 0.16 mmol) in 10 mL of THF was added a solution of **6** (0.040 g, 0.19 mmol) in 5 mL of THF. To the solution was added NEt_3 (42 µL, 0.32 mmol) dropwise. The reaction was stirred at room temperature over 18 h. The solvent was evaporated under vacuum and re-dissolved in 8 mL of toluene. The white solid (Et_3NHCl) was filtered off by pipetting solution through glass wool and the supernatant was concentrated to ~2 mL *in vacuo* and layered

with 8 mL of pentane to obtain as colourless needles in 77 % yield (0.097 g). ^{1}H NMR (400 MHz, $CDCl_3$): δ = 7.49 (t, 2H, $^{3}J_{HH}$ = 8 Hz, (^{i}Pr)$_2$Ar-*H*), 7.28 (d, 4H, $^{3}J_{HH}$ = 8 Hz, (^{i}Pr)$_2$Ar-*H*), 7.15 (s, 2H, HC=C*H*), 6.91 (s, 1H, Ar-*H*), 6.83 (s, 1H, Ar-*H*), 4.19 (s, 2H, CH_2N$_3$), 3.50 (s, 2H, CH_2SAu), 2.60 (sept, 4H, $^{3}J_{HH}$ = 7 Hz, (CH$_3$)$_2$C*H*), 2.19 (s, 3H, Ar-CH_3), 2.06 (s, 3H, Ar-CH_3), 1.34 (d, 12H, $^{3}J_{HH}$ = 8 Hz, (CH_3)$_2$CH), 1.22 (d, 12H, $^{3}J_{HH}$ = 8 Hz, (CH_3)$_2$CH). ^{13}C{^{1}H} NMR (150 MHz, $CDCl_3$): δ = 187.5, 145.9, 144.0, 134.5, 133.8, 133.3, 131.2, 130.6, 130.3, 129.2, 128.4, 124.2, 122.9, 53.2, 34.3, 28.9, 28.6, 27.7, 24.6, 24.2, 22.5, 18.8, 18.6, 14.2. m.p. 180 – 184 ºC. Anal. Calcd for $C_{37}H_{48}AuN_5S$: N, 8.84; C, 56.13; H, 6.11; S, 4.04. Found N, 8.13; C, 55.70; H, 6.42; S, 3.58. UV-Vis (CH_2Cl_2): λ_{max} = 286 nm (ε = 23,000 $M^{-1}cm^{-1}$), 291 nm (22,400 $M^{-1}cm^{-1}$), 300 nm (20,400 $M^{-1}cm^{-1}$).

2.1.4 [(IPr)Ag-1-SCH$_2$-2,5-(CH$_3$)$_2$Ph-4-CH$_2$N$_3$] (3)

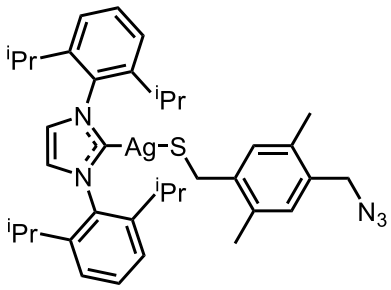

To a 6 mL solution of [(IPr)AgOAc] (0.10 g, 0.1 mmol) in THF was added azide terminated benzyl trimethylsilylsulfide, **7** (0.061 g, 0.22 mmol) in 6 mL of THF. (Synthesis of **7** is discussed in chapter 3.) The reaction was stirred for 5 h at room temperature after which the solvent was removed under vacuum. The white solid was re-dissolved in 4 mL of toluene and layered with 10 mL of pentane to get colourless rods in 68 % yield (0.048 g). ^{1}H NMR (400 MHz, $CDCl_3$): δ = 7.49 (t, 2H, $^{3}J_{HH}$ = 8 Hz, (^{i}Pr)$_2$Ar-*H*), 7.29 (d, 4H, $^{3}J_{HH}$ = 8 Hz, (^{i}Pr)$_2$Ar-*H*), 7.13 (s, 2H, HC=C*H*), 7.11 (s, 1H, Ar-*H*), 7.03 (s, 1H, Ar-*H*), 4.29 (s, 2H, CH_2N$_3$), 3.67 (s, 2H, CH_2SAg), 2.57 (sept, 4H, $^{3}J_{HH}$ = 7 Hz, (CH$_3$)$_2$C*H*), 2.37 (s, 3H, Ar-CH_3), 2.30 (s, 3H, Ar-CH_3), 1.30 (d, 12H, $^{3}J_{HH}$ = 8 Hz, (CH_3)$_2$CH), 1.23 (d, 12H, $^{3}J_{HH}$ = 8 Hz, (CH_3)$_2$CH). ^{13}C{^{1}H} NMR (150 MHz, $CDCl_3$): δ = 145.8, 145.3, 138.0, 134.9, 131.6, 131.26, 131.0, 130.7, 129.2,

128.4, 125.4, 124.3, 53.2, 28.9, 28.7, 27.7, 24.9, 24.7, 24.1, 21.6, 18.7. m.p. 174 – 179 ºC. UV-Vis (CH_2Cl_2): λ_{max} = 286 nm (ε = 23,600 $M^{-1}cm^{-1}$), 290 nm (22,900 $M^{-1}cm^{-1}$), 300 nm (20,700 $M^{-1}cm^{-1}$).

2.1.5 [(IPr)Cu-1-SCH$_2$-2,5-(CH$_3$)$_2$Ph-4-CH$_2$N$_3$] (4)

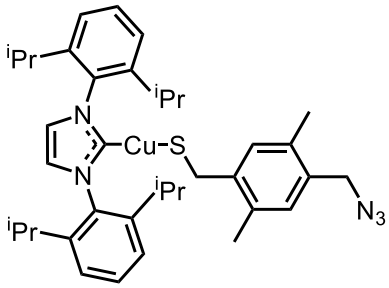

To a 6 mL solution of [(IPr)CuCl] (0.13 g, 0.25 mmol) in THF was added **7** (0.085 g, 0.30 mmol) in 6 mL of THF. The reaction was stirred for 5 h at room temperature after which the solvent was removed under vacuum. The yellow-white solid was re-dissolved in 4 mL of toluene and layered with 10 mL of pentane to obtain colourless plates in 65 % yield (0.10 g). ^{1}H NMR (400 MHz, $CDCl_3$): δ = 7.48 (t, 2H, $^3J_{HH}$ = 8 Hz, (^{i}Pr)$_2$Ar-*H*), 7.29 (d, 4H, $^3J_{HH}$ = 8 Hz, (^{i}Pr)$_2$Ar-*H*), 7.13 (s, 2H, HC=C*H*), 6.88 (s, 1H, Ar-*H*), 6.81 (s, 1H, Ar-*H*), 4.18 (s, 2H, C*H*$_2$N$_3$), 3.17 (s, 2H, C*H*$_2$SCu), 2.61 (sept, 4H, $^3J_{HH}$ = 7 Hz, (CH$_3$)$_2$C*H*), 2.19 (s, 3H, Ar-C*H*$_3$), 2.07 (s, 3H, Ar-C*H*$_3$), 1.32 (d, 12H, $^3J_{HH}$ = 8 Hz, (C*H*$_3$)$_2$CH), 1.23 (d, 12H, $^3J_{HH}$ = 8 Hz, (C*H*$_3$)$_2$CH). ^{13}C{^{1}H} NMR (150 MHz, $CDCl_3$): δ = 179.2, 145.9, 145.1, 134.8, 133.7, 131.2, 131.1, 130.6, 129.2, 128.4, 125.44, 124.3, 122.9, 53.2, 29.3, 29.1, 28.9, 24.6, 24.2, 22.5, 18.8, 18.6, 14.2. m.p. 174 – 178 ºC. Anal. Calcd for $C_{37}H_{48}CuN_5S$: N, 10.64; C, 67.49; H, 7.35; S, 4.87. Found. N, 10.62; C, 67.01; H, 7.49; S, 5.34. UV-Vis (CH_2Cl_2): λ_{max} = 285 nm (ε = 22,200 $M^{-1}cm^{-1}$), 289 nm (21,500 $M^{-1}cm^{-1}$), 302 nm (18,000 $M^{-1}cm^{-1}$).

2.1.6 Cycloadduct of 2 and BCN_{exo}-OH (5)

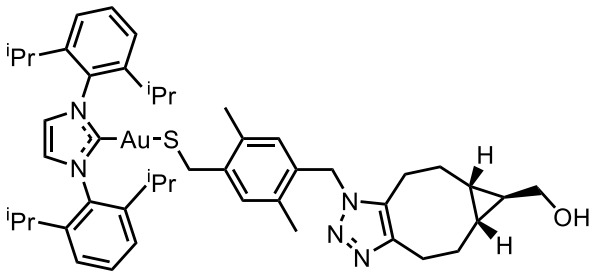

To a 5 mL solution of **2** (0.064 g, 0.080 mmol) in CH_2Cl_2 was added BCN-OH (0.016 g, 0.11 mmol) and left to stir at room temperature for 12 h. The solvent was removed under vacuum. The white solid was washed with 5 × 5 mL of Et_2O and re-dissolved in 3 mL of THF and a few drops of heptane to obtain the white solid in 76 % yield (0.057 g). ^{1}H NMR (400 MHz, CD_2Cl_2): δ = 7.54 (t, 2H, $^3J_{HH}$ = 8 Hz, (^{i}Pr)$_2$Ar-*H*), 7.34 (d, 4H, $^3J_{HH}$ = 8 Hz, (^{i}Pr)$_2$Ar-*H*), 7.23 (s, 2H, HC=C*H*), 6.83 (s, 1H, Ar-*H*), 6.19 (s, 1H, Ar-*H*), 5.31 (s, 2H, CH_2N$_3$), 3.43 (s, 2H, CH_2SAu), 3.43 (m, 4H, $^3J_{HH}$ = 7 Hz), 3.03 (m, 1H), 2.87 (m, 1H), 2.68 (m, 1H), 2.61 (sept, 4H, $^3J_{HH}$ = 7 Hz, (CH$_3$)$_2$C*H*), 2.50 (m, 1H), 2.38 (1H, m), 2.21 (s, 3H, Ar-CH_3), 1.92 (s, 3H, Ar-CH_3), 1.80 (br s, 1H), 1.34 (d, 12H, $^3J_{HH}$ = 8 Hz, (CH_3)$_2$CH), 1.24 (d, 12H, $^3J_{HH}$ = 8 Hz, (CH_3)$_2$CH), 1.17 (t, 3H, $^3J_{HH}$ = 7 Hz), 0.77 (m, 1H), 0.65 (m, 1H). ^{13}C{^{1}H} NMR (150 MHz, CD_2Cl_2): δ = 187.4, 146.2, 145.3, 134.7, 134.0, 133.9, 132.6, 131.2, 131.0, 130.8, 128.3, 124.5, 123.4, 66.53, 66.04, 49.89, 29.14, 28.55, 28.18, 27.60, 26.63, 26.08, 24.53, 24.09, 23.24, 22.44, 22.15, 18.83, 18.77, 15.48. m.p. 93 – 97 ºC. HRMS (ESI): Calc. [M] 1035.5123 found 1035.5124.

2.1.7 Photophysical studies

Solution-state UV-Vis absorption spectra were acquired with a Varian Cary 300 Bio Spectrophotometer (for solution-state measurements) and Varian Cary 5000 (for solid-state measurements). 10^{-5} M solutions of the complexes **1**-**4** and [(IPr)AuCl], and thiol (**6**) were prepared in spectroscopic grade CH_2Cl_2. For solution state measurements, a 1 cm quartz cuvette was used. For solid state measurements, samples were dissolved in trichlorobenzene, and then spin-coated

onto quartz slides. The solvent and background were subtracted from each spectrum. Steady-state excitation and emission spectra were collected on a QuantaMaster Luminescence Fluorimeter (Photon Technology International) at room temperature using a 1 cm quartz cuvette. 10^{-6} M solutions of the complexes **1-4** and [(IPr)AuCl], and thiol (**6**) were prepared in spectroscopic grade CH_2Cl_2. The solid-state samples were prepared by dissolving the samples in trichlorobenzene and spin-coating onto a quartz slide.

2.2 Results and Discussion

2.2.1 Synthesis

The synthesis of azide-terminated ligand to the NHC-terminated gold thiolate in **1** and **2** involves the deprotonation of –SH group of **6**, followed by reaction with either [(^{i}Pr$_2$bimy)AuCl] (to give **1**) or [(IPr)AuCl] (to give **2**) in the presence of a base, where the chloride is replaced by the thiolate ligand (**Scheme 2.1**). For the synthesis of **2** in method 1a, the thiolate ligand was formed by deprotonating the thiol with sodium hydride. Following subsequent reaction with the [(NHC)AuCl], the salt by-product NaCl was filtered off and colourless plates of **2** were obtained in 72 % yield after crystallization from 1:4 toluene:pentane. In method 1b, which was used for the synthesis of both **1** and **2**, the thiolate is formed by conducting the reaction of the thiol and [(NHC)AuCl] in the presence of a mild base such as triethylamine. Following filtration of $NEt_3 \cdot HCl$, the purification step involved crystallization out of 1:4 toluene:pentane. The reaction gave rise to **1** and **2** in the form of white crystals in 74 % and 77 % yield, respectively. The complexes characterized by ^{1}H NMR spectroscopy and X-ray crystallography.

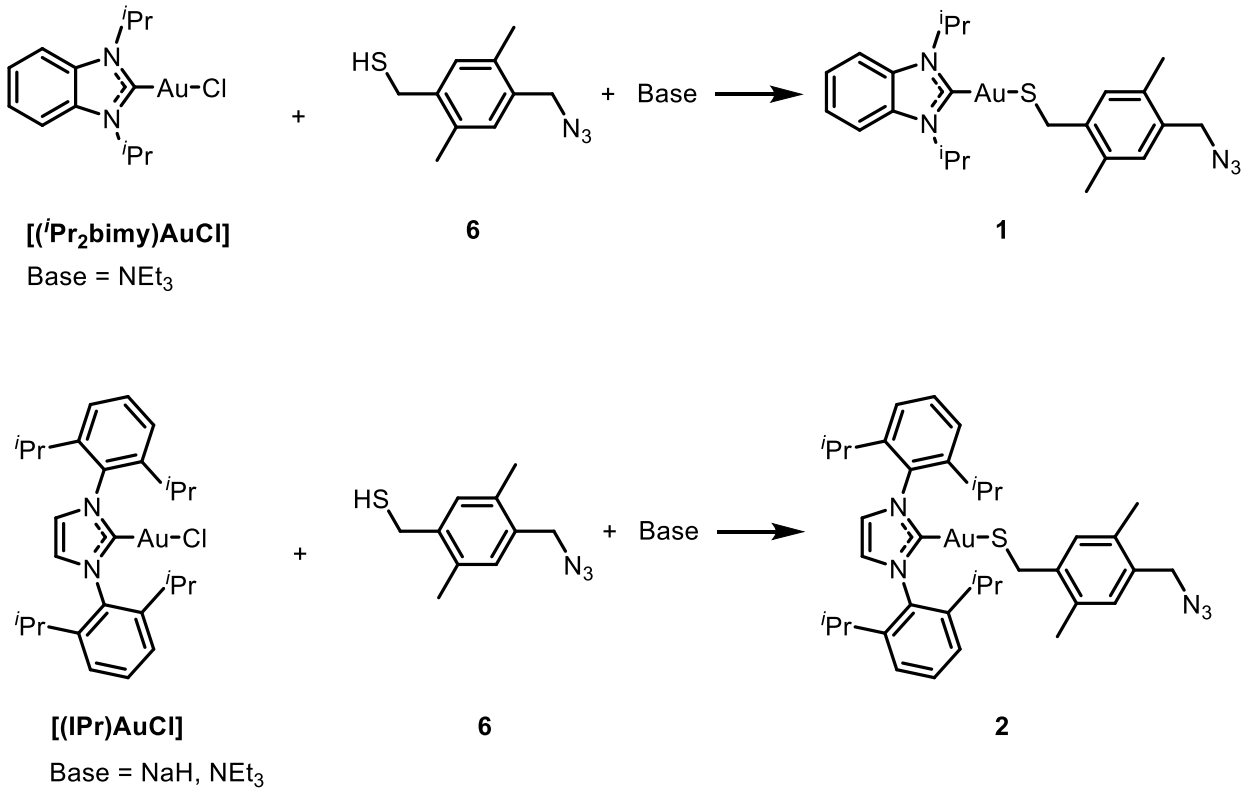

Scheme 2.1: Reaction of [(^{i}Pr$_2$bimy)AuCl] and [(IPr)AuCl] with **6** and a base (either NaH or NEt_3).

The Ag congener containing a relatively small NHC, [(^{n}Bu$_2$)bimy)AgBr], was treated with **6** in the presence of NEt_3 which lead to the formation of a suspension and the reaction was tracked by ^{1}H NMR spectroscopy (**Fig 2.1**). Unlike the previous examples, instead of a terminally bound thiolate, a cyclic structure, where the Ag atoms are bridged by thiolates was expected due to the nature of the metal and the relatively smaller NHC whose sterics and electronics are comparable to ^{i}Pr$_2$-bimy.[2] The product was filtered and a ^{1}H NMR spectrum was acquired of the filtrate. A resonance was observed at 11.24 ppm, which corresponds to protonated carbene suggesting that the thiolate sources **6**, and **7** were too nucleophilic as they regenerated the protonated NHC.

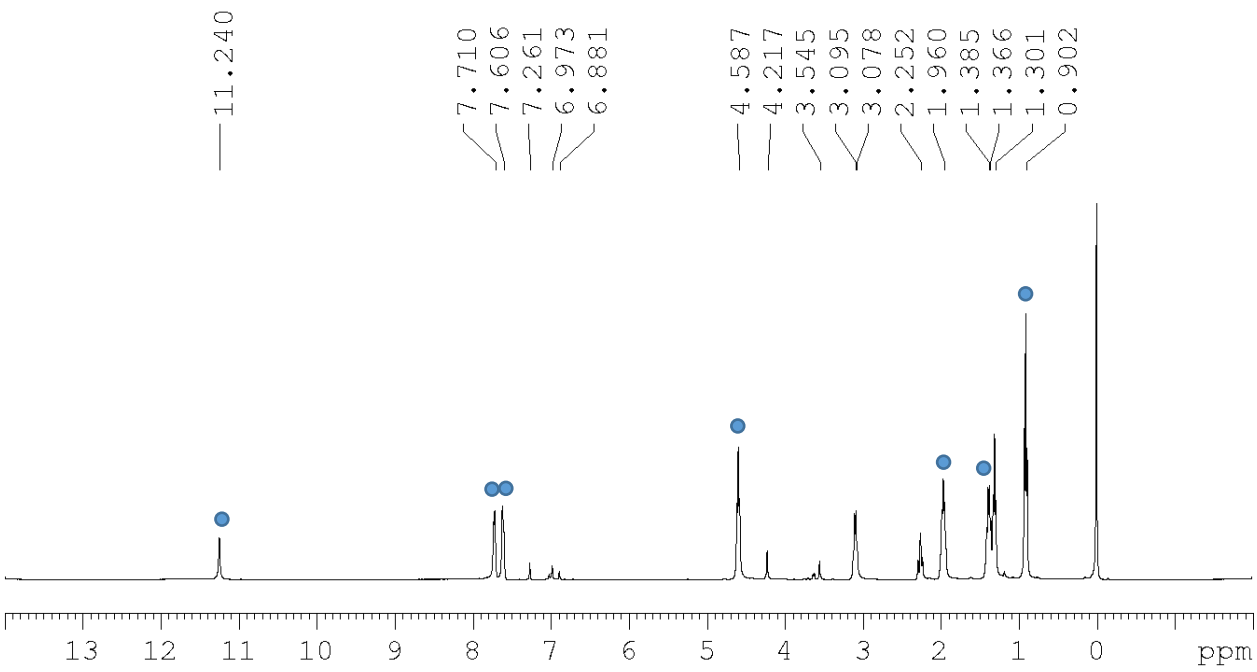

Fig 2.1: ^{1}H NMR spectrum of the reaction of [(^{n}Bu$_2$bimy)AgBr] with **6** in THF. Imidazolium salt that was regenerated indicated by (●).

The solid from the suspension was found to insoluble in common organic solvents (THF, toluene, CH_2Cl_2, CH_3CN and DMF). It was speculated that the insoluble material was a silver-thiolate coordination polymer.[11] This was further confirmed by the fact that the ratio of ligand: carbene was 1:10 in the filtrate, indicating that most of the ligand was part of the insoluble material that had formed from the reaction. This result suggested that the carbene was protonated and the resultant thiolate was reacting with silver salt to form a silver thiolate polymer shown in **Fig 2.2**. These results demonstrated the known lability of the $C_{carbene}$–Ag bond, and the tendency of Ag to adopt higher coordination modes when reacting with relatively smaller NHCs,[12] which was not observed in the Au congener.

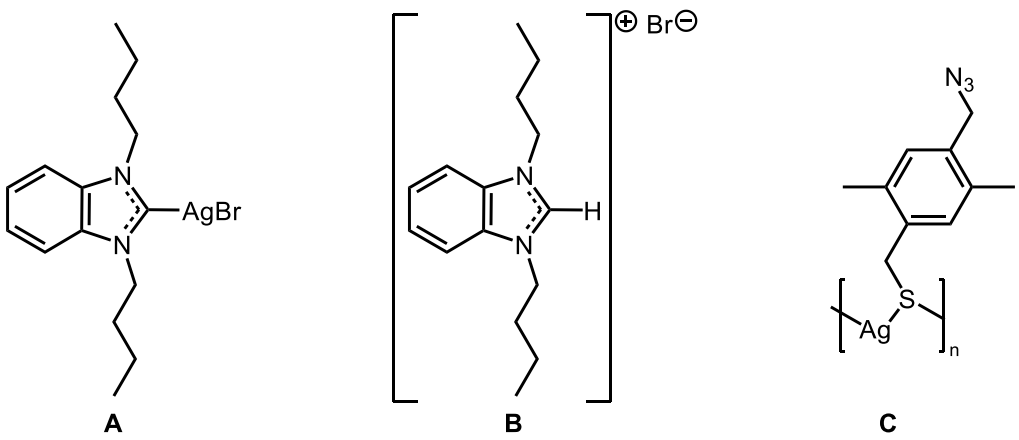

Fig. 2.2: (A) [(^{n}Bu$_2$bimy)AgBr] (B) Protonated carbene: [(^{n}Bu$_2$bimy)HBr] (C) Coordination polymer.

Due to the high nucleophilicity of the thiolate sources used, an alternate approach was taken for the introduction of the azide-terminated ligand. It has been demonstrated that the Ag–OAc bond can be cleaved by trimethylsilyl halide reagents to form complexes of the type [(IPr)AgX] (**Scheme 2.2**).[2,3] It was confirmed by NMR spectroscopy and X-ray crystallography that treatment of the NHC terminated AgOAc salt with **7** yielded **3**. This method was also repeated for the synthesis of the analogous Cu complex, **4** using [(IPr)CuOAc]. The yellow oily solid obtained from the reaction was purified by crystallization from a 2:5 mixture of toluene:pentane to get colourless plates and **3** and **4** were obtained in comparable yields (68 % and 65 % yields, respectively).

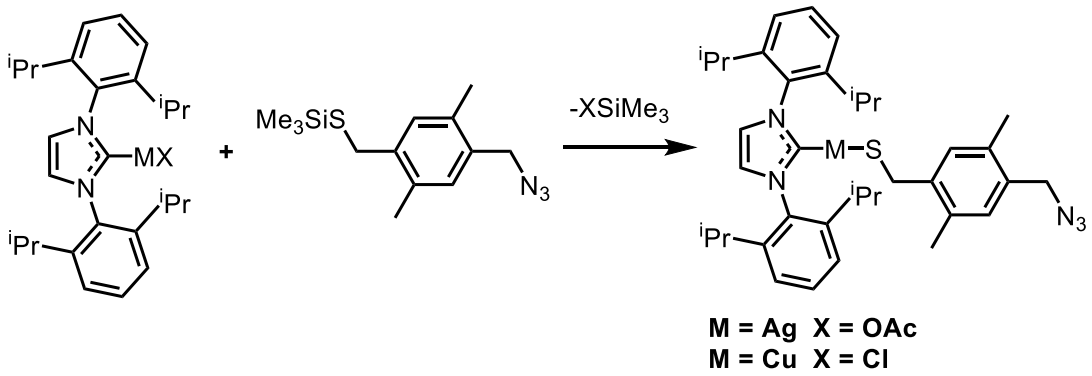

Scheme 2.2: Treatment of [(IPr)MX] with trimethylsilyl halide reagents.

2.2.2 NMR Spectroscopy

The four complexes were characterized by NMR spectroscopy. As depicted in **Fig. 2.3**, the ^{1}H NMR spectra exhibit resonances consistent with the structure of each of the coinage-metal complexes **2, 3**, and **4**. Expectedly, the resonances from the methylene protons alpha to the azide were unaffected by coordination to any of the metals (orange dot, **Fig 2.3**). However, there is a notable change to the resonances corresponding to the methylene protons alpha to the sulfur of the thiolate functionality (blue dot, **Fig 2.3**) in the Cu, Au and Ag complexes, which appeared at 3.17, 3.50 and 3.67 ppm respectively. The deshielding effect of the π component of the metal thus follows the order: Cu(I) > Au(I) > Ag(I), which is also expected given the trend in the ionization potentials of these ions [Cu(I), 20.29 eV; Au(I), 20.50 eV; Ag(I) 21.49 eV].[13] Additionally, the doublet corresponding to the methylene group adjacent to the thiol becomes a singlet upon coordination to the metal centre. For these reasons, the position of these methylene protons in the ^{1}H NMR spectrum is indicative of the coinage metal to which the thiolate is bonded.

In the case of the CH_3-Ar protons (red dot, **Fig 2.3**) and the H-Ar (purple dot, **Fig 2.3**) closest in proximity to the thiolate functionality, it was found that the resonances for these protons in **3** (2.30 and 7.03 ppm) had significantly higher frequencies than the same protons in **2** (2.06 and

6.83 ppm) and **4** (2.07 and 6.81 ppm). These proton resonances appear to be shifted downfield in **3** relative to **2** and **4**, indicating that they are in a more deshielded environment, which as with methylene protons alpha to the thiolate, provides information on the electronic nature of the thiolate-silver bond in comparison the thiolate-copper and thiolate-gold bond. Interestingly, there was also a small downfield shift for CH_3-Ar protons (grey dot, **Fig 2.3**) and the H-Ar protons (green dot, **Fig 2.3**) closest to the azide moiety in **3** (2.37 and 7.11 ppm), compared to those seen in **4** (2.19, and 6.88 ppm) and **2** (2.19 and 6.91 ppm).

The resonance from the methylene alpha to the azide in the $^{13}C\{^1H\}$ NMR spectra of **2**, **3** and **4** is unaffected by metal coordination (53.2 ppm in all three complexes), (**see Section 2.1**) which is consistent with the ^1H NMR data indicating that the electronic influence of each of the three different metals has no effect on the electronic nature of the azide functionality. The $^{13}C\{^1H\}$ spectra for **2** and **4** exhibit a prototypical downfield resonance for the carbene carbon atom ($C_{carbene}$) at 187.5 ppm for **2**, and 179.2 ppm for **4**.[15] There were no observable resonances that could be assigned to the $C_{carbene}$ resonance of the Ag complex, which has been reported previously for complexes of this type. The resonance values corresponding to the central carbon of the NCN moiety of the carbene in NHC-Ag complexes fall over a wide range 163.2 – 213.7 ppm.[3,4] This resonance was not observed because of the broadening of the signal as a result of coupling to the two isotopes of Ag (^{107}Ag and ^{109}Ag).[16]

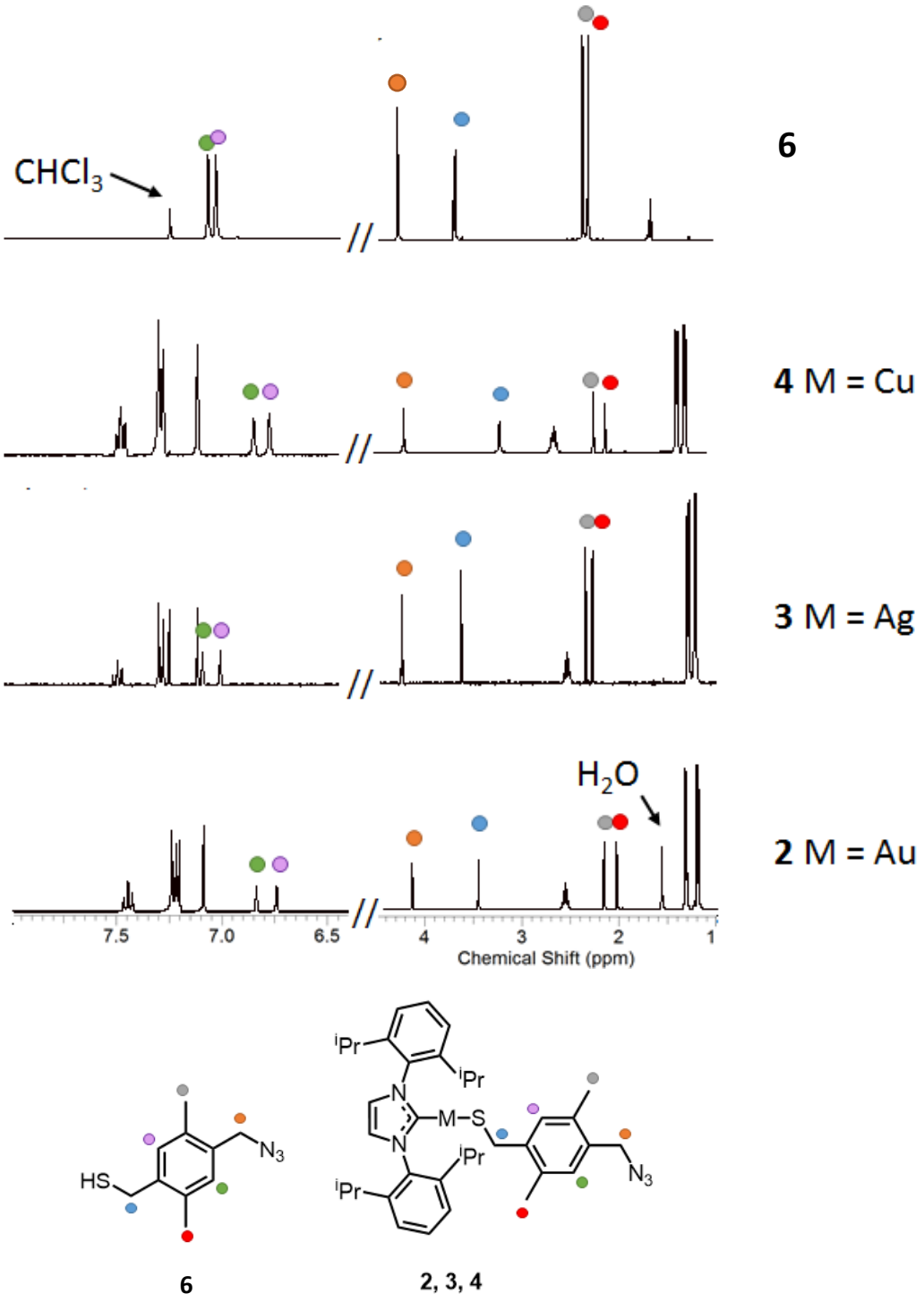

Fig 2.3: Stacked ^{1}H NMR spectra of **6** and **2, 3** and **4**. Dots represent the protons on 1-SCH_2-2,5-$(CH_3)_2$Ph-4-CH_2N_3.

In the ^{1}H NMR spectrum of **1**, similar to the other complexes, a significant shift of the resonance corresponding to the protons alpha to the sulfur was observed which appeared at 4.02 ppm compared to 3.50 ppm for **6**. The $C_{carbene}$ resonance in the $^{13}C\{^{1}H\}$ NMR spectrum was found at 190.3 ppm. Overall, ^{1}H and ^{13}C NMR spectroscopy overall provides clear evidence for the successful synthesis of the novel and clickable azide-modified Cu- (**4**), Ag- (**3**) and Au-(**1,2**) thiolate complexes.

2.2.3 X-Ray Crystallography

Compound **1** was obtained by layering a sample in toluene with heptane. It crystallizes in the monoclinic space group $P2_1/c$ with four molecules in the unit cell (**Fig 2.4A**). Crystals of **2-4** were obtained by layering in a 1:4 mixture of toluene with pentane. All three complexes crystallize in the triclinic space group P–1 with two molecules in the unit cell (see **Fig. 2.4 B,C**). The samples are in fact isomorphous. Selected bond angles and lengths are listed in **Table 2.1** and it was found that the values were consistent with those reported in literature for NHC terminated complexes of Cu, Ag, and Au.[3,17] The metal to carbene (M1–C1) bond distances were 2.0093(14) Å and 2.0168(16) Å for Au (**1** and **2**, respectively) and 2.0815(9) Å for Ag (**3**). They were found to be shorter in the case of Cu (**4**) at 1.8957(9) Å. The metal to sulfur (M1-S1) bond distances were slightly larger at 2.3243(3) Å for Ag (**3**) and 2.2792(6) Å and 2.2901(5) Å for Au (**1** and **2**, respectively) and relatively shorter for Cu (**4**) (2.1371(3) Å). M1-C1 and M1-S1 bond lengths of **1** were found to be slightly longer compared to **2**. The geometry around the metal atom was found to be nearly linear, with the bond angles for S1–M1–C1 deviating away from linearity from Au (178.23(4)º for **1** and 174.88(4)º for **2**) to Ag (174.46(3)º for **3**) to Cu (173.00(3)º for **4**). For the case of **1**, the S1-M1-C1 bond angle was slightly closer to linearity than **2** and the thiolate group

in **2** was rotated out of the plane as a result the steric hindrance imposed by the ^{i}Pr phenyl groups of the NHC in **2**.

In all 4 complexes, terminal coordination was favourable due to the relatively sterically encumbered IPr, $^{i}Pr_2$bimy ligands, and the methyl groups on the thiolate ligand. The intermolecular bond distances were greater than the sum of the Van der Waals radii for the metals thereby concluding that no metallophilic interaction is present.[18] The bond angles and distances were also found to be comparable to crystal structures of existing coinage metal thiolate complexes.[19]

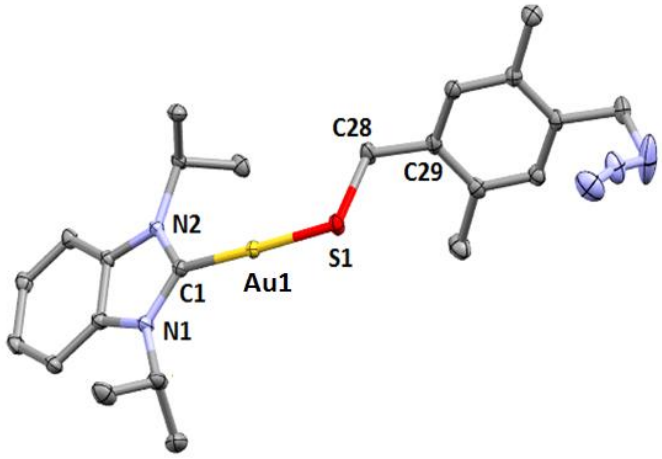

A

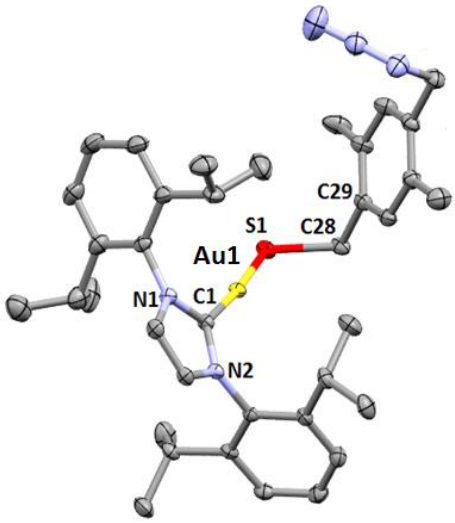

B

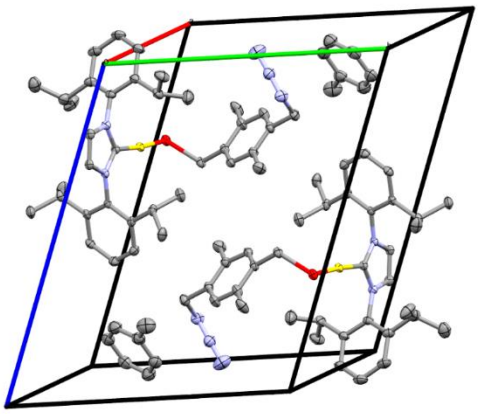

C

Fig 2.4: (A) Molecular structure of **1** (B) Molecular structure of **2** (C) Unit cell of **2**. Ellipsoids shown at 50% probability. Hydrogen atoms are omitted for clarity.

Table 2.1: Selected bond angles and bond lengths for complexes **1**, **2**, **3** and **4**. R = {$CH_2Ph(CH_3)_2CH_2N_3$}.

Selected Bond Angles (º)	**1-[(^{i}Pr$_2$bimy)AuSR]**	**2-[(IPr)AuSR]**	**3-[(IPr)AgSR]**	**4-[(IPr)CuSR]**
S1–M1–C1	178.23(4)	174.88(4)	174.46(3)	173.00(3)
S1–C28–C29	112.03(11)	115.48(11)	115.32(8)	115.51(7)
M1–S1–C28	101.20(6)	106.97(5)	106.15(4)	107.94(4)
C32–C35–N3	111.74(19)	111.90(15)	112.08(10)	111.95(9)
N1–C1–M1	126.57(11)	124.86(10)	124.94(7)	124.98(7)
N2–C1–M1	126.43(11)	130.45(10)	130.89(8)	131.16(7)
Selected Bond Lengths (Å)				
C1–M1	2.0168(16)	2.0093(14)	2.0815(9)	1.8957(9)
M1–S1	2.2901(5)	2.2792(6)	2.3243(3)	2.1371(3)
C16-N1	1.477(2)	1.4447(19)	1.4434(13)	1.4432(12)
C4-N2	1.483(2)	1.4448(19)	1.4458(13)	1.4450(12)

2.2.4 SPAAC Reactivity of NHC-Gold Thiolate – Characterization and Rate of Reaction

Azide-alkyne cycloaddition at the periphery of the ligands bound to metal ions has been previously demonstrated.[16] Having developed a synthetic protocol for four novel azide-modified coinage metal complexes and fully characterizing them, the SPAAC reactivity of one of the metal

complexes was explored to demonstrate its reactivity towards its corresponding click partner, namely, a strained-alkyne such as BCN-OH (see **scheme 2.3**).

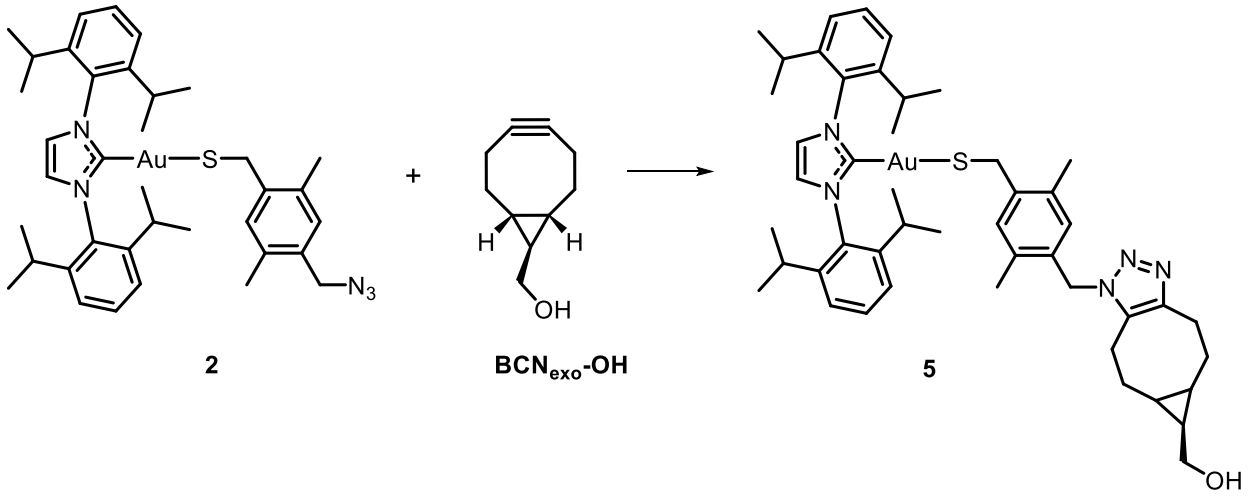

2 **BCN_{exo}-OH** **5**

Scheme 2.3: SPAAC Reaction of **2** with BCN-OH to obtain cycloadduct, **5**.

To this end, **2** was reacted with a 1.2 eq. excess of BCN-OH in deuterated CH_2Cl_2 for 12 h, after which residual starting material were removed by trituration in ether and a ^{1}H NMR spectrum was obtained of the cycloadduct, **5**. As can be seen in **Fig 2.5**, changes to the ^{1}H NMR signals of the cyclooctene ring in the 0.5 – 3.0 ppm region as a result of loss of symmetry in the ring and the formation of the cycloadduct and its corresponding regioisomer can be observed (orange, **Fig 2.5**).[20] Further confirmation of the SPAAC reaction can be seen in the well-documented upfield shift of the ^{1}H NMR signal from the methylene protons alpha to the hydroxyl group from 3.5 ppm to between 2.0 and 2.5 ppm,[16] as BCN-OH is consumed to form the corresponding triazole cycloadduct, **5**.

Expectedly, the ^{1}H NMR signal from the methylene protons alpha to the thiolate functionality did not undergo a shift subsequent to the SPAAC reaction. However, since the chemical environment of the methylene alpha to the azide/triazole cycloadduct changes during the

SPAAC reaction, the resonance from the methylene protons alpha to the azide in **2** underwent a downfield shift from 4.19 ppm to 5.31 ppm represented by (★), which provides diagnostic confirmation that the SPAAC reaction had indeed occurred. Additionally, the ratio of the resonances of the azide thiolate:BCN moieties of the cycloadduct integrated to 1:1, thereby further confirming that the reaction had gone to completion. ^{13}C NMR shows resonances at 133.9 and 132.6 ppm in **5** that did not appear in the ^{13}C NMR of either BCN-OH or **2**, and can be assigned to the carbons of the alkene (C-4 and C-5) in the cycloadduct.

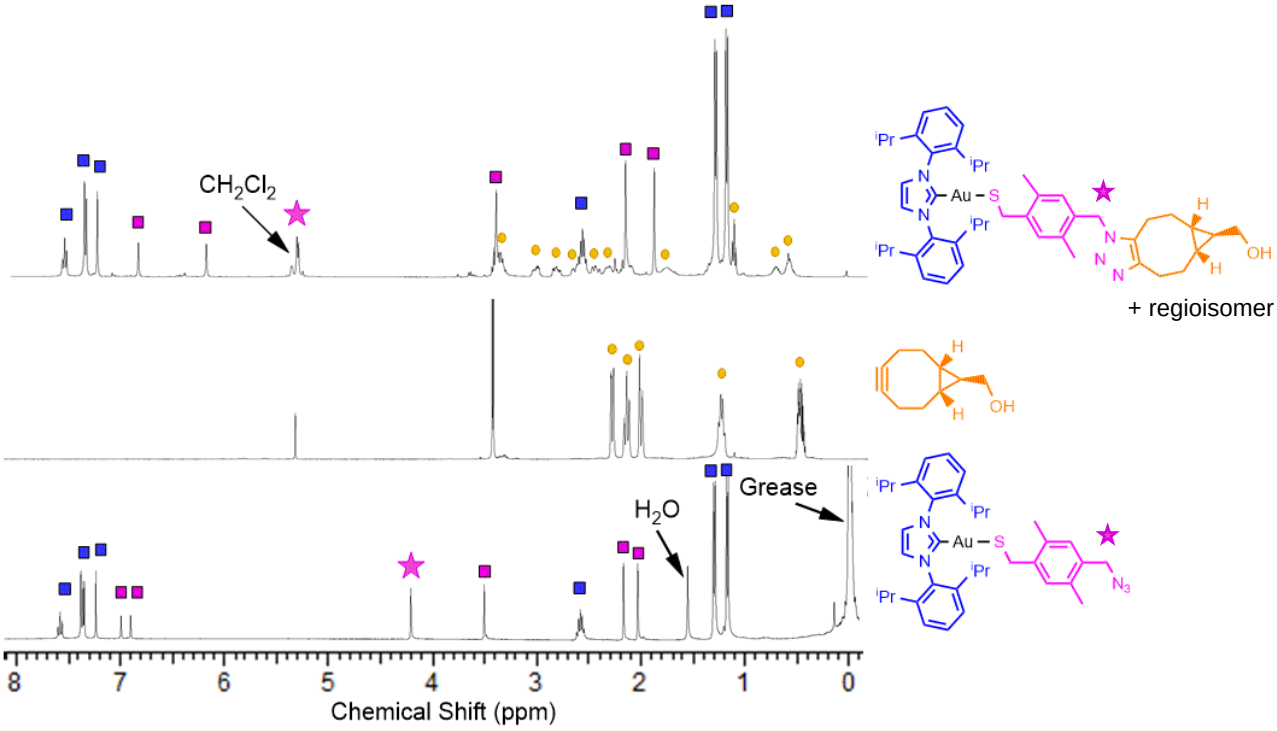

Fig 2.5: Stacked ^{1}H NMR spectra of cycloadduct, **5** (top), BCN-OH (middle), **2** (bottom). Azide thiolate protons (■), NHC protons (■), and BCN protons (●). (★) represents diagnostic shift of methylene protons alpha to the nitrogen atom following reaction.

Having successfully demonstrated the SPAAC reactivity of **2** toward BCN-OH and characterized the corresponding triazole cycloadduct, the estimated rate of reaction of SPAAC was determined in order to probe the accessibility of the azide functionality in **Fig 2.6**.

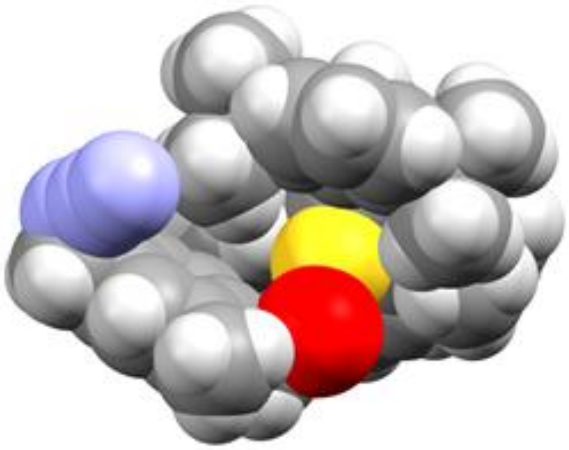

Fig 2.6: Space-filling model of **2**. C: grey, H: white, N: purple, S: red, Au: yellow.

The reactivity of **2**, which is coordinated to a gold atom bearing a relatively sterically demanding NHC, was probed and compared to that of a free simple organic azide, namely benzyl azide. The estimated rate kinetics for the reaction between the equimolar quantities of the terminally bound azide in **2** or benzyl azide with BCN was tracked by ^{1}H NMR spectroscopy under second order conditions. The second order rate constants were calculated using **equation 2.1**:

$$kt = \frac{1}{[B]_o - [A]_0} x\ ln \frac{[A]_0([B]_0 - [P])}{[B]_0([A]_0 - [P])} \qquad (2.1)$$

with k_2 = 2nd order rate constant ($M^{-1}s^{-1}$), t = reaction time (s), $[A]_0$ = the initial concentration of A ($mol \cdot L^{-1}$), $[B]_0$= the initial concentration of B ($mol \cdot L^{-1}$), [P] = the concentration of the product,

[P] (mol·L^{-1}). In this case, substrate A represented the azide in either **2** or benzyl azide, substrate B represented BCN and the product was the cycloadduct, **5**. Since equimolar quantities of **2**/benzyl azide and BCN were added, **equation 2.1** can be simplified to **equation 2.2**:

$$\frac{-d[A]}{dt} = k[A]^2 \qquad (2.2)$$

This means the integrated second order rate law (**equation 2.3**) is:

$$\frac{1}{[A]} = kt + \frac{1}{[A]_0} \qquad (2.3)$$

As can be seen, **equation 2.3** is in the form of y = mx + b. In this way, graphing 1/ [$azide$] against time (in seconds) gives a straight line, since the reaction is second order, which has a slope that is the rate constant, k_2.

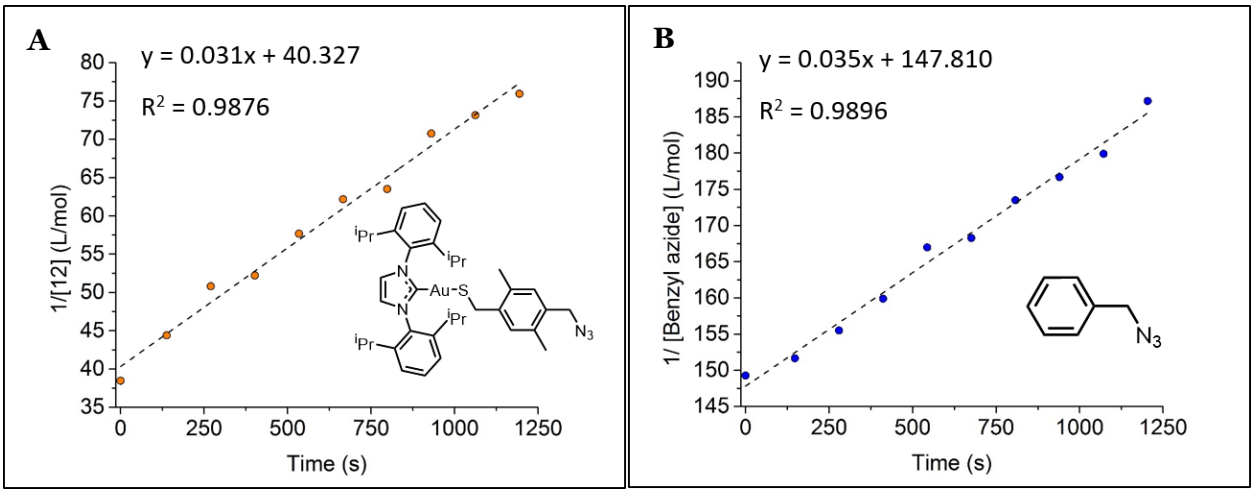

Fig 2.7: Regression analysis of estimated second order rate kinetics from ^{1}H NMR between BCN-OH and (A) **2** and (B) benzyl azide. Data reported within ±5% error.

Fig 2.7 shows the regression analysis of the ^{1}H NMR kinetic analysis of **2** and benzyl azide with BCN-OH. As can be seen, the estimated second order rate constant between **2** and BCN-OH is $0.031 M^{-1}s^{-1}$, which is very similar to the estimated second order rate constant of the electronically similar benzyl azide ($0.035 M^{-1}s^{-1}$). These data indicate that the accessibility of the azide functionality is unaltered by coordination to the NHC-Au center, indicating that this coinage metal complex is as readily available for SPAAC reaction with strained alkynes as its organic azide counterparts. The electronic environment of the azide functionality is very similar between all coinage-metal complexes, based on the NMR analysis described above, suggesting that the second order SPAAC kinetics between all NHC-metal complexes and BCN-OH should be similar to both one another and to benzyl azide. Additionally, the steric demand resulting from the large NHC groups did not seem to encumber the cycloaddition reaction, as the estimated rate kinetics were comparable to that of free benzyl azide.

2.3 Photoluminescence

Mono- and multi-nuclear gold(I) complexes produce characteristic luminescence in the range of 350 to 700 nm.[17,19] These complexes are well-known to demonstrate solid-state and solution based luminescence. One of the interesting properties of gold compounds is the presence of aurophilic interactions in the form of weak Au(I)···Au(I) interactions which can lead to aggregation-based luminescence in these complexes. Complexes that crystallize without Au–Au interactions can also be luminescent with their luminescence assigned to charge transfer transitions between the ligand and gold metal or inter- and intra-ligand transitions.[17,19] Although aurophilic interactions are likely in Au(I) complexes, there are none present in complexes **1-4**. **Fig 2.8** (top) shows the absorption spectra of complexes **1-4** in CH_2Cl_2 solution. **Fig 2.8** (bottom) shows the solid-state emission of the complexes. The optical solution state spectrum exhibits an onset at approximately 310 nm and two peaks at 285 nm and 290 nm. The bands displayed at 285 and 290 nm are very similar in terms of band shape and position to carbene precursors and are also consistent with the aromatic thiol.[19] Therefore, they were assigned to the n-π* intraligand transitions in the azide group and π-π* transitions arising from the phenyl ring of the thiol and carbene. The aforementioned bands are assigned as a superposition of intraligand transitions (IL) involving the carbene and thiol ligands. Reports on bands at 300 – 320 nm present in analagous NHC- and phosphine- gold complexes have been ascribed to S→M (thiolate ligand to metal) charge transfer transitions[17] and the lower energy transitions of the complexes at 305 nm for **2-4** and 320 nm for **1** have similar band positions and molar absorptivities.[17] However, the position of the bands were unaffected by the metal center (Cu, Ag, and Au) suggesting that the transition is a ligand based transition that is centered around the NHC and the thiolate. Hence, the additional band at 305 nm in the IPr complexes and at 320 nm in the $^{i}Pr_2$bimy complexes were assigned as

arising from interligand transitions. Density functional theory (DFT) calculations are necessary to supplement this assignment and can elucidate the nature of the orbitals involved in these transitions. The absorption spectra in the solid-state, which was obtained by spin coating a solution of the sample in trichlorobenzene onto a quartz slide exhibited bands at 240 nm and 310 nm. The former was assigned to intraligand transitions involving the phenyl group, and the latter to interligand transitions. All the complexes were found to be luminescent at room temperature in the solid-state, emitting blue-green light. **Fig 2.8** (bottom) shows the excitation and emission spectra of the complexes in the solid-state. The photophysical properties of the complexes were analysed in the solid-state in order to detect high energy charge transfer transitions. Upon excitation at 250 nm (and other wavelengths) the corresponding emission spectra were found to exhibit the same profile, with a peak at roughly 400 nm as well as a small relatively less intense shoulder at 290 nm. The high energy emission at 290 nm and low energy emission at 400 nm are assigned to originate from IL excited states.[17,19] The independency of the emission and the excitation wavelength provides strong evidence that the observed emission is a real luminescence from the relaxed states, rather than scattering. Moreover, the solid-state fluorescent excitation spectrum roughly follows the profile of the UV-vis absorption spectrum with the peak at 250 nm lying near the absorbance maximum at 240 nm. The Stoke's shift of the samples was 150 nm which is characteristic to the Stoke's shifts that are documented for NHC-coinage metal systems.[12,17,19]

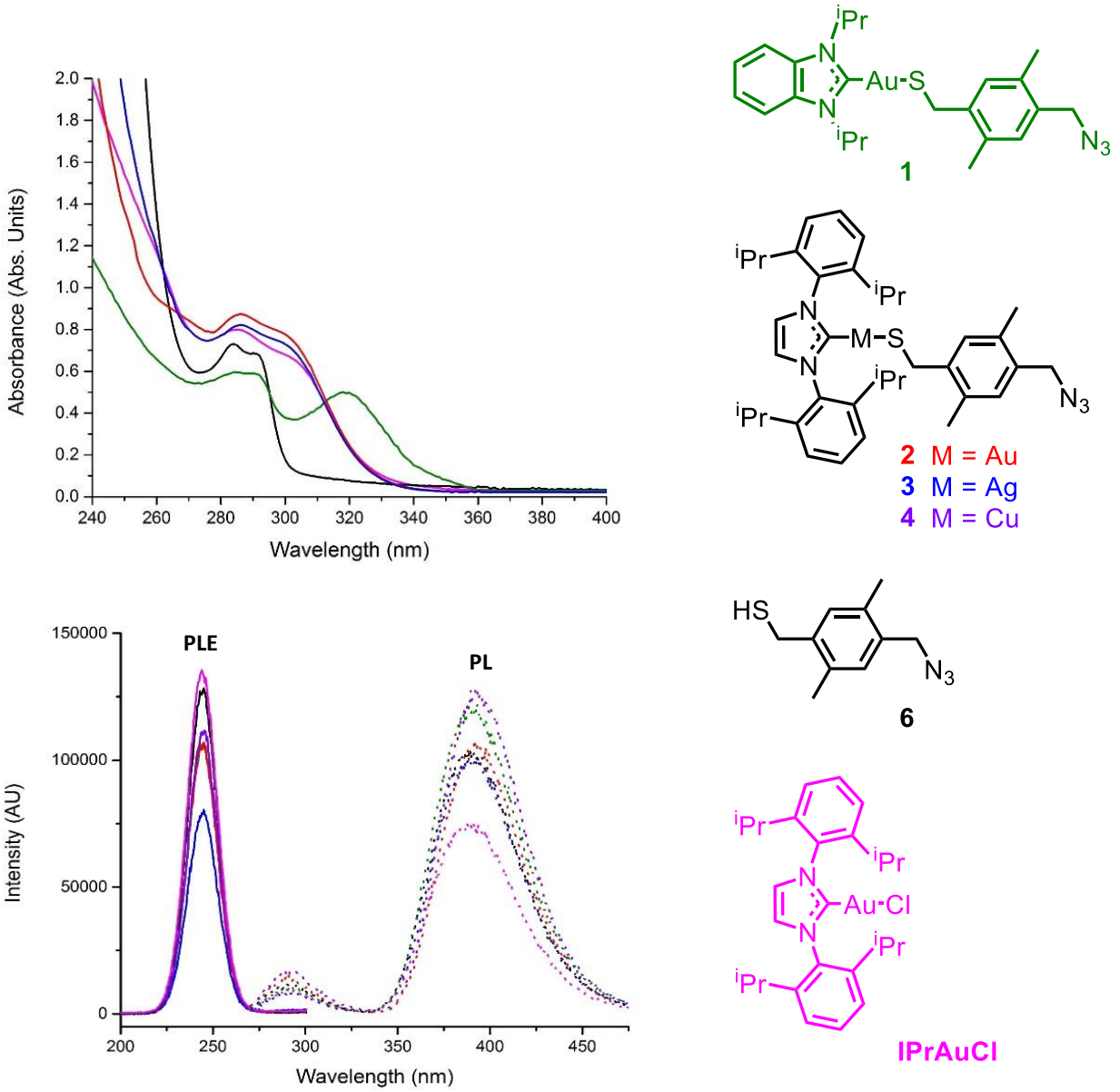

Fig 2.8: Solution-state absorption spectra of complexes and thiol **(top).** PL and PLE Spectra in the solid-state of complexes and thiol **(bottom).** λ_{ex} = 250 nm. Concentrations ($\times 10^{-6}$ M): **1**-2.8, **2**-3.8, **3**-3.5, and **4**-3.6, [(IPr)AuCl]-3.5.

2.4 Conclusion

Having established a facile synthetic protocol for a novel azide-modified thiolate ligand, four novel clickable coinage-metal complexes (**1-4**) have been successfully developed containing Cu, Ag and Au centers. In order to coordinate the azide-terminated ligand to each of the metal centers, **6** was deprotonated or converted to the trimethyl silyl sulfide (**7**), and subsequently coordinated to NHC-metal centers. In addition to the facile synthetic approach, these novel clickable complexes were characterized by multinuclear spectroscopy, and X-ray crystallography which confirmed the coordination of the azide-terminated thiolate to the NHC-metal salt. After having fully characterized the clickable complexes, the reactivity of **2** towards a strained alkyne (BCN-OH) was explored to demonstrate that these complexes are both facile to synthesize and easy to modify via SPAAC reaction. The accessibility of the azide group of **2** to SPAAC reaction was investigated and the rate of formation of the cycloadduct was determined and compared to a model azide. This kinetic study has revealed that the azide-functionality is as readily available when bound to the coinage-metal as it is in a simple organic compound, confirming the true practicality of the clickable complex. The complexes were also found to be luminescent in the solid-state, and the emissive properties were attributed to the phenyl and azide functionalities on the thiolate, and carbene moieties.

2.5 References

[1] Zhong-Ning Chen, Z.; Zhao, N.; Fan, Y.; Ni, J. *Coord. Chem. Rev.* **2009**, 253, 1.

[2] Humenny, W. J.; Mitzinger, S.; Khadka, C. B.; Khalili Najafabadi, B.; Vieira, I.; Corrigan, J. F. *Dalton Trans.* **2012**, 41, 4413.

[3] Azizpoor, F. M.; Levchenko, T. I.; Cadogan, C; Humenny, W. J.; Corrigan, J. F. *Chem. Eur. J.* **2016**, 22, 4543.

[4] Delp, S. A.; Munro-Leighton, C.; Goj, L. A.; Ramirez, M. A.; Gunnoe, T. B.; Petersen, J. L.; Boyle, P. D. *Inorg. Chem.* **2007**, 46, 2365.

[5] a) Satoshi, T.; Yukinao, O.; Toshio, K.; Keun, A. D.; Sentaro, O. *Tet. Lett*. **2004**, 45, 5585. b) Baker, M. V.; Barnard, P. J.; Berners-Price, S. J.; Brayshaw, S. K.; Hickey, J. L.; Skelton, B. W.; White, A. H. *J. Org. Chem.* **2005**, 690, 5625.

[6] Bruker-AXS, SAINT version 2013.8, **2013**, Bruker-AXS, Madison, WI 53711, USA.

[7] Bruker-AXS, SADABS version 2012.1, **2012**, Bruker-AXS, Madison, WI 53711, USA.

[8] Sheldrick, G. M., *Acta Cryst.* **2015**, A71, 3.

[9] Sheldrick, G. M., *Acta Cryst.* **2015**, C71, 3.

[10] Gabe, E. J.; Le Page, Y.; Charland, J. P.; Lee, F. L.; White, P. S. *J. Appl. Cryst*. **1989**, 22, 384.

[11] Dance, I. G.; Fisher, K. J.; Banda, H.; Scudder, M. L. *Inorg. Chem*. **1991**, 30, 183.

[12] Khalili Najafabadi, B.; Corrigan, J. F. *Dalton Trans.* **2014**, 43, 2104.

[13] Salomon, R. G.; Kochi, J. K. *J. Am. Chem. Soc.* **1973**, 95, 1889.

[14] a) Tonner, R.; Heydenrych, G.; Frenking, G. *Chem. Asian. J.* **2007**, 2, 1555. b) Hu, X.; Castro-Rodriguez, I.; Olsen, K.; Meyer, K. *Organometallics.* **2004**, 23, 755.

[15] Zhu, S.; Liang, R.; Jiang, H. *Tetrahedron*. **2012**, 68, 7949.

[16] Garner, M. E.; Niu, W.; Chen, X.; Ghiviriga, I.; Tan, W.; Veige, A. S. *Dalton Trans.* **2015**, 44, 1914.

[17] a) Wang, H. M.; Chen, C. Y.; Lin, I. J. *Organometallics*. **1999,** 18, 1216. b) Assefa, Z.; Staples, J.; Fackler, J. P. *J. Inorg. Chem.* **1994**, 33, 2790. c) Narayanaswamy, R.; Young, M. A.; Parkhurst, E.; Ouellette, M.; Kerr, M. E.; Ho, D. M.; Elder, R. C.; Bruce, A. E.; Bruce, M. R. M. *Inorg. Chem.* **1993**, 32, 2506.

[18] Mingos, M. P. *Dalton Trans*. **1996**, 5, 561.

[19] a) Forward, J. M.; Bohmann, D.; Fackler, J. P.; Staples, R. J. *Inorg. Chem*. **1995**, 34, 6330. b) Ho, S. Y.; Cheng, E.; Tiekink, E.; Yam, V. *Inorg. Chem*. **2006**, 45, 8165.

[20] Oliva, C. G.; Jagerovic, N.; Goya, P.; Alkorta, I.; Elquero, J.; Cuberes, R.; Dordal, A. *Arkivoc*. **2010**, 127.

3. Preparation and Characterization of Azide Functionalized Thiolate Ligands

3.1 Introduction

Ligands that are incorporated into metal complexes can be designed with a functional handle of a non-natural origin for bio-orthogonal reactions that can be coupled onto target biomolecules that contain the complementary functional group.[1-4] The azide moiety is truly bio-orthogonal – it is essentially unreactive with any biological functional groups under physiological conditions. It is also absent from virtually all biological systems and is thermodynamically a high energy species prone to specific reactivity as a 1,3 – dipole.[5] The robustness of the reaction and the fact that there is virtually no cross-reactivity with any other functional group gives it vast potential to be exploited in chemistry for applications on biomolecules.[6-9]

X-ray crystallography is a powerful means to model and understand anticipated properties and reactivity of azide modified ligands. One of the factors that can influence the propensity of a ligand for crystallization is torsional freedom, which can be curtailed by crystallizing relatively small molecules. Numerous studies have been published which incorporate aryl and benzyl thiolates onto Ag and Au nanoclusters (tuning properties of silver thiolates). In 2015, Bakr *et al.* published a synthetic procedure for the synthesis of Ag nanoclusters using a terminally bound 2,4-benzenethiolate.[10] With these aspects in mind, we targeted the synthesis of a simple propyl thiol and phenyl thiol that would also incorporate an azide. The optimal conditions, including reaction temperature, solvent, ratio of starting materials, and time of reaction, were explored. The azide terminated thiol with the best stability and yields was selected as a precursor for the synthesis of NHC terminated coinage metal thiolates.

3.2 Experimental

3.2.1 General Synthetic Techniques and Characterization

Experimental procedures for the synthesis of the thiol ligands **6**, **9** and **12** were performed using standard double manifold Schlenk line techniques under a dry and high purity nitrogen or argon atmosphere. Chemicals were used as received from Alfa Aesar and/or Aldrich. Azido-3-iodopropane was synthesized per literature procedure.[11] ^{1}H NMR (400 MHz, $CDCl_3$): δ = 3.46 (t, J = 8 Hz, C*H*$_2$I), 3.25 (t, J = 8 Hz, 2H, C*H*$_2$N$_3$), 2.06 (quin, J = 8 Hz, 2H, C*H*$_2$(CH$_2$)$_2$). ^{13}C NMR (150 MHz, CDCl3): δ = 51.5 (C*H*$_2$I), 32.3 (C*H*$_2$N$_3$), 2.3 (C*H*$_2$(CH$_2$)$_2$).

Solution ^{1}H and ^{13}C{^{1}H} NMR spectra were obtained on a Varian Mercury VX 400 MHz spectrometer. ^{1}H and ^{13}C{^{1}H} chemical shifts are referenced to $SiMe_4$, using the solvent peak as a secondary reference. High-resolution mass spectrometry was recorded on a Finnigan MAT 8400 Mass Spectrometer. UV/Vis absorption spectra were acquired on Varian Cary 1000 and 300 Bio UV/Vis spectrophotometers. Infrared spectra were collected using a Perkin Elmer Spectrum Two ATR-FTIR spectrometer. The wave number range scanned was 4000 – 400 nm.

3.3.0 4-Azidomethyl-2,5-dimethylbenzyl-1-thiol (6)

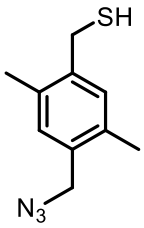

To a solution of compound **15** (2.0 g, 0.01 mol) in 3 mL of ethanol was added 0.4 mL of 1M NaOH (0.010 mol) in ethanol. The reaction was left stirring for 15 min under an Ar atmosphere after which 0.4 mL of 2M HCl (0.020 mol) was added and left to stir for an additional 15 min under Ar. The cloudy mixture was extracted into 5 mL CH_2Cl_2 and the resultant yellow solution was extracted with 3 × 10 mL of deionized H_2O and removed by rotoevaporation. The yellow solid was then purified by column chromatography using 1:1 CH_2Cl_2:hexanes as the eluent. The product **6** was obtained as a white solid in 82 % yield

(1.60 g). ^{1}H NMR (400 MHz, $CDCl_3$): δ = 7.10 (s, 1H, Ar-*H*), 7.06 (s, 1H, Ar-*H*), 4.30 (s, 2H, C*H*$_2$N$_3$), 3.70 (d, 2H, C*H*$_2$SH, $^{3}J_{HH}$ = 8 Hz), 2.37 (s, 3H, Ar-*H*), 2.31 (s, 3H, Ar-*H*), 1.67 (t, 1H, S*H*, $^{3}J_{HH}$ = 8 Hz) ppm. ^{13}C{^{1}H} NMR (150 MHz, $CDCl_3$): δ = 139.5, 134.8, 133.6, 132.5, 131.8, 131.1, 52.8, 26.6, 18.6, 18.5 ppm. IR: 2161, 2550 cm^{-1}. HRMS (ESI): Calc. [M] 208.0664, found 208.0662. λ_{max} = 285 nm (ε = 11 600 M^{-1}cm^{-1}), 290 nm (ε = 11 400M^{-1}cm^{-1}).

3.3.1 4-Azidomethyl-2,5-dimethyl-1-trimethylsilylthiomethylbenzene (7)

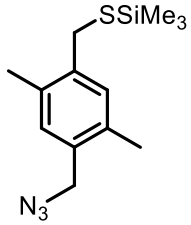

To a solution of **6** (0.15 g, 0.72 mmol) in 8 mL of toluene was added trimethylsilyl chloride (TMSCl) (0.3 mL, 2.2 mmol) followed by trimethylamine (0.1 mL, 0.74 mmol). The reaction was left to stir for 18 h after which the mixture was filtered through a plug of glass wool. The solvent and excess trimethylsilyl chloride (TMSCl) were evaporated off under vacuum to yield **7** a colourless oil in 92 % yield (0.19 g). ^{1}H NMR ($CDCl_3$, 400 MHz): δ = 7.11 (s, 1H, Ar-*H*), 7.03 (s, 1H, Ar-*H*), 4.28 (s, 2H, C*H*$_2$N$_3$), 3.67 (s, 2H, C*H*$_2$Si(CH$_3$)$_3$), 2.37 (s, 3H, Ar-C*H*$_3$), 2.30 (s, 3H, Ar-C*H*$_3$), 0.33 (s, 9H, CH$_2$Si(*CH*$_3$)$_3$) ppm. ^{13}C{^{1}H} NMR (150 MHz, $CDCl_3$): δ = 138.8, 134.4, 134.2, 132.2, 131.8, 131.7, 52.9, 28.3, 18.7, 185, 1.16 ppm. IR: 2162 cm^{-1}. HRMS (ESI): Calc. [M] 280.4822, found 280.4862.

3.2.2 Synthesis of 3-Azidopropyl Ethanethioate (8)

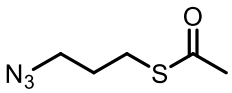

To azido-3-iodopropane (6.8 g, 32 mmol) in 50 mL of acetonitrile (CH_3CN) was added potassium thioacetate (KSAc) (4.1 g, 36 mmol). The reaction mixture was heated to reflux for a period of 24 h, after which the solvent was evaporated. The crude residue was then washed with 2 x 20 mL of hexanes to obtain **8** as a yellow oil in 62 % yield (2.9 g). ^{1}H NMR (400 MHz, $CDCl_3$): δ = 3.36 (t, $^{3}J_{HH}$ = 8 Hz, 2H), 2.94 (t, $^{3}J_{HH}$ = 8 Hz, 2H),

2.35 (s, 3H), 1.86 (quin, $^{3}J_{HH}$ = 8 Hz, 2H). $^{13}C\{^{1}H\}$ NMR (150 MHz, $CDCl_3$): δ = 195.4, 50.1, 30.6, 28.9, 26.1. HRMS (CI) Calc. [M + H^+] 160.0566, found 160.0545.

3.2.3 Synthesis of 3-Azidopropane-1-thiol (9)

A solution of **8** (2.9 g, 20 mmol) in 5 mL of ethanol was purged with argon for 20 min after which 21 mL of a 1M (21 mmol) stock solution of NaOH in ethanol was added to the solution and left to stir under argon for an additional 20 min. 21 mL of 2M HCl (21 mmol) in deionized H_2O was added to the reaction mixture and allowed to mix for 20 min under argon. The crude mixture was diluted with 10 mL of 2M deionized H_2O, extracted with 3 x 10 mL of CH_2Cl_2, dried over Na_2SO_4 and concentrated *in vacuo* to give **9** in 78 % yield (1.6 g). ^{1}H NMR (400 MHz, $CDCl_3$): δ = 3.42 (t, $^{3}J_{HH}$ = 8 Hz, 2H), 2.61 (quartet, $^{3}J_{HH}$ = 8 Hz, 2H), 1.86 (quin, $^{3}J_{HH}$ = 8 Hz, 2H), 1.35 (t, $^{3}J_{HH}$ = 8 Hz, 1H). $^{13}C\{^{1}H\}$ NMR (150 MHz, $CDCl_3$): δ = 49.5, 32.7, 21.6. HRMS (CI) Calc. [M + H^+] 118.0461, found 118.0440.

3.2.4 Synthesis of *p*-Bromomethyl-benzyl ethanethioate (10)

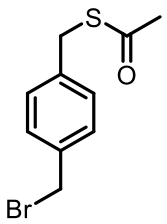

To a solution of 1,4-bis(bromomethyl)benzene (2.0 g, 7.5 mmol) in 10 mL of CH_3CN was added KSAc (0.40 g, 3.1 mmol). The reaction mixture was refluxed for 48 h after which the salt was filtered off and solvent was evaporated. The crude mixture was purified by flash column chromatography (1:2 CH_2Cl_2:hexanes) to give the product as a white solid in 50 % yield (0.41 g). ^{1}H NMR (400 MHz, $CDCl_3$): δ = 7.33 (d, $^{3}J_{HH}$ = 8 Hz, 2H), 7.26 (d, $^{3}J_{HH}$ = 8 Hz, 2H), 4.48 (s, 2H), 4.11 (s, 2H), 2.36 (s, 3H). $^{13}C\{^{1}H\}$ NMR (150 MHz, $CDCl_3$): δ = 138.4, 137.1, 129.6, 129.5, 33.4, 33.3, 30.6. HRMS (ESI): Calc. [M] 257.9714, found 257.9602.

3.2.5 Synthesis of *p*-Azidomethyl-benzyl ethanethioate (11)

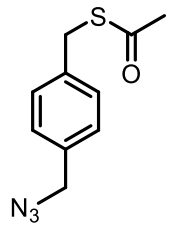

To a solution of **10** (0.30 g, 1.2 mmol) in 50 mL of CH_3CN was added NaN_3 (0.800 g, 12 mmol). The reaction mixture was refluxed for 24 h after which 120 mL deionized H_2O was added and the product was extracted with 3 x 20 mL of CH_2Cl_2 and dried over Na_2SO_4 to give **11** as a yellow oil in 87 % yield (0.23 g). ^1H NMR (400 MHz, $CDCl_3$): δ = 7.32 (d, $^3J_{HH}$ = 8 Hz, 2H), 7.26 (d, $^3J_{HH}$ = 8 Hz, 2H), 4.32 (s, 2H), 4.13 (s, 2H), 2.36 (s, 3H). $^{13}C\{^1H\}$ NMR (150 MHz, $CDCl_3$): δ = 194.9, 137.9, 134.4, 129.2, 128.5, 54.4, 33.0, 33.3. The spectroscopic data are in agreement with those reported.[12] HRMS (ESI): Calc. [M] 221.0623, found 221.0625.

3.2.6 Synthesis of *p*-Azidomethyl-benzyl-ethanethiol (12)

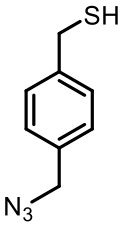

11 (0.23 g, 1.0 mmol) in 5 mL of ethanol was bubbled with Ar for 15 min after which (1.1 mL, 1.1 mmol) of a 1M stock solution of NaOH in ethanol was added to the solution and left stir under argon for an additional 15 min. (1.1 mL, 2.2 mmol) of 2M HCl in deionized H_2O was added to the reaction mixture and allowed to mix for 15 min under argon. The crude mixture was diluted with 10 mL of 2M deionized H_2O and extracted with 3 x 5 mL of CH_2Cl_2. CH_2Cl_2 was evaporated off to give **12** in 71 % yield (0.13 g). ^1H NMR (400 MHz, $CDCl_3$): δ = 7.33 (d, $^3J_{HH}$ = 8 Hz, 2H), 7.25 (d, $^3J_{HH}$ = 8 Hz, 2H), 4.30 (s, 2H), 3.73 (d, $^3J_{HH}$ = 8 Hz, 1H), 1.74 (s, 3H). $^{13}C\{^1H\}$ NMR (150 MHz, $CDCl_3$): δ = 136.5, 134.0, 128.5, 127.3, 56.2, 34.0, 29.1.

3.2.7 1,4-Bis(bromomethyl)-2,5-dimethyl-benzene (13)

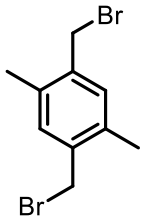

Followed procedure with a few modifications and data is consistent with literature:[13] To a round-bottom flask charged with *p*-xylene (25 mL, 0.20 mol) and paraformaldehyde (PFA) (11 g, 0.37 mol) was added 150 mL of 48 % HBr. After 48 h of stirring at reflux, the white precipitate was collected by vacuum filtration and washed with deionized H_2O. The crude was then purified by column chromatography in 1:2 CH_2Cl_2:hexanes to afford the product as white needles in 89 % yield (52 g). ^{1}H NMR (400 MHz, $CDCl_3$): δ = 7.13 (s, 2H, Ar-*H*), 4.46 (s, 4H, C*H*$_2$Br), 2.36 (s, 6H, Ar-C*H*$_3$) ppm. ^{13}C{^{1}H} NMR (150 MHz, $CDCl_3$): δ = 136.5, 135.3, 132.5, 31.87, 18.30. HRMS (ESI): Calc. [M] 292.9285, found 292.9281.

3.2.8 1-Bromomethyl-4-thioacetomethyl-2,5-dimethyl-benzene (14)

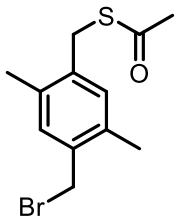

To a solution of **13** (15 g, 0.05 mol) in 150 mL of CH_3CN was added KSAc (2.3 g, 0.02 mol). After 48 h of stirring at reflux, the CH_3CN was removed by rotary evaporation and the mixture was re-dissolved in 80 mL of CH_2Cl_2. The salt by-product was removed by gravity filtration. **14** was purified by column chromatography using 1:3 CH_2Cl_2:hexanes as the eluent and obtained as a yellow oil in 30 % yield (5.2 g). ^{1}H NMR (400 MHz, $CDCl_3$): δ = 7.10 (s, 2H, Ar-*H*), 4.46 (s, 2H, CH_2N_3), 4.10 (s, 2H, C*H*$_2$S(C=O)CH_3), 2.35 (s, 3H, CH_2S(C=O)C*H*$_3$), 2.27 (s, 6H, Ar-C*H*$_3$) ppm. ^{13}C{^{1}H} NMR (150 MHz, $CDCl_3$): δ = 195.1, 135.2, 134.3, 132.5, 132.2, 101.4, 51.3, 32.2, 31.3, 30.5, 18.9, 18.3 ppm. HRMS (ESI): Calc. [M] 287.0027, found 287.0031.

3.2.9 4-Azidomethyl-1-thioacetomethyl-2,5-dimethyl-benzene (15)

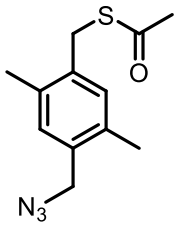

To a solution of compound **14** (5.2 g, 0.02 mol) in 50 mL of CH_3CN was added NaN_3 (4.6 g, 0.070 mol). The reaction flask was purged with Ar and heated to reflux overnight. CH_3CN was removed by rotoevaporation and re-dissolved in 10 mL of CH_2Cl_2. Salt by-products were removed by extraction with distilled H_2O to yield **13** as a yellow oil in 83 % yield (6.0 g). ^{1}H NMR (400 MHz, $CDCl_3$): δ = 7.13 (s, 1H, Ar-*H*), 7.04 (s, 1H, Ar-*H*), 4.28 (s, 2H, CH_2N_3), 4.10 (s, 2H, CH_2S(C=O)CH_3), 2.34 (s, 3H, CH_2S(C=O)C*H*$_3$), 2.30 (s, 3H, Ar-C*H*$_3$), 2.29 (s, 3H, Ar-C*H*$_3$) ppm. ^{13}C{^{1}H} NMR (150 MHz, $CDCl_3$): δ = 195.3, 135.5, 134.6, 134.4, 132.8, 132.3, 101.5, 52.8, 31.3, 30.5, 19.9, 18.5 ppm. IR: 2155 cm^{-1}. HRMS (ESI): Calc. [M] 250.0936, found 250.0935.

3.3 Results and Discussion

3.3.1 Synthesis

The azide modified ligand precursors used for the synthesis of the complexes were 4-azidomethyl-2,5-dimethylbenzyl-1-thiol (**6**) and 4-azidomethyl-2,5-dimethyl-1-trimethylsilylthiomethylbenzene (**7**). Other azide terminated thiol ligands that were also synthesized were 3-azidopropane-1-thiol (**9**) and *p*-azidomethyl-benzyl-ethanethiol (**12**). The synthetic approach used for the preparation of the mixed thiol/azide ligand utilized a di-halide as the template onto which subsequent S_N2 substitution reactions would take place. Overall yields in the synthesis of **9 (Scheme 3.1** (1)**)** and **12 (Scheme 3.1** (2)**)** were found to be low, and small molecules of this type are particularly hard to work with due to their volatility.[14]

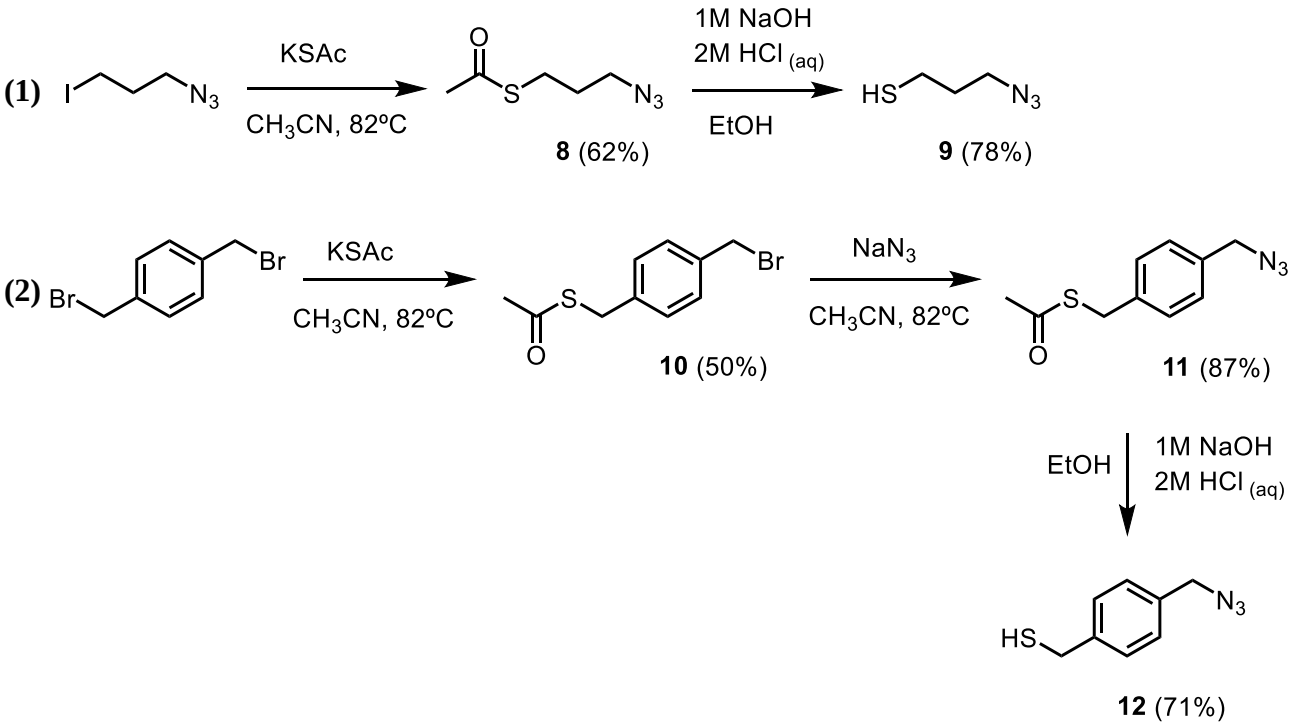

Scheme 3.1: Synthetic Pathway for (1) **9** and (2) **12**.

For this reason, attention was directed towards the synthesis of a benzyl thiol containing methyl substituents, which tend to be solids at room temperature and hence easier to handle and purify. To this end, **6** was synthesized in quantitative yield by following established procedures with minor modifications. The reaction proceeds via an electrophilic aromatic substitution mechanism.[15] The addition of 2 equivalents of the acid allows for a di-substitution on the *p*-xylene ring (**Scheme 3.2**).

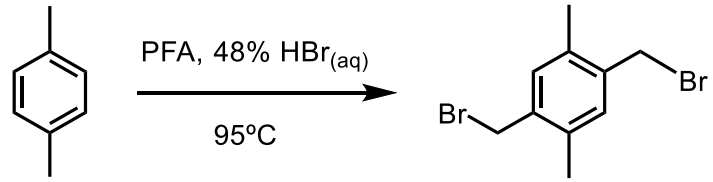

13 (89%)

Scheme 3.2: Synthesis of compound **13**.

The advantages of this synthetic approach are that the methyl groups are both *ortho* and *para* directing substituents in electrophilic aromatic substitution providing good control over the regiochemistry and the two alkyl groups are added *para* to each other to reduce steric congestion.

In order to incorporate a thiol functionality, a protected thiol was introduced by heating **13** with potassium thioacetate (KSAc) over 18 h in CH_3CN to give compound **14** (**Scheme 3.3**). Monosubstitution reactions often occur in poor yield, so in order to maximize the yield of **13**, the ratios of the two reagents, solvent system, temperature and time of reaction were altered and optimized (**Table 3.1**). In all experimental trials, the di-substituted thioacetate was found as a by-product of the reaction along with unreacted **13**. In order to minimize the amount of di-substituted

thioacetate, potassium thioacetate had to be added in limiting amounts. Adjusting the ratio of **13**: KSAc from 2:1 to 1.43:1 also resulted in improved yield. To further reduce the formation of the disubstituted thioacetate, the volume of reaction was increased to dilute the reaction enough to limit disubstitution, but still concentrated enough for the reaction to proceed efficiently. The reaction was heated to reflux using various solvents and in the case of CH_2Cl_2 or acetone, the reaction had not proceeded to completion after 48 h giving rise to the low yields. Allowing the reaction to proceed for longer time did not change the progress. Switching to a higher boiling solvent improved yields slightly, however it also led to the production of the di-substituted thioacetate. Due to this the reaction time was decreased from 48 h to 24 h which significantly improved yields.

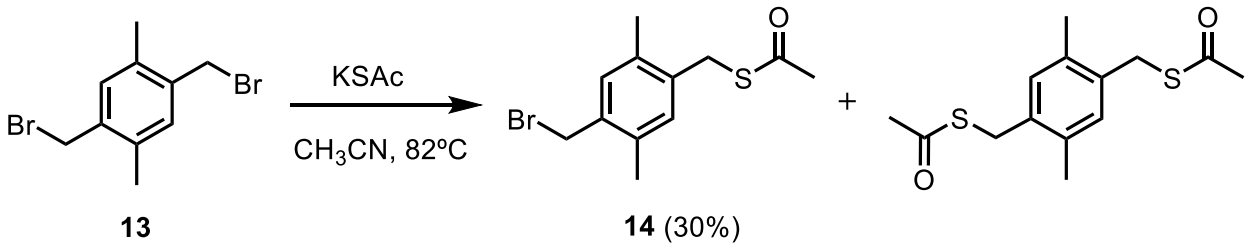

13 **14** (30%)

Scheme 3.3: Reaction of **13** with KSAc.

Table 3.1: Optimizing conditions to maximize yield of **14.**

Solvent	Time (h)	Yield (%)
CH_2Cl_2	48	10
Acetone	48	15
CH_3CN	48	18
CH_3CN	24	25(30)*

*Adjusting ratio of 1:KSAc to 1.43:1 increased yield to 30%

Compound **14** was purified by flash column chromatography to give a white solid in 30% yield. It was found that **14** has poor solubility in CH_2Cl_2, whereas the other two by-products were very soluble. Hence, filtration of the crude product mixture in CH_2Cl_2 removed the majority of **13** and made the overall purification easier.

Compound **14** was reacted with NaN_3 in CH_3CN which substituted the remaining bromide with a 'clickable' azide group (**Scheme 3.4**). Purification was achieved through a simple extraction to give **15** as a yellow oil in quantitative yield. The acetate group of compound **15** was deprotected by the addition of NaOH, which results in an acyl substitution to generate $ArCH_2S^-$, which was subsequently protonated to generate **6**.

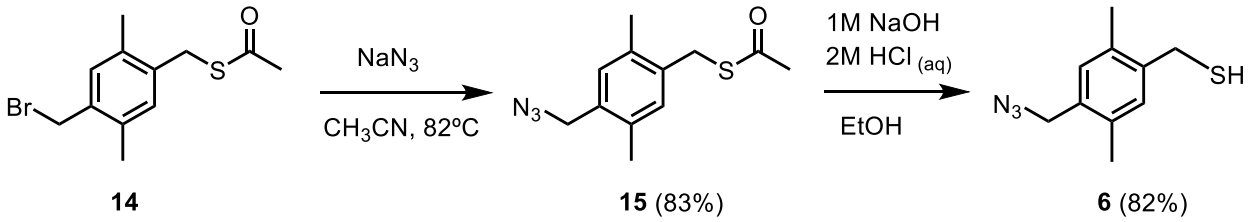

14 **15** (83%) **6** (82%)

Scheme 3.4: The synthesis of **6**.

The thiol functionality in compound **6** was reacted TMSCl and NEt_3 with the elimination of Et_3NHCl to afford **7**. The sodium thiolate salt of **6** was prepared by deprotonation of the thiol with NaH (**Scheme 3.5**). Compound **7** and the sodium thiolate salt served as precursors for the synthesis of the coinage metal chalcogenolates described in Chapter 2. The sodium thiolate was not isolated due to its susceptibility to oxidation, and served therefore as an intermediate for the synthesis of the complexes.

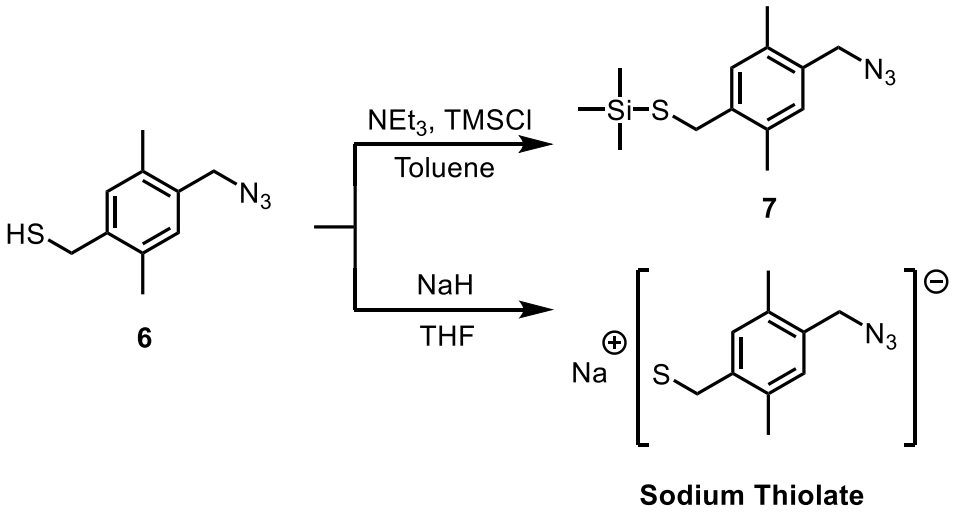

Scheme 3.5: Synthesis of **7** and the sodium salt of **6**.

3.3.2 NMR Spectroscopy

The synthesis of compounds **6 – 15** was followed by NMR spectroscopy in order to confirm successful S_N2 substitution at each step. As shown in **Fig. 3.1**, the aromatic proton ^1H NMR signals were observed as singlets ~ 7 ppm, the methyl groups yielded signals ~ 2.2 – 2.4 ppm, whereas the resonances corresponding to methylene protons were located between 3.5 to 4.5 ppm. Monosubstitution of bromide of **13** with a thioacetate group (**14**) was confirmed by the splitting of the methylene resonances into two separate signals corresponding to the now asymmetric molecule and differing shielding effects of each of the substituents. The shielding effect of the thioacetate compared to the bromide groups shifted the methylene signal adjacent to the thioacetate slightly upfield. Substitution did not have a significant effect on the chemical shifts for the aromatic and methyl proton signals. Upon substitution of the bromide with the more electronegative azide group, the aromatic and methyl proton signals shifted such that the two environments were resolved for each. Interestingly, after substitution of the bromide group with an azide to give **15**, the aromatic proton signal shifted upfield from 7.10 ppm to 7.04 ppm and the methyl signal shifted slightly

from 2.27 ppm to 2.30 ppm, which can likely be explained by the resonance contribution from the azide group and is consistent with literature.[16] Deprotection of the acetate with NaOH and subsequent protonation with HCl leads to the formation of azide thiol **6**. The resonance corresponding to proton of the thiol functionality appears at 1.66 ppm as a triplet due to splitting by the adjacent protons on the methylene group. Generation of the thiol from the deprotection of the thioacetate group leads to a shift in the signal of the adjacent methylene protons, upfield from 4.10 to 3.70 ppm and a downfield shift in the signal of the two sets of methyl protons from 2.30 and 2.29 to 2.37 and 2.31 ppm. Reaction of the thiol with TMSCl in the presence of NEt_3 results in the formation of **7**. The methyl groups of the $SSiMe_3$ functionality appear as a singlet at 0.33 ppm and the chemical shifts of the methylene groups do not change upon transformation from the thiol to the sulfide.

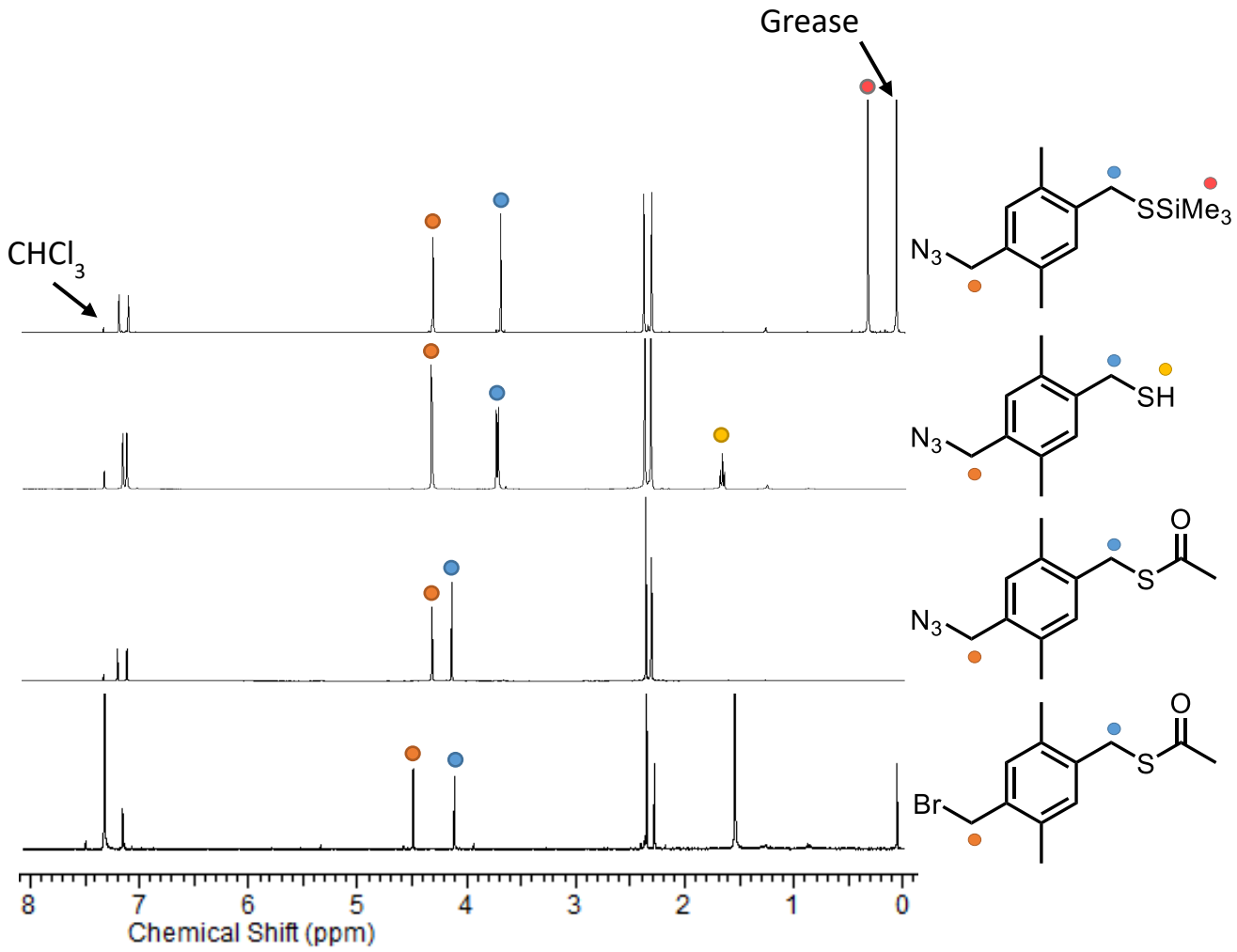

Fig 3.1: Stacked NMR spectra of **14, 15, 6 and 7** (bottom to top) in $CDCl_3$. Dots indicate proton resonances that were tracked to monitor reaction completion.

3.3.3 Infrared and UV/Vis Spectroscopy

In addition to ^1H NMR spectroscopy, the incorporation the azide functionality and deprotection of the thioacetate to generate the thiol could be confirmed using infrared spectroscopy. The azide functionality displays a strong, narrow band at ~2161 cm^{-1} which is characteristic of the N_3 asymmetric stretch in the azide group present in the thiol (**6**).[17] The thiol functionality was confirmed by observing a broad signal at 2550 cm^{-1}.[18] Compound **6** was further

characterized by UV/VIS spectroscopy, which showed bands at 285 nm and 290 nm. The former is the result of π to π* transitions of the aromatic ring and the latter is characteristic of azides.[19] Together, ^{1}H NMR, infrared and UV/Vis spectroscopy provide conclusive evidence for both the presence of the clickable azide group and the thiol functionality that can be attached to metal complexes.

3.4 Conclusion

A series of simple substitution reactions on a dihalogenated benzyl template produced a novel clickable aromatic ligand was successfully synthesized that also possessed a terminal thiol that can be incorporated onto coinage metal complexes. The advantage to using aromatic-based ligands over aliphatic ligands is that aromatic ligands are easier to handle and prepare, providing better synthetic control. The success of each reaction could be easily tracked by ^{1}H NMR spectroscopy due to the appearance and disappearance of signals that were easily resolved, further enhancing the practicality of the clickable ligand that was chosen. Dihalogenated xylyl template **13** was substituted first with a protected thiol and then subsequently with an azide group, to generate a protected azido-xylyl intermediate in good yield that was successfully deprotected in quantitative yield to generate the reactive thiol functionality. Due to the relative inertness of the azide moiety, it was unaltered during the deprotection strategy, providing a facile approach to generating thiol-modified clickable ligands. Furthermore, unlike the propyl and non-methylated aromatic counterparts, azido thiol **6** was a solid at room temperature and stable towards undesired oxidation, making it an ideal ligand for reaction with coinage metal salts. The thiol group was successfully converted to a thiolate through deprotonation and/or reaction with TMSCl, which was

subsequently used towards the development of coinage metal complexes containing the clickable azide moiety.

3.5 References

[1] Ibrahim, H.; Gibard, C.; Hesling, C.; Guillot, R.; Morel, L.; Gautier, A.; Cisnetti, F. *Dalton Trans*. **2014**, 43, 6981.

[2] Hohloch, S.; Hettmanczyk, L.; Bipraji, S. *Eur. J. Inorg. Chem.* **2014**, 20, 3164.

[3] Baeza, B.; Casarrubios, L.; Sierra, M. A. *Chem. Eur. J*. **2013**, 19, 1429.

[4] Del Castillo, T. J.; Sarkar, S.; Abboud, K. A.; Veige, A. S. *Dalton Trans.* **2011**, 40, 8140.

[5] Agard, N. J.; Prescher, J. A.; Bertozzi, C. R. *J. Am. Chem. Soc.* **2004**, 126, 15046.

[6] Gabano, E.; Ravera, M.; Tinello, S.; Osella, D. *Eur. J. Inorg. Chem.* **2015**, 32, 5335.

[7] Connell, T. U.; James, J. L.; White, A. R.; Donnelly, P. S. *Chem. Eur. J.* **2015**, 21, 14146.

[8] Richters, T.; Krug, O.; Koesters, J.; Hepp, A.; Mueller, J. *Chem. Eur. J.* **2014**, 20, 7811.

[9] Pola, R.; Braunova, A.; Laga, R.; Pechar, M.; Ulbrich, K. *Poly. Chem*. **2014**, 5, 1340.

[10] Joshi, C. P.; Bootharaju, M. S.; Alhilaly, M. J.; Bakr, O. M. *J. Am. Chem. Soc.* **2015**, 137, 11578.

[11] Gobbo, P.; Gunawardene, P. N.; Luo, W.; Workentin, M. S. *Synlett*. **2015**, 26, 1169.

[12] Saha, S.; Nicolaï, A.; Owens, J. R.; Krawicz, A.; Dinolfo, P. H.; Meunier, V.; Lewis, K. M. *ACS Appl. Mater. Interfaces*. **2015**, *7*, 19, 10085.

[13] Dahrouch, M. R.; Mendez, P. L.; Portilla, Y.; Abril, D.; Alfonso, G.; Chavez, I.; Manriquez, J. M.; Rivière-Baudet, M.; Rivière, P.; Castel, A.; Rouzaud, J.; Gornitzka, H. *Organometallics*. **2001**, 20, 5591.

[14] Cossar, B. C.; Fournier, J. O.; Fields, D. L.; Reynolds, D. D. *J. Org. Chem.* **1961**, 27, 93.

[15] Izmant, H. H.; Dudek, J. *J. Am. Chem. Soc.* **1949**, 71, 3763.

[16] Graaf, A. J.; Mastrobattista, E.; Nostrum C. F.; Rijkers, D. T. S.; Hennink, W. E.; Vermonden, T. *Chem. Commun.* **2011**, 47, 6972.

[17] Scott, F. L. *Experientia*. **1957**, 13, 275.

[18] Menefee, A.; Dorman, A.; Scott, C. B. *J. Chem. Phys.* **1956**, 25, 370.

[19] Abu-Eittah, R.; El-Shahawy, *A. Appl. Spectrosc*. **1971**, 25, 90.

4. Conclusions

Herein a straightforward and optimized synthesis for novel and easy-to-handle azide-terminated thiolate ligands is presented, which can be extended towards the development of clickable coinage-metal thiolate complex or nanocluster system. The development of this ligand involved simple-to-perform S_N2 substitution reactions onto a di-halogenated precursor that underwent a mono-substitution with an azide salt, followed by substitution with a thioacetate salt. Deprotection of the thioacetate moiety in basic solution yielded the thiol functionality in high yield. For complexes **1** and **2**, it was found that direct reaction of the thiol with the NHC-stabilized coinage-metal salts afforded the thiolate complexes in high yields. For complexes **3** and **4** the thiol was first deprotected and then underwent reaction with a TMSCl to produce a trimethylsilyl sulfide which was subsequently incorporated into NHC-Cu and NHC-Ag thiolates. The complexes were synthesized using a facile protocol and synthetically-accessible precursors.

The formation of the two-coordinate, nearly linear complexes was monitored by ^{1}H NMR spectroscopy, and the formation of complexes **1-4** were further confirmed by elemental analysis, and single crystal X-ray analysis. Their photophysical properties were analyzed by UV-Vis and photoluminescence spectroscopy at 298 K. Bands corresponding to intraligand transitions originating from the phenyl and azide groups of the NHCs and ligand were observed. Excitation of these wavelengths produced an intense emission band centered at approximately 400 nm. Finally, the SPAAC reactivity of these complexes were successfully determined through reaction with BCN-OH, demonstrating that the clickable azide group is sterically available for SPAAC chemistry. The reaction was monitored by ^{1}H NMR spectroscopy for the shift of the peak corresponding to the methylene adjacent to the azide group, and splitting of the signals

corresponding to the cyclooctyne moiety. Additionally, the rate at which the clickable complexes react with BCN-OH has shown to be nearly identical to the rate at which an electronically similar azide reacts, further confirming that the clickable azide group is available for reaction with strained-alkyne moieties.

Aside from being synthetically facile, the true utility of the overall approach presented herein is that it bypasses the necessity of more synthetically-difficult thiolated ligands that would be required to incorporate functionality to such coinage metal systems for applications in catalysis, nanotechnology and biology. Instead, functionality can be more easily incorporated to azide-modified complexes through SPAAC chemistry, allowing for straightforward post-assembly modifications to the metal complexes. Furthermore, these novel azide-modified complexes represent precursors for the synthesis of large, clickable nuclearity Ag_2S clusters.

5. Recommendations for Future Work

The development of clickable coinage-metal complexes represents an exciting avenue towards the development of functional coinage-metal complexes, through post-assembly modifications using synthetically-facile SPAAC chemistry. These complexes represent models to the synthesis of functional, large-nuclearity Ag_2S nanoclusters, through the reaction of the azide-terminated silver thiolate with $S(SiMe_3)_2$ shown in **scheme 5.1**.

$$xLAgSR + yE(SiMe_3)_2 \rightarrow L_{x-w}Ag_xE_y(SR)_{x-z} + zRSSiMe_3 + wL$$

Scheme 5.1: Synthesis of Ag_2S nanoclusters using azide terminated thiolate precursor.

In this particular system, formation of the Ag_2S core is accompanied by the dissociation of the ancillary NHC ligands[2] which can potentially undergo reaction with the azide moiety, rendering it inaccessible for SPAAC chemistry. As a result, sources that can react with the dissociated NHC prior to reaction with the chalcogenide agent can also be explored such as good Lewis scavengers like BH_3.

Another interesting topic to explore would be the usage of other clickable moieties, such as the nitrone group. The nitrone, like the azide, can undergo click reaction with an alkyne, in the Strain-promoted-alkyne-nitrone cycladdition (SPANC). The synthetic strategy for a proposed nitrone thiol which is considerably easier to make and high-yielding is presented below in **Scheme 5.2**. The advantage of using a nitrone is also its inertness in the presence of phosphines and NHC ancillary ligands.

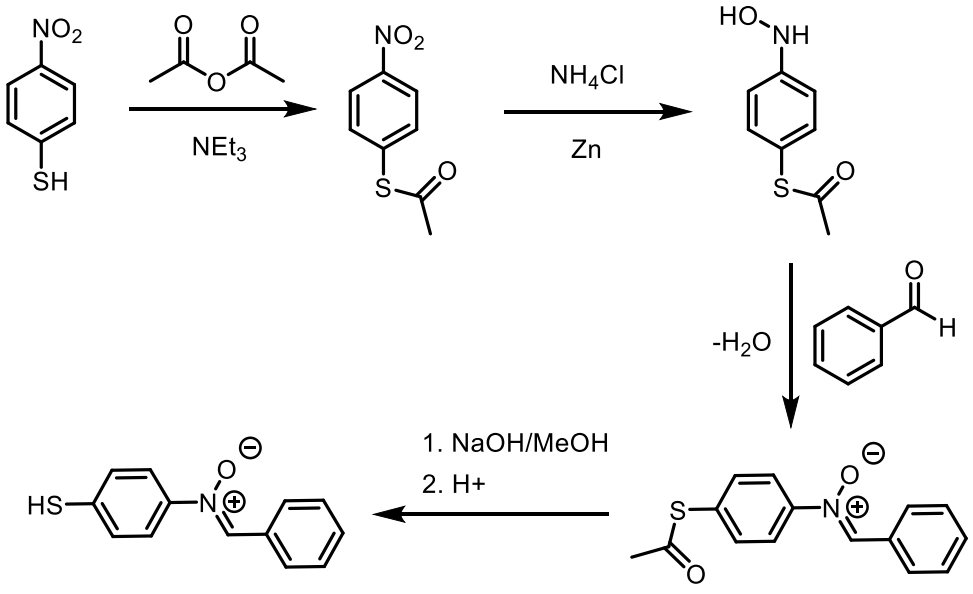

Scheme 5.2: Proposed synthesis of a nitrone-modified thiol precursor.

5.1 References

[1] Xie, Y.-P.; Jin, J.-L.; Duan, G.-X.; Lu, X.; Mak, T. *Coord. Chem. Rev.* **2017**, 331, 54.

[2] Ibrahim, H.; Gibard, C.; Hesling, C.; Guillot, R.; Morel, L.; Gautier, A.; Cisnetti, F. *Dalton Trans.* **2014**, 43, 6981.

[3] Staudinger, H.; Meyer, J. *Helv. Chim. Acta*. **1919**, 2, 619.

Appendices

Appendix A: Crystal data and structure refinement for [(^{i}Pr$_2$bimy)AuSR] **(1)**

Formula	$C_{23}H_{30.27}AuN_5O_0S$
Formula Weight (*g/mol*)	605.82
Crystal Dimensions (*mm*)	0.395 × 0.103 × 0.101
Crystal Color and Habit	colourless Needle
Crystal System	monoclinic
Space Group	P 2_1/c
Temperature, K	110
a, Å	8.7046(18)
b, Å	11.026(3)
c, Å	24.680(6)
α,°	90
β,°	95.511(12)
γ,°	90
V, Å^3	2357.7(9)
Number of reflections to determine final unit cell	9385
Min and Max 2□ for cell determination, °	5.98, 74.44
Z	4
F(000)	1193
ρ (*g/cm*)	1.707
λ, Å, (MoKα)	0.71073
μ, (*cm^{-1}*)	6.348
Diffractometer Type	Bruker Kappa Axis Apex2
Scan Type(s)	φ and ω scans
Max 2θ for data collection, °	75.68
Measured fraction of data	0.999
Number of reflections measured	81809
Unique reflections measured	12659
R_{merge}	0.0324
Number of reflections included in refinement	12659
Cut off Threshold Expression	I > 2σ(I)
Structure refined using	full matrix least-squares using F^2
Weighting Scheme	w=1/[sigma^2(Fo^2)+(0.0183P)^2+ 2.2379P] where P=(Fo^2+2Fc^2)/3
Number of parameters in least-squares	305
R_1	0.0238
wR_2	0.0464
R_1 (all data)	0.0315
wR_2 (all data)	0.0483
GOF	1.016
Maximum shift/error	0.011
Min & Max peak heights on final ΔF Map (*e$^-$*/Å)	-1.508, 3.471

Appendix B: Atomic Coordinates for [(^{i}Prbimy)AuSR] (**1**)

Atom	**x**	**y**	**z**	**$U_{iso/equiv}$**
Au01	0.24249(2)	0.58741(2)	0.64359(2)	0.01311(2)
S1	0.45539(4)	0.48731(4)	0.61879(2)	0.01653(7)
N1	0.03984(15)	0.74616(13)	0.70711(5)	0.0162(2)
N2	-0.09181(15)	0.66642(12)	0.63632(5)	0.0136(2)
C21	0.7503(2)	-0.04075(16)	0.53489(8)	0.0223(3)
N3	0.9060(4)	-0.0333(3)	0.5690(3)	0.0555(14)
N4	0.9673(4)	0.0676(3)	0.56905(16)	0.0299(7)
N5	1.0337(3)	0.1539(3)	0.57789(12)	0.0370(8)
C21A	0.7503(2)	-0.04075(16)	0.53489(8)	0.0223(3)
N3A	0.9166(5)	-0.0184(5)	0.53684(19)	0.0116(10)
N4A	0.9667(12)	0.0166(18)	0.5821(3)	0.061(4)
N5A	1.0294(13)	0.031(2)	0.6245(4)	0.122(8)
C1	0.05103(18)	0.67306(15)	0.66349(6)	0.0145(2)
C2	0.17104(19)	0.77361(18)	0.74777(7)	0.0212(3)
C3	0.2029(2)	0.90967(19)	0.75093(9)	0.0269(4)
C4	0.1458(3)	0.7167(2)	0.80222(8)	0.0289(4)
C5	-0.13470(18)	0.59871(14)	0.58519(6)	0.0149(3)
C6	-0.0438(2)	0.64372(17)	0.53954(6)	0.0188(3)
C7	-0.1212(2)	0.46249(16)	0.59432(7)	0.0201(3)
C8	-0.11195(18)	0.78617(15)	0.70855(6)	0.0149(3)
C9	-0.18351(19)	0.85997(16)	0.74450(7)	0.0179(3)
C10	-0.3414(2)	0.87982(16)	0.73307(7)	0.0189(3)
C11	-0.42458(19)	0.82748(16)	0.68768(7)	0.0177(3)
C12	-0.35383(17)	0.75458(15)	0.65168(6)	0.0155(3)
C13	-0.19585(17)	0.73460(14)	0.66303(6)	0.0134(2)
C14	0.36616(19)	0.37887(16)	0.56817(8)	0.0199(3)
C15	0.46850(17)	0.27148(15)	0.56093(7)	0.0164(3)
C16	0.54291(18)	0.26136(15)	0.51333(7)	0.0165(3)
C17	0.63399(17)	0.16133(15)	0.50276(7)	0.0155(3)
C18	0.65283(18)	0.06978(14)	0.54221(7)	0.0156(3)
C19	0.58143(19)	0.08128(15)	0.59018(7)	0.0175(3)
C20	0.48755(19)	0.17945(16)	0.60026(7)	0.0182(3)
C22	0.7049(2)	0.15134(17)	0.44948(7)	0.0204(3)
C23	0.4097(2)	0.18355(19)	0.65226(8)	0.0272(4)
H21A	0.7676	-0.0489	0.4960	0.027
H21B	0.6943	-0.1138	0.5455	0.027
H21A	0.7317	-0.1001	0.5636	0.027
H21B	0.7155	-0.0783	0.4994	0.027
H3A	0.9725	-0.0288	0.5093	0.014

H2	0.2644	0.7343	0.7349	0.025
H3A	0.2159	0.9408	0.7144	0.040
H3B	0.2973	0.9246	0.7750	0.040
H3C	0.1159	0.9511	0.7654	0.040
H4A	0.1331	0.6288	0.7977	0.043
H4B	0.0528	0.7511	0.8156	0.043
H4C	0.2352	0.7333	0.8284	0.043
H5	-0.2460	0.6164	0.5741	0.018
H6A	-0.0832	0.6049	0.5053	0.028
H6B	0.0655	0.6234	0.5479	0.028
H6C	-0.0552	0.7319	0.5361	0.028
H7A	-0.1584	0.4199	0.5608	0.030
H7B	-0.1835	0.4387	0.6236	0.030
H7C	-0.0129	0.4412	0.6045	0.030
H9	-0.1271	0.8952	0.7754	0.021
H10	-0.3937	0.9300	0.7566	0.023
H11	-0.5323	0.8423	0.6814	0.021
H12	-0.4104	0.7198	0.6207	0.019
H14A	0.2668	0.3503	0.5800	0.024
H14B	0.3441	0.4207	0.5328	0.024
H16	0.5311	0.3248	0.4872	0.020
H19	0.5975	0.0197	0.6171	0.021
H22A	0.6586	0.0828	0.4286	0.031
H22B	0.8164	0.1385	0.4567	0.031
H22C	0.6857	0.2263	0.4286	0.031
H23A	0.2975	0.1846	0.6435	0.041
H23B	0.4419	0.2569	0.6727	0.041
H23C	0.4391	0.1118	0.6743	0.041

Appendix C: Crystal data and structure refinement for [(IPr)AuSR] (**2**)

Formula	$C_{44}H_{56}AuN_5S$
Formula Weight (*g/mol*)	883.96
Crystal Dimensions (*mm*)	0.337 × 0.295 × 0.086
Crystal Color and Habit	colourless Plate
Crystal System	Triclinic
Space Group	P -1
Temperature, K	110
a, Å	9.935(2)
b, Å	13.781(5)
c, Å	16.237(5)
α,°	112.118(11)
β,°	94.491(8)
γ,°	90.223(11)
V, $Å^3$	2051.8(11)
Number of reflections to determine final unit cell	9144
Min and Max 2θ for cell determination, °	4.92, 72.06
Z	2
F(000)	900
ρ (*g/cm*)	1.431
λ, Å, (MoKα)	0.71073
μ, (cm^{-1})	3.672
Diffractometer Type	Bruker Kappa Axis Apex2
Scan Type(s)	φ and ω scans
Max 2θ for data collection, °	75.624
Measured fraction of data	0.999
Number of reflections measured	149238
Unique reflections measured	21937
R_{merge}	0.0310
Number of reflections included in refinement	21937
Cut off Threshold Expression	I > 2σ (I)
Structure refined using	full matrix least-squares using F^2
Weighting Scheme	$w=1/[sigma^2(Fo^2)+(0.0293P)^2+0.6998P]$ where $P=(Fo^2+2Fc^2)/3$
Number of parameters in least-squares	471
R_1	0.0277
wR_2	0.0568
R_1 (all data)	0.0355
wR_2 (all data)	0.0586
GOF	1.046
Maximum shift/error	0.008
Min & Max peak heights on final ΔF Map (e^-/Å)	-0.946, 4.183

Appendix D: Atomic coordinates for [(IPr)AuSR] (**2**)

Atom	**x**	**y**	**z**	$\mathbf{U_{iso/equiv}}$
Au1	0.44287(2)	0.09725(2)	0.29880(2)	0.01474(2)
S1	0.67113(3)	0.12290(3)	0.30735(3)	0.01942(6)
N1	0.17012(11)	0.02506(10)	0.20018(8)	0.0167(2)
N2	0.15144(11)	0.07513(9)	0.34084(8)	0.01470(19)
N3	0.45681(18)	0.54820(13)	0.17239(11)	0.0325(3)
N4	0.48376(17)	0.47433(14)	0.10653(12)	0.0328(3)
N5	0.4990(3)	0.40450(19)	0.04237(15)	0.0568(6)
C1	0.24302(13)	0.06415(11)	0.28068(10)	0.0156(2)
C2	0.03485(13)	0.01241(12)	0.21030(10)	0.0193(3)
C3	0.02289(13)	0.04344(12)	0.29848(10)	0.0175(2)
C4	0.18703(13)	0.10742(11)	0.43558(9)	0.0150(2)
C5	0.23037(13)	0.03090(11)	0.46804(10)	0.0168(2)
C6	0.26892(15)	0.06419(13)	0.55930(11)	0.0216(3)
C7	0.26451(16)	0.16883(14)	0.61471(11)	0.0244(3)
C8	0.21696(16)	0.24197(13)	0.58068(11)	0.0231(3)
C9	0.17577(14)	0.21264(12)	0.49040(10)	0.0181(2)
C10	0.23544(15)	-0.08412(12)	0.40959(11)	0.0206(3)
C11	0.38094(19)	-0.12049(16)	0.40578(16)	0.0358(4)
C12	0.1465(2)	-0.15040(15)	0.44282(14)	0.0315(4)
C13	0.11921(16)	0.29187(12)	0.45373(11)	0.0220(3)
C14	0.03492(19)	0.37366(14)	0.51890(14)	0.0305(4)
C15	0.2315(2)	0.34582(16)	0.42572(14)	0.0333(4)
C16	0.22812(14)	-0.00476(13)	0.11561(10)	0.0196(3)
C17	0.22805(17)	0.06658(14)	0.07328(11)	0.0241(3)
C18	0.2817(2)	0.03342(17)	-0.00980(12)	0.0324(4)
C19	0.3333(2)	-0.06535(18)	-0.04758(12)	0.0348(4)
C20	0.33362(19)	-0.13340(16)	-0.00296(13)	0.0321(4)
C21	0.28159(17)	-0.10463(14)	0.08007(11)	0.0255(3)
C22	0.1785(2)	0.17700(15)	0.11563(13)	0.0308(4)
C23	0.2986(3)	0.25631(18)	0.14385(17)	0.0471(5)
C24	0.0718(2)	0.20093(19)	0.05339(15)	0.0393(5)
C25	0.2887(2)	-0.17932(16)	0.12927(14)	0.0349(4)
C26	0.4364(3)	-0.19219(18)	0.15755(16)	0.0470(6)
C27	0.2191(2)	-0.28542(18)	0.07344(17)	0.0421(5)
C28	0.71048(15)	0.26001(13)	0.38226(11)	0.0216(3)
C29	0.67528(14)	0.34106(12)	0.34315(11)	0.0198(3)
C30	0.75231(15)	0.35629(14)	0.27982(12)	0.0237(3)
C31	0.71628(16)	0.43555(14)	0.24925(12)	0.0259(3)
C32	0.60820(16)	0.50000(13)	0.27947(11)	0.0233(3)
C33	0.53149(16)	0.48488(13)	0.34235(11)	0.0224(3)

C34	0.56732(15)	0.40535(13)	0.37259(11)	0.0214(3)
C35	0.57399(18)	0.58244(14)	0.24191(12)	0.0275(3)
C36	0.87211(18)	0.29136(17)	0.24575(15)	0.0345(4)
C37	0.4151(2)	0.55408(17)	0.37809(14)	0.0341(4)
C1S	-0.0858(3)	-0.5587(3)	-0.22565(19)	0.0557(7)
C2S	0.0218(2)	-0.60184(19)	-0.17777(14)	0.0374(4)
C3S	0.0542(2)	-0.70613(19)	-0.21095(15)	0.0417(5)
C4S	0.1530(2)	-0.74448(19)	-0.16656(15)	0.0398(5)
C5S	0.2190(2)	-0.67771(19)	-0.08879(16)	0.0400(5)
C6S	0.1870(2)	-0.5728(2)	-0.05378(16)	0.0432(5)
C7S	0.0882(2)	-0.53548(18)	-0.09851(15)	0.0382(4)
H2	-0.0360	-0.0133	0.1639	0.023
H3	-0.0578	0.0436	0.3263	0.021
H6	0.2986	0.0144	0.5837	0.026
H7	0.2942	0.1906	0.6762	0.029
H8	0.2125	0.3132	0.6196	0.028
H10	0.1990	-0.0936	0.3478	0.025
H11A	0.4360	-0.0770	0.3845	0.054
H11B	0.3823	-0.1939	0.3649	0.054
H11C	0.4177	-0.1138	0.4655	0.054
H12A	0.1812	-0.1428	0.5032	0.047
H12B	0.1478	-0.2242	0.4028	0.047
H12C	0.0536	-0.1266	0.4438	0.047
H13	0.0583	0.2525	0.3990	0.026
H14A	-0.0285	0.3385	0.5428	0.046
H14B	-0.0156	0.4124	0.4876	0.046
H14C	0.0948	0.4225	0.5680	0.046
H15A	0.2920	0.3865	0.4783	0.050
H15B	0.1918	0.3928	0.3985	0.050
H15C	0.2829	0.2928	0.3824	0.050
H18	0.2826	0.0796	-0.0409	0.039
H19	0.3686	-0.0864	-0.1042	0.042
H20A	0.3698	-0.2008	-0.0293	0.038
H22	0.1353	0.1822	0.1707	0.037
H23A	0.3631	0.2399	0.1852	0.071
H23B	0.2663	0.3272	0.1734	0.071
H23C	0.3430	0.2525	0.0910	0.071
H24A	0.1104	0.1933	-0.0024	0.059
H24B	0.0426	0.2729	0.0823	0.059
H24C	-0.0060	0.1520	0.0404	0.059
H25	0.2406	-0.1473	0.1846	0.042
H26A	0.4856	-0.2240	0.1043	0.070
H26B	0.4400	-0.2375	0.1919	0.070
H26C	0.4780	-0.1233	0.1945	0.070
H27A	0.1238	-0.2755	0.0591	0.063
H27B	0.2256	-0.3312	0.1073	0.063

H27C	0.2633	-0.3177	0.0181	0.063
H28A	0.6616	0.2752	0.4364	0.026
H28B	0.8084	0.2676	0.4013	0.026
H31	0.7675	0.4460	0.2061	0.031
H34	0.5154	0.3947	0.4154	0.026
H35A	0.5521	0.6478	0.2909	0.033
H25B	0.6537	0.5978	0.2153	0.033
H36A	0.9031	0.3062	0.1957	0.052
H36B	0.8461	0.2168	0.2256	0.052
H36C	0.9452	0.3087	0.2937	0.052
H37A	0.4478	0.6274	0.4053	0.051
H37B	0.3758	0.5339	0.4231	0.051
H37C	0.3462	0.5459	0.3291	0.051
H1SA	-0.0456	-0.5411	-0.2717	0.084
H1SB	-0.1222	-0.4956	-0.1825	0.084
H1SC	-0.1590	-0.6117	-0.2535	0.084
H3S	0.0082	-0.7526	-0.2651	0.050
H4S	0.1742	-0.8164	-0.1902	0.048
H5S	0.2872	-0.7031	-0.0585	0.048
H6S	0.2326	-0.5266	0.0006	0.052
H7S	0.0662	-0.4637	-0.0744	0.046

Appendix E: Crystal data and structure refinement for [(IPr)AgSR] (**3**)

Formula	$C_{44}H_{56}AgN_5S$
Formula Weight (*g/mol*)	794.86
Crystal Dimensions (*mm*)	0.411 × 0.271 × 0.104
Crystal Color and Habit	colourless Rod
Crystal System	triclinic
Space Group	P -1
Temperature, K	110
a, Å	10.0465(4)
b, Å	13.7120(6)
c, Å	16.2168(7)
α,°	112.088(2)
β,°	94.365(2)
γ,°	90.084(2)
V, $Å^3$	2062.93(15)
Number of reflections to determine final unit cell	9878
Min and Max 2θ for cell determination, °	5.16, 69.96
Z	2
F(000)	836
ρ (*g/cm*)	1.280
λ, Å, (MoKα)	0.71073
μ, (cm^{-1})	0.575
Diffractometer Type	Bruker Kappa Axis Apex2
Scan Type(s)	φ and ω scans
Max 2θ for data collection, °	70.382
Measured fraction of data	0.999
Number of reflections measured	66419
Unique reflections measured	18278
R_{merge}	0.0285
Number of reflections included in refinement	18278
Cut off Threshold Expression	I > 2σ (I)
Structure refined using	full matrix least-squares using F^2
Weighting Scheme	$w=1/[sigma^2(Fo^2)+(0.0341P)^2+0.4496P]$ where $P=(Fo^2+2Fc^2)/3$
Number of parameters in least-squares	471
R_1	0.0303
wR_2	0.0697
R_1 (all data)	0.0387
wR_2 (all data)	0.0730
GOF	1.041
Maximum shift/error	0.002
Min & Max peak heights on final ΔF Map (e^-/Å)	-0.901, 1.018

Appendix F: Atomic coordinates for [(IPr)AgSR] (**3**)

Atom	**x**	**y**	**z**	$\mathbf{U_{iso/equiv}}$
Ag1	0.44416(2)	0.10021(2)	0.30015(2)	0.01518(2)
S1	0.67461(2)	0.12358(2)	0.30789(2)	0.01899(5)
N1	0.14832(8)	0.07656(7)	0.34197(6)	0.01317(15)
N2	0.16704(8)	0.02810(7)	0.20173(6)	0.01455(15)
N3	0.45902(11)	0.54971(9)	0.17242(8)	0.0270(2)
N4	0.48574(11)	0.47343(10)	0.10663(8)	0.0273(2)
N5	0.50079(14)	0.40394(12)	0.04373(10)	0.0451(3)
C1	0.23943(9)	0.06657(8)	0.28196(7)	0.01388(17)
C2	0.02110(9)	0.04550(9)	0.30008(7)	0.01650(18)
C3	0.03286(9)	0.01522(9)	0.21150(8)	0.01744(19)
C4	0.18430(9)	0.10774(8)	0.43645(7)	0.01388(17)
C5	0.17247(10)	0.21349(9)	0.49240(7)	0.01636(18)
C6	0.21476(11)	0.24218(10)	0.58247(8)	0.0209(2)
C7	0.26350(11)	0.16798(10)	0.61515(8)	0.0220(2)
C8	0.26927(11)	0.06342(10)	0.55929(8)	0.0198(2)
C9	0.22954(9)	0.03083(9)	0.46805(7)	0.01558(18)
C10	0.11525(11)	0.29373(9)	0.45693(8)	0.0201(2)
C11	0.03244(13)	0.37545(10)	0.52344(10)	0.0280(3)
C12	0.22572(14)	0.34878(12)	0.42867(10)	0.0317(3)
C13	0.23561(11)	-0.08434(9)	0.40873(8)	0.01905(19)
C14	0.14889(14)	-0.15173(11)	0.44168(10)	0.0303(3)
C15	0.37991(14)	-0.12040(12)	0.40416(12)	0.0357(3)
C16	0.22427(10)	-0.00142(9)	0.11687(7)	0.01732(19)
C17	0.27992(11)	-0.10091(10)	0.08148(8)	0.0228(2)
C18	0.33148(13)	-0.12870(12)	-0.00176(9)	0.0301(3)
C19	0.32788(14)	-0.06080(13)	-0.04699(9)	0.0326(3)
C20	0.27465(14)	0.03760(12)	-0.00920(9)	0.0305(3)
C21	0.22154(12)	0.07008(10)	0.07408(8)	0.0225(2)
C22	0.28990(14)	-0.17554(11)	0.13040(10)	0.0300(3)
C23	0.43747(17)	-0.18807(13)	0.15752(12)	0.0424(4)
C24	0.22239(16)	-0.28287(12)	0.07538(11)	0.0363(3)
C25	0.16982(14)	0.18014(11)	0.11636(9)	0.0285(3)
C26	0.28699(19)	0.26143(13)	0.14625(13)	0.0455(4)
C27	0.06490(16)	0.20386(14)	0.05343(11)	0.0368(3)
C28	0.71304(11)	0.26104(10)	0.38310(8)	0.0206(2)
C29	0.67698(10)	0.34247(9)	0.34441(8)	0.01795(19)
C30	0.75362(10)	0.36022(10)	0.28240(8)	0.0207(2)
C31	0.71704(11)	0.43943(10)	0.25181(8)	0.0214(2)
C32	0.60748(11)	0.50191(9)	0.28069(8)	0.01885(19)
C33	0.53012(11)	0.48431(9)	0.34234(8)	0.0198(2)

C34	0.56678(11)	0.40492(9)	0.37263(8)	0.0196(2)
C35	0.87481(12)	0.29682(12)	0.24947(11)	0.0320(3)
C36	0.41138(14)	0.55087(12)	0.37627(10)	0.0310(3)
C37	0.57273(12)	0.58486(10)	0.24343(8)	0.0230(2)
C1S_2	-0.02021(13)	-0.39785(12)	0.17508(9)	0.0295(3)
C2S_2	-0.05299(14)	-0.29184(12)	0.20905(10)	0.0334(3)
C3S_2	-0.15287(14)	-0.25397(12)	0.16655(10)	0.0308(3)
C4S_2	-0.22250(14)	-0.32131(12)	0.08912(10)	0.0310(3)
C5S_2	-0.19025(14)	-0.42655(12)	0.05420(10)	0.0331(3)
C6S_2	-0.08996(14)	-0.46405(12)	0.09684(10)	0.0303(3)
C7S_2	0.08790(17)	-0.43946(15)	0.22128(12)	0.0447(4)
H2	-0.0586	0.0455	0.3281	0.020
H3	-0.0370	-0.0099	0.1651	0.021
H6	0.2101	0.3135	0.6220	0.025
H7	0.2932	0.1892	0.6766	0.026
H8	0.3005	0.0132	0.5830	0.024
H10	0.0546	0.2548	0.4024	0.024
H11A	-0.0184	0.4149	0.4930	0.042
H11B	0.0921	0.4241	0.5723	0.042
H11C	-0.0294	0.3397	0.5476	0.042
H12A	0.2749	0.2960	0.3836	0.047
H12B	0.2871	0.3877	0.4808	0.047
H12C	0.1858	0.3978	0.4035	0.047
H13	0.1992	-0.0933	0.3471	0.023
H14A	0.0563	-0.1294	0.4414	0.045
H14B	0.1819	-0.1430	0.5026	0.045
H14C	0.1529	-0.2259	0.4022	0.045
H15A	0.3817	-0.1942	0.3634	0.054
H15B	0.4171	-0.1133	0.4639	0.054
H15C	0.4333	-0.0767	0.3823	0.054
H18	0.3698	-0.1956	-0.0278	0.036
H19	0.3620	-0.0818	-0.1040	0.039
H20	0.2741	0.0841	-0.0403	0.037
H22	0.2431	-0.1437	0.1863	0.036
H23A	0.4858	-0.2185	0.1038	0.064
H23B	0.4426	-0.2347	0.1909	0.064
H23C	0.4778	-0.1190	0.1951	0.064
H24A	0.1271	-0.2739	0.0631	0.054
H24B	0.2330	-0.3292	0.1089	0.054
H24C	0.2638	-0.3143	0.0189	0.054
H25	0.1260	0.1843	0.1709	0.034
H26A	0.3343	0.2568	0.0943	0.068
H26B	0.3486	0.2469	0.1898	0.068
H26C	0.2528	0.3323	0.1737	0.068
H27A	0.1052	0.1995	-0.0010	0.055
H27B	0.0322	0.2749	0.0832	0.055

H27C	-0.0098	0.1524	0.0378	0.055
H28A	0.6652	0.2759	0.4375	0.025
H28B	0.8099	0.2687	0.4016	0.025
H31	0.7687	0.4514	0.2096	0.026
H34	0.5145	0.3926	0.4144	0.023
H35A	0.8507	0.2216	0.2275	0.048
H35B	0.9450	0.3138	0.2986	0.048
H35C	0.9075	0.3139	0.2009	0.048
H36A	0.3453	0.5421	0.3261	0.047
H36B	0.4407	0.6251	0.4049	0.047
H36C	0.3712	0.5286	0.4198	0.047
H37A	0.5485	0.6497	0.2924	0.028
H37B	0.6520	0.6019	0.2181	0.028
H2S_2	-0.0059	-0.2449	0.2623	0.040
H3S_2	-0.1736	-0.1816	0.1906	0.037
H4S_2	-0.2917	-0.2958	0.0601	0.037
H5S_2	-0.2371	-0.4732	0.0007	0.040
H6S_2	-0.0687	-0.5363	0.0721	0.036
H7SA_2	0.1174	-0.5067	0.1793	0.067
H7SB_2	0.0531	-0.4501	0.2722	0.067
H7SC_2	0.1637	-0.3887	0.2424	0.067

Appendix G: Crystal data and structure refinement for [(IPr)CuSR] (**4**)

Formula	$C_{44}H_{56}CuN_5S$
Formula Weight (*g/mol*)	750.53
Crystal Dimensions (*mm*)	0.437 × 0.231 × 0.068
Crystal Color and Habit	colourless Plate
Crystal System	triclinic
Space Group	P -1
Temperature, K	110
a, Å	9.8285(5)
b, Å	13.7300(7)
c, Å	16.3274(9)
α,°	111.800(3)
β,°	94.632(2)
γ,°	90.644(2)
V, $Å^3$	2037.03(19)
Number of reflections to determine final unit cell	9928
Min and Max 2θ for cell determination, °	4.9, 66.34
Z	2
F(000)	800
ρ (*g/cm*)	1.224
λ, Å, (MoKα)	0.71073
μ, (cm^{-1})	0.624
Diffractometer Type	Bruker Kappa Axis Apex2
Scan Type(s)	phi and omega scans
Max 2θ for data collection, °	66.478
Measured fraction of data	0.999
Number of reflections measured	59551
Unique reflections measured	15507
R_{merge}	0.0275
Number of reflections included in refinement	15507
Cut off Threshold Expression	I > 2σ (I)
Structure refined using	full matrix least-squares using F^2
Weighting Scheme	$w=1/[sigma^2(Fo^2)+(0.0455P)^2+0.5630P]$ where $P=(Fo^2+2Fc^2)/3$
Number of parameters in least-squares	471
R_1	0.0321
wR_2	0.0839
R_1 (all data)	0.0418
wR_2 (all data)	0.0889
GOF	1.022
Maximum shift/error	0.016
Min & Max peak heights on final ΔF Map (e^-/Å)	-0.312, 0.607

Appendix H: Atomic coordinates for [(IPr)CuSR] (**4**)

Atom	**x**	**y**	**z**	$\mathbf{U_{iso/equiv}}$
Cu1	0.43436(2)	0.59856(2)	0.29953(2)	0.01439(3)
S1	0.65135(2)	0.61799(2)	0.30483(2)	0.01810(5)
N1	0.14907(8)	0.57629(6)	0.34036(5)	0.01281(13)
N2	0.16950(8)	0.52813(6)	0.20151(5)	0.01339(14)
N3	0.46195(10)	1.04855(8)	0.17116(7)	0.02428(18)
N4	0.48896(10)	0.97335(8)	0.10538(7)	0.02391(18)
N5	0.50397(13)	0.90464(10)	0.04235(8)	0.0385(3)
C1	0.24340(9)	0.56715(7)	0.28174(6)	0.01308(15)
C2	0.01903(9)	0.54409(8)	0.29770(7)	0.01554(16)
C3	0.03206(10)	0.51388(8)	0.20992(7)	0.01604(17)
C4	0.18392(9)	0.60812(7)	0.43448(6)	0.01308(15)
C5	0.17144(10)	0.71364(7)	0.48911(7)	0.01532(16)
C6	0.21260(11)	0.74298(8)	0.57906(7)	0.01905(18)
C7	0.26088(11)	0.66953(9)	0.61284(7)	0.02023(19)
C8	0.26633(10)	0.56481(8)	0.55804(7)	0.01783(17)
C9	0.22802(9)	0.53185(7)	0.46724(6)	0.01446(16)
C10	0.11352(11)	0.79242(8)	0.45231(7)	0.01909(18)
C11	0.22675(14)	0.84730(10)	0.42429(9)	0.0301(2)
C12	0.02827(13)	0.87369(9)	0.51673(9)	0.0269(2)
C13	0.23485(10)	0.41696(8)	0.40886(7)	0.01744(17)
C14	0.38341(13)	0.38434(10)	0.40263(10)	0.0317(3)
C15	0.15152(13)	0.34803(9)	0.44322(8)	0.0271(2)
C16	0.22840(10)	0.49856(8)	0.11782(6)	0.01608(16)
C17	0.22658(11)	0.56967(9)	0.07473(7)	0.02052(19)
C18	0.28014(13)	0.53673(10)	-0.00783(8)	0.0276(2)
C19	0.33305(13)	0.43870(11)	-0.04464(8)	0.0289(2)
C20	0.33555(12)	0.37104(10)	0.00057(8)	0.0261(2)
C21	0.28353(11)	0.39939(8)	0.08321(7)	0.01991(18)
C22	0.17564(13)	0.67953(9)	0.11604(8)	0.0256(2)
C23	0.29696(17)	0.75980(11)	0.14497(11)	0.0405(3)
C24	0.06865(14)	0.70327(12)	0.05315(9)	0.0335(3)
C25	0.29278(13)	0.32541(9)	0.13284(8)	0.0256(2)
C26	0.44329(15)	0.31397(10)	0.16032(10)	0.0364(3)
C27	0.22239(14)	0.21826(10)	0.07864(9)	0.0318(3)
C28	0.70151(11)	0.75416(8)	0.37932(7)	0.01926(18)
C29	0.67067(10)	0.83721(8)	0.34151(7)	0.01670(17)
C30	0.56508(10)	0.90497(8)	0.37263(7)	0.01820(18)
C31	0.53277(10)	0.98583(8)	0.34311(7)	0.01827(17)
C32	0.61030(10)	0.99898(8)	0.27939(7)	0.01767(17)
C33	0.71566(10)	0.93175(8)	0.24808(7)	0.01956(18)

C34	0.74799(10)	0.85093(8)	0.27787(7)	0.01860(18)
C35	0.57902(12)	1.08225(8)	0.24208(7)	0.02110(19)
C36	0.41892(13)	1.05750(10)	0.37975(8)	0.0277(2)
C37	0.86524(12)	0.78278(10)	0.24241(9)	0.0272(2)
C1S_2	-0.02060(12)	0.09814(10)	0.17804(8)	0.0258(2)
C2S_2	-0.08730(12)	0.03274(10)	0.09771(8)	0.0264(2)
C3S_2	-0.18560(13)	0.07091(10)	0.05276(8)	0.0281(2)
C4S_2	-0.21870(13)	0.17564(10)	0.08766(8)	0.0266(2)
C5S_2	-0.15179(13)	0.24199(10)	0.16742(8)	0.0273(2)
C6S_2	-0.05393(13)	0.20351(10)	0.21219(8)	0.0287(2)
C7S_2	0.08587(15)	0.05591(13)	0.22623(10)	0.0407(3)
H2	-0.0628	0.5434	0.3248	0.019
H3	-0.0390	0.4880	0.1632	0.019
H6	0.2075	0.8141	0.6177	0.023
H7	0.2905	0.6912	0.6741	0.024
H8	0.2964	0.5150	0.5825	0.021
H10	0.0517	0.7526	0.3980	0.023
H11A	0.2780	0.7946	0.3811	0.045
H11B	0.2886	0.8879	0.4764	0.045
H11C	0.1862	0.8945	0.3974	0.045
H12A	-0.0236	0.9119	0.4853	0.040
H12B	0.0890	0.9232	0.5652	0.040
H12C	-0.0352	0.8380	0.5408	0.040
H13	0.1942	0.4071	0.3480	0.021
H14A	0.3858	0.3108	0.3625	0.048
H14B	0.4248	0.3924	0.4616	0.048
H14C	0.4346	0.4290	0.3798	0.048
H15A	0.0567	0.3694	0.4457	0.041
H15B	0.1904	0.3560	0.5027	0.041
H15C	0.1541	0.2744	0.4033	0.041
H18	0.2800	0.5828	-0.0392	0.033
H19	0.3677	0.4177	-0.1010	0.035
H20	0.3733	0.3042	-0.0249	0.031
H22	0.1312	0.6841	0.1702	0.031
H23A	0.3449	0.7546	0.0932	0.061
H23B	0.3599	0.7454	0.1884	0.061
H23C	0.2637	0.8307	0.1718	0.061
H24A	0.1088	0.6966	-0.0016	0.050
H24B	0.0386	0.7749	0.0816	0.050
H24C	-0.0099	0.6534	0.0392	0.050
H25	0.2453	0.3574	0.1880	0.031
H26A	0.4926	0.2844	0.1073	0.055
H26B	0.4485	0.2672	0.1934	0.055
H26C	0.4847	0.3831	0.1978	0.055
H27A	0.1249	0.2269	0.0667	0.048
H27B	0.2336	0.1720	0.1120	0.048

H27C	0.2636	0.1872	0.0225	0.048
H28A	0.6543	0.7707	0.4339	0.023
H28B	0.8009	0.7581	0.3965	0.023
H30	0.5130	0.8955	0.4159	0.022
H33	0.7676	0.9412	0.2048	0.023
H35A	0.5564	1.1474	0.2904	0.025
H35B	0.6612	1.0981	0.2171	0.025
H36A	0.3502	1.0530	0.3314	0.041
H36B	0.4560	1.1299	0.4086	0.041
H36C	0.3765	1.0361	0.4231	0.041
H37A	0.8394	0.7094	0.2310	0.041
H37B	0.9451	0.8053	0.2860	0.041
H37C	0.8875	0.7892	0.1872	0.041
H2S_2	-0.0654	-0.0390	0.0732	0.032
H3S_2	-0.2304	0.0252	-0.0021	0.034
H4S_2	-0.2865	0.2016	0.0572	0.032
H5S_2	-0.1730	0.3139	0.1914	0.033
H6S_2	-0.0089	0.2495	0.2669	0.034
H7SA_2	0.0578	-0.0156	0.2194	0.061
H7SB_2	0.0955	0.1009	0.2893	0.061
H7SC_2	0.1736	0.0550	0.2014	0.061

Appendix I:

Appendix IA: ^{13}C NMR spectrum of [($^{i}Pr_2$bimy)AuSR] **(1)**

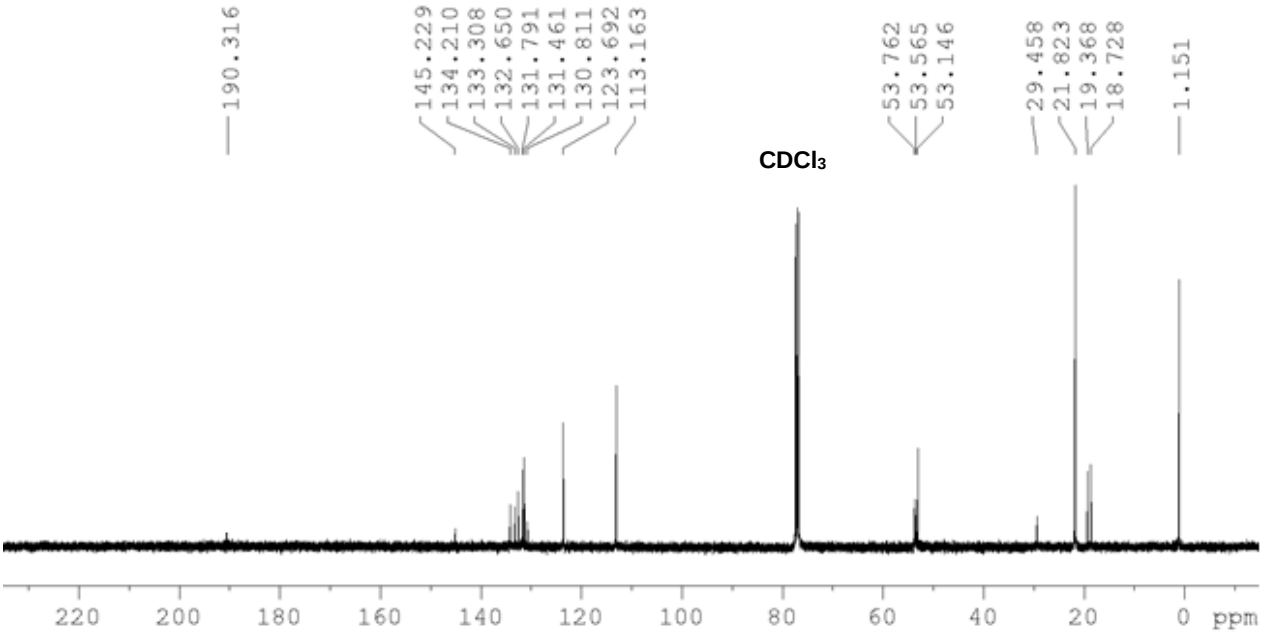

Appendix IB: ^{13}C NMR of [(IPr)AuSR] **(2)**

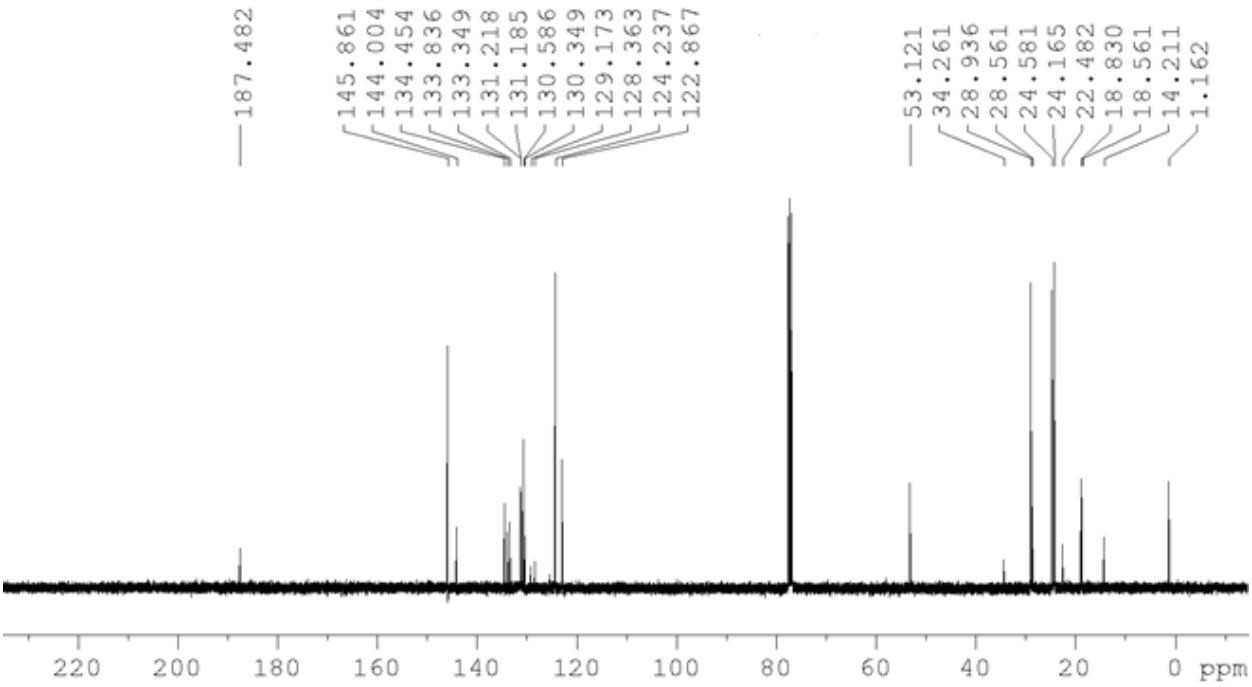

Appendix IC: ^{13}C NMR of [(IPr)AgSR] **(3)**

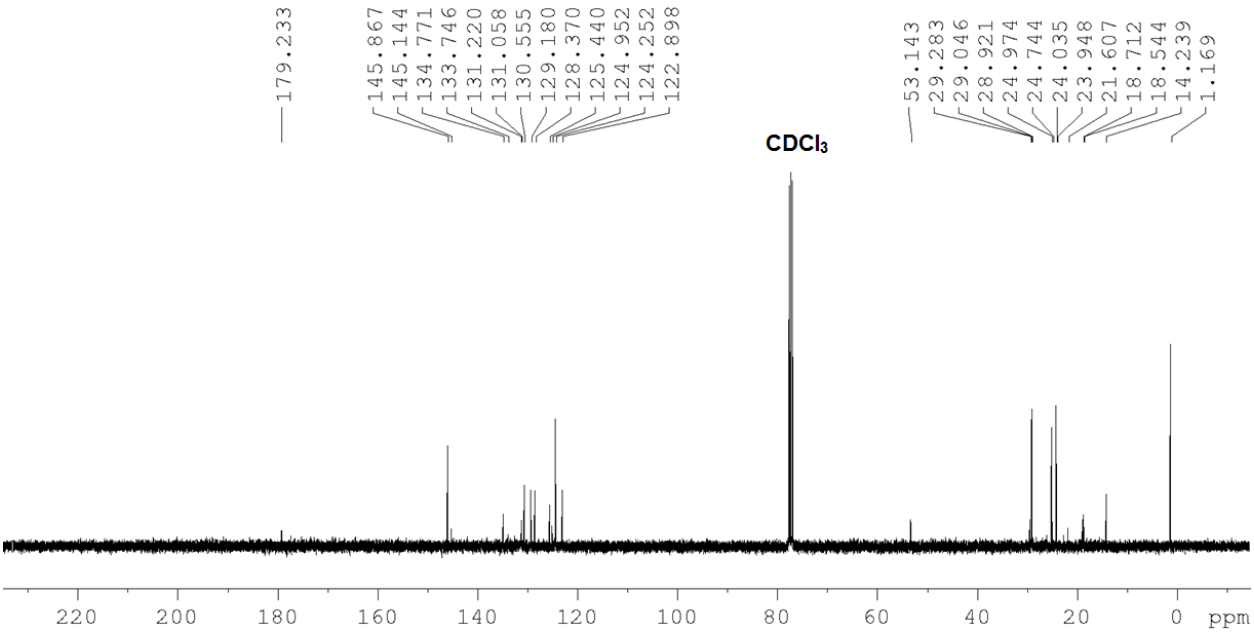

Appendix ID: ^{13}C NMR of [(IPr)CuSR] **(4)**

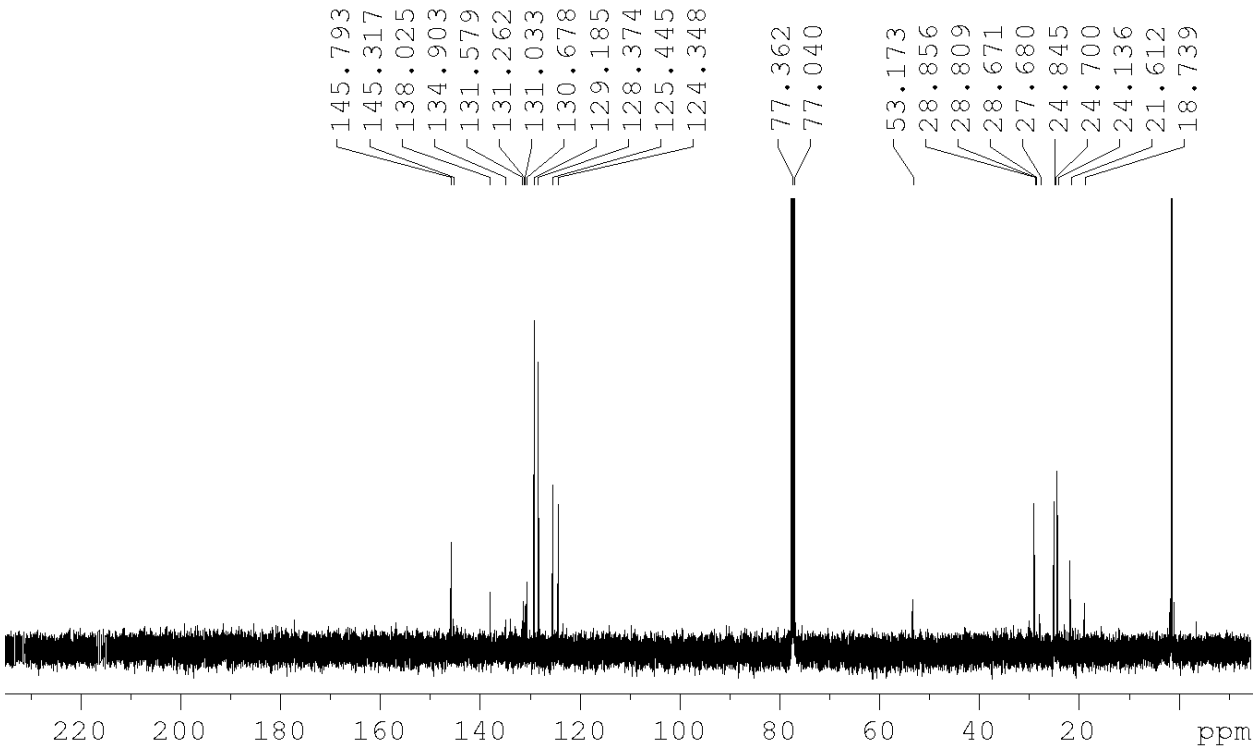

Appendix J:

Appendix JA: ^{1}H NMR spectrum of [(^{i}Pr$_2$bimy)AuSR] **(1)**

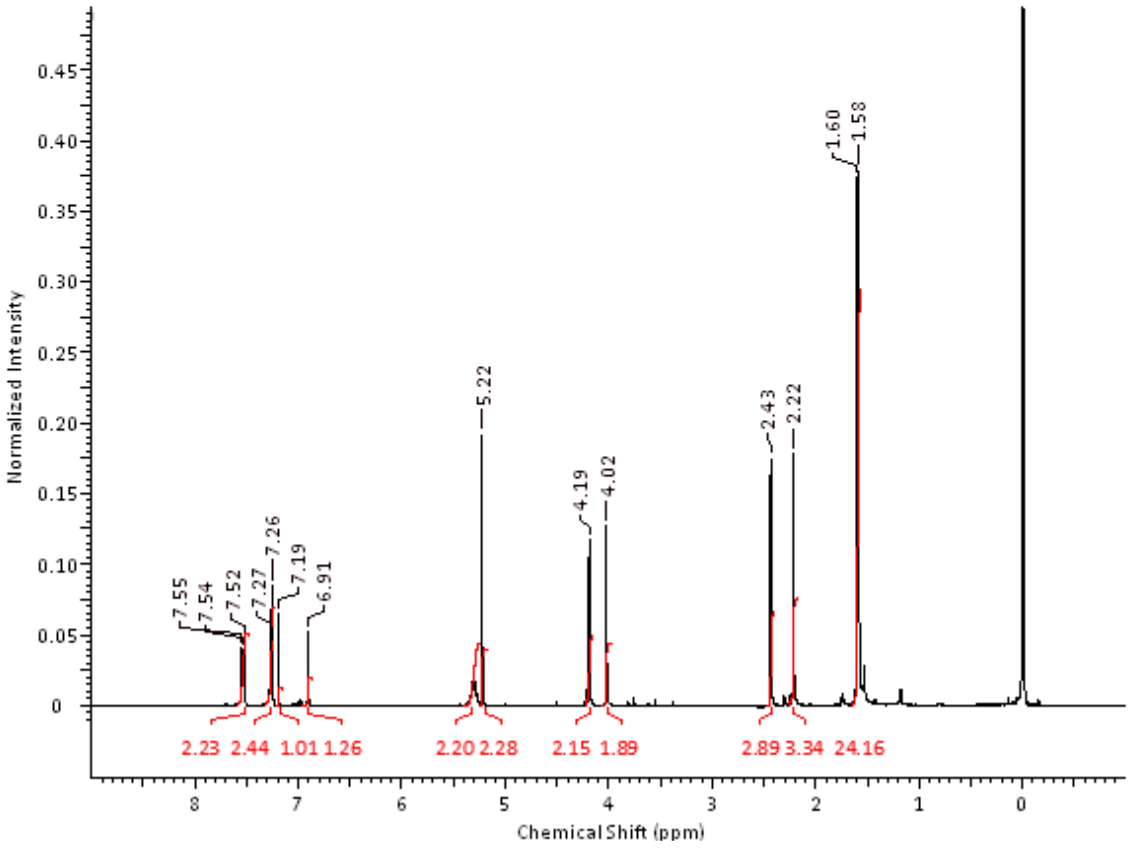

Appendix JB: ^{1}H NMR of [(IPr)AuSR] **(2)**:

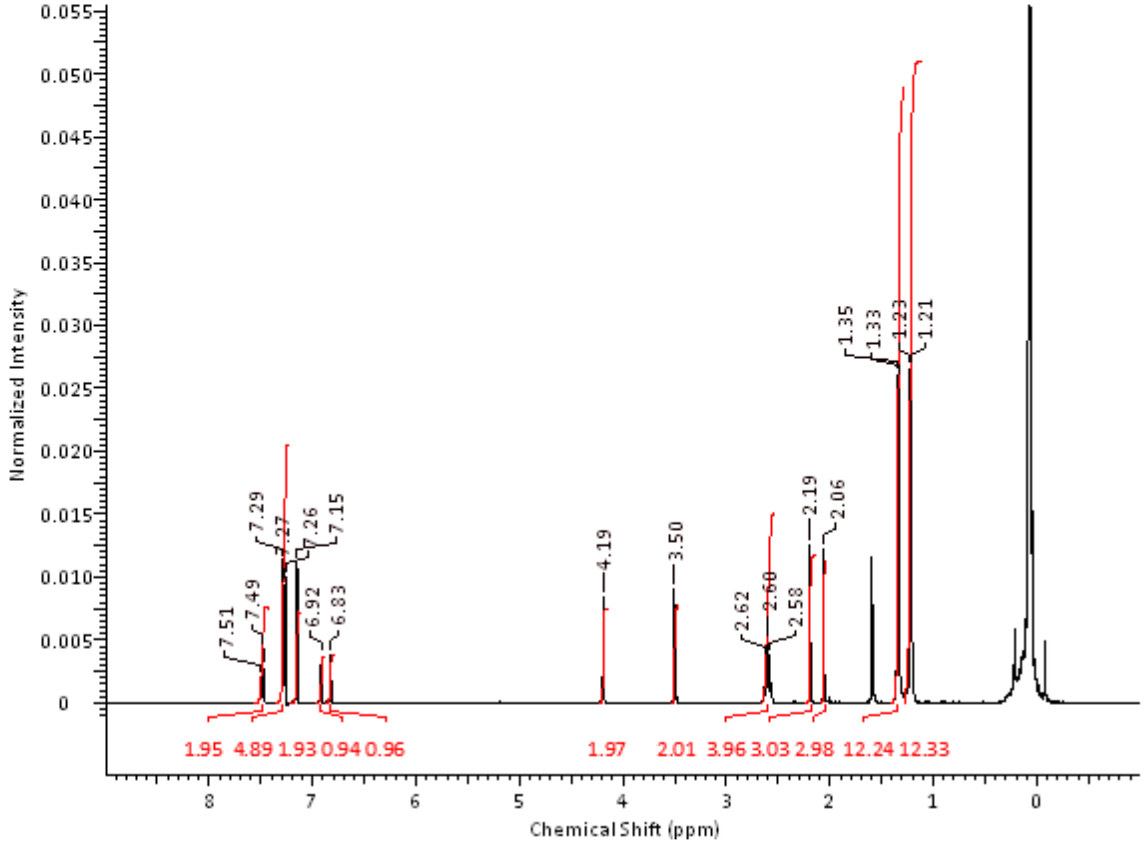

Appendix JC: ^{1}H NMR of [(IPr)AgSR] **(3)**:

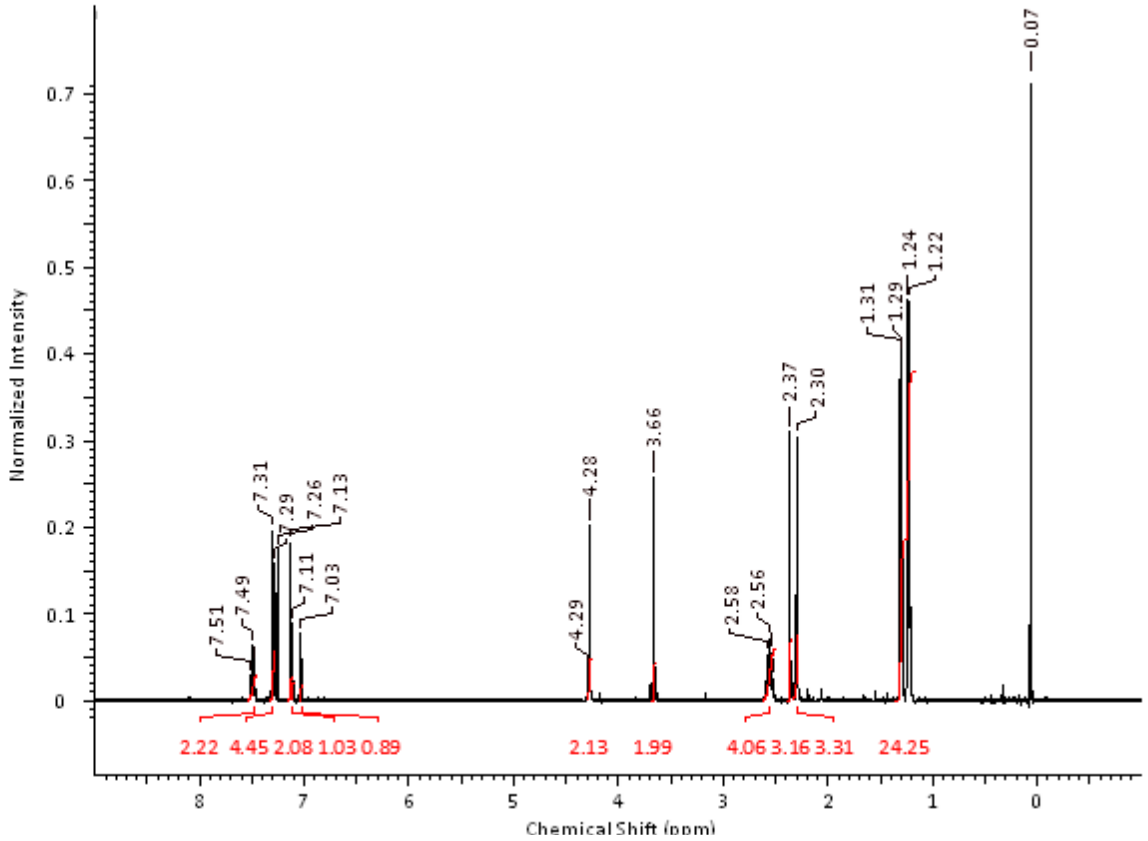

Appendix JD: ^{1}H NMR of [(IPr)CuSR] **(4)**:

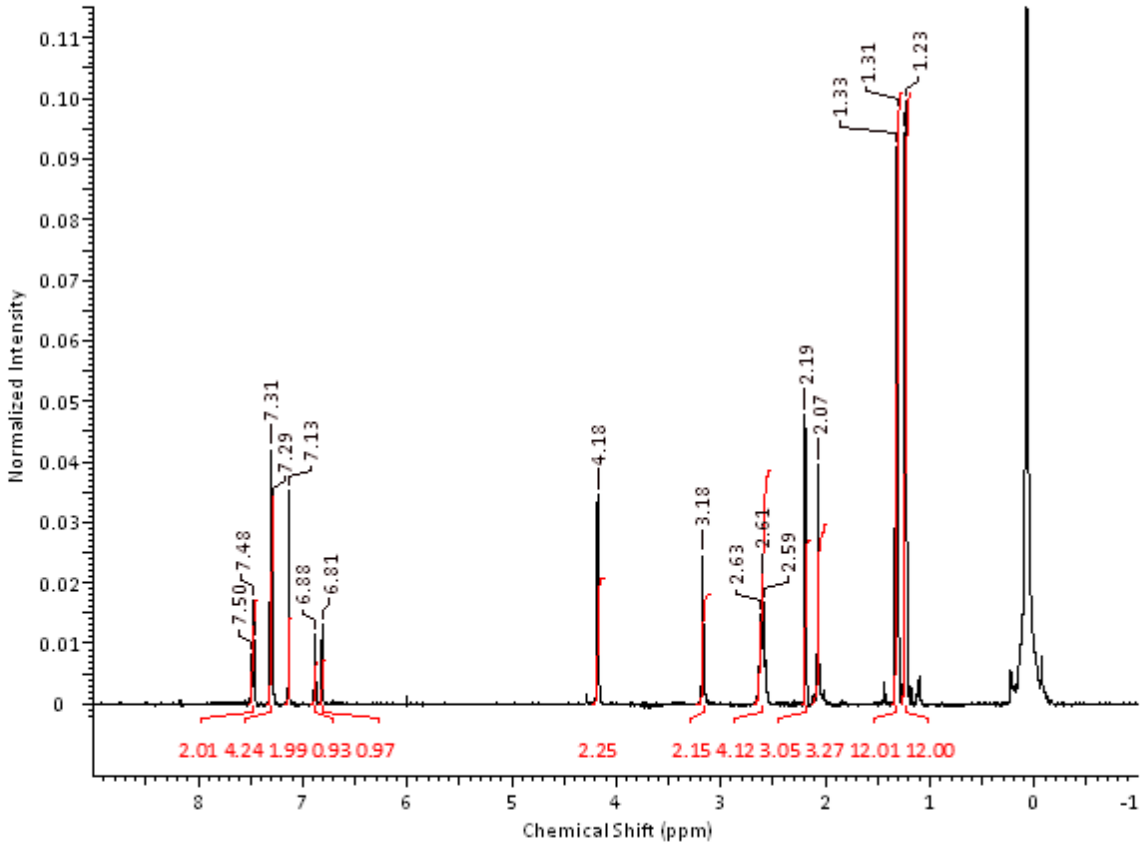

CURRICULUM VITAE

Vaishnavi Somasundaram

EDUCATION

M.Sc., Inorganic Chemistry Sept. 2014 – Jan. 2017
Western University, London, ON

M.Sc., Chemistry Co-op Sept. 2009 – Apr. 2014
McMaster University, Hamilton, ON
Minor: French Studies

TEACHING EXPERIENCE

Western University, London, ON Sept. 2014 – Jan. 2017

- General Chemistry (1302A) Fall 2014
- Bioinorganic Chemistry (2211A) Fall 2014
- Nuclear Magnetic Resonance Facility Winter 2015
- Organic Chemistry (2213A) Fall 2015
- Organic Chemistry (2223B) Winter 2016

CONFERENCES

- **98th Conference of the Canadian Society for Chemistry** – Ottawa, ON
  Somasundaram, V.; Corrigan, J.F., Workentin M.S.* (2015) "Immobilization of Small Molecules onto the Surface of Silver Nanoclusters."

- **41st Annual Southern Ontario Undergraduate Student Chemistry Conference** – Hamilton, ON
  Somasundaram V., Vargas-Baca I.* 0098 Inorganic Materials: "Alkali-Metal Derivatives of Highly-Charged Conjugated Anions."